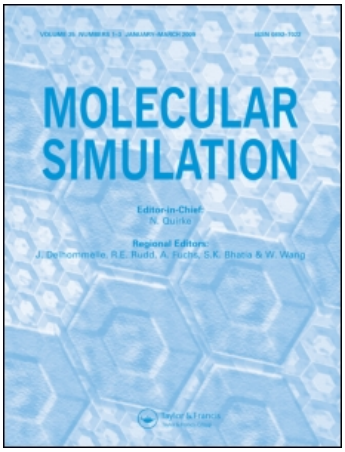

Molecular Simulation
Publication details, including instructions for authors and subscription information:
http://www.informaworld.com/smpp/title~content=t713644482

Homogeneous non-equilibrium molecular dynamics simulations of viscous flow: techniques and applications

B. D. Todd[a]; Peter J. Daivis[b]
[a] Centre for Molecular Simulation, Swinburne University of Technology, Hawthorn, Vic., Australia [b] Applied Physics, School of Applied Sciences, RMIT University, Melbourne, Vic., Australia

To cite this Article Todd, B. D. and Daivis, Peter J.(2007) 'Homogeneous non-equilibrium molecular dynamics simulations of viscous flow: techniques and applications', Molecular Simulation, 33: 3, 189 — 229
To link to this Article: DOI: 10.1080/08927020601026629
URL: http://dx.doi.org/10.1080/08927020601026629

Molecular Simulation, Vol. 33, No. 3, 15 March 2007, 189–229

Taylor & Francis
Taylor & Francis Group

Homogeneous non-equilibrium molecular dynamics simulations of viscous flow: techniques and applications

B. D. TODD†* and PETER J. DAIVIS‡¶

†Centre for Molecular Simulation, Swinburne University of Technology, PO Box 218, Hawthorn, Vic. 3122, Australia
‡Applied Physics, School of Applied Sciences, RMIT University, GPO Box 2476V, Melbourne, Vic. 3001, Australia

(Received August 2006; in final form September 2006)

We provide a review of the literature for non-equilibrium molecular dynamics (NEMD) simulations of homogeneous fluids. Our review focuses on techniques for simulations of shear and elongational flows in viscous fluids and covers the formulation and application of NEMD algorithms for atomic and molecular fluids. We provide a set of expositions that can be effectively used as guidelines to formulate the relevant equations of motion, periodic boundary conditions and thermostats. We also provide a survey of applications in a convenient tabular form as an aid to researchers who wish to use NEMD to study transport phenomena.

Keywords: Non-equilibrium molecular dynamics; Rheology; Non-equilibrium statistical mechanics; Shear flow; Elongational flow; Transport

1. Introduction

The past decade has witnessed a significant rise in the number of researchers using non-equilibrium molecular dynamics (NEMD) simulation techniques to study liquids under the influence of various types of flow fields [1,2]. These studies have been almost equally divided between liquids under bulk conditions (homogeneous fluids), and those in highly confined geometries (inhomogeneous fluids). A review that could do full justice to both types of systems would need to be several hundred pages in length, and would also probably tire the reader beyond endurance. Instead, we have taken a more moderate (and hopefully more useful) approach and focused on an extensive review of homogeneous fluids under homogeneous non-equilibrium flows. This is motivated largely by the rapid increase in the use of NEMD techniques for homogeneous molecular fluids, such as alkanes and polymers under shear or elongation. Therefore, we focus exclusively on shear and elongational flows, although homogeneous dilational flows can also be studied using these methods. Apart from assumptions about the nature of intermolecular forces and the degree of coarse-graining, NEMD methods allow one to obtain accurate transport properties of molecularly structured fluids of any arbitrary molecular architecture and composition. Nevertheless, the correct determination of these transport properties requires carefully formulated equations of motion and due attention to issues such as periodic boundary conditions and thermostatting details. In surveying the literature over the past two decades it is clear to us that there is still considerable doubt in the simulation community as to what the most appropriate equations of motion should be for molecular systems, and how such systems should be coupled to a thermostatting mechanism. To enable us to concentrate on these rather technical details we also restrict our review to viscous flow and only comment on thermal or mass transport where appropriate. This is again motivated by the contents of the literature itself: the overwhelming majority of publications with NEMD simulations as the theme have concentrated on momentum transport in viscous fluids.

We have chosen to exclusively discuss homogeneous flows generated by deterministic equations of motion, but algorithms using various types of momentum reservoir algorithms have been proposed [3,4]. These algorithms sometimes use an *ad-hoc* device such as particle momentum interchange to generate shear flow [4]. Although they are effective under some circumstances, these techniques have significant disadvantages. They

*Corresponding author. Email: btodd@swin.edu.au
¶Email: peter.daivis@rmit.edu.au

Molecular Simulation
ISSN 0892-7022 print/ISSN 1029-0435 online © 2007 Taylor & Francis
http://www.tandf.co.uk/journals
DOI: 10.1080/08927020601026629

induce substantial density and temperature inhomogeneity, which is undesirable unless the inhomogeneity is itself the subject of study. Unlike algorithms based on the SLLOD equations of motion, they sometimes lack a firm basis in statistical mechanics and cannot be verified with response theory. In cases where the perturbation is applied by *ad-hoc* algorithmic rules rather than deterministic equations of motion, the advantages of a strong connection to non-linear response theory, such as the applicability of the transient-time correlation function formalism, are lost. In addition, it is not clear how to simulate flows other than simple planar shear (e.g. elongational and dilational flows) by such methods. Flows with time dependent velocity gradient tensors are also not easily studied with reservoir methods. For these reasons, we have decided to restrict our attention to algorithms in which spatially homogeneous perturbations appear explicitly in the equations of motion.

Our review is structured as follows. In section 2 we first introduce the pre-requisites to NEMD simulation, namely a discussion on thermodynamic forces and fluxes—the fundamental cause and effect relationship for systems out of equilibrium. After identifying the macroscopic and microscopic forms of these forces and fluxes, we take into account the importance of introducing periodic boundary conditions in molecular dynamics simulations. We then delve into the equations of motion for generalised homogeneous flows in section 3 and concentrate on the specific examples of planar shear and planar elongational flows, as these are the two most important types of flows for NEMD applications. We do this for both atomic and molecular fluids. For both types of fluids, we pay careful attention to the momentum and energy balance requirements as well as the formulation of thermostats. In surveying the literature in section 4, rather than specifically commenting on individual papers in the literature, we provide a summary of some of the most relevant work done in the field for atomic and molecular systems. This summary is in the form of tables 1 (atomic fluids) and 2 (molecular fluids). To our knowledge, this is the first time that the literature for NEMD simulation of viscous flows has been so conveniently presented. We hope readers will find these tables useful when seeking out specific papers in the relevant literature. We conclude our review in section 5.

Our motive in writing this review has been to provide readers with the most useful, up-to-date and practical information they require in order to perform NEMD simulations of viscous flow for homogeneous systems. We do not provide a detailed discussion of response theory in this review. The relevant papers that deal with response theory are summarised in table 1. Response theory has been an indispensable tool for the validation of NEMD algorithms. It is also the basis of the transient-time correlation function (TTCF) formalism, which is the most practical application of non-linear response theory. We expect that TTCF is likely to be useful in the study of transport in molecular fluids in the years to come. This is because TTCF can be used at strain rates many orders of magnitude smaller than direct time-averaged NEMD simulations, enabling the computation of useful transport properties at strain rates that approach experimentally accessible strain rates. However, at the current time there have been only a limited number of studies that use the TTCF technique, and we refer to these in table 1.

Finally, it is our hope that this review proves to be a useful contribution to the NEMD literature. We have surveyed around 300 references that span some 50 years in the hope of putting together not just a review of the existing literature, but rather a practical guide to reliable and proven methods for NEMD simulations of homogeneous fluids under various flow geometries.

2. Thermodynamic fluxes and forces

2.1 Atomic representation

In the theory of non-equilibrium thermodynamics, the thermodynamic fluxes and forces are identified by analysing the bilinear expression for the entropy production. For simple viscous flow, the relevant term in the entropy production is

$$\sigma_{\text{visc}} = -\frac{1}{T}(\mathbf{P} - p_0\mathbf{1}) : \nabla\mathbf{v} \tag{2.1}$$

where $\mathbf{P}$ is the pressure tensor and p_0 is the equilibrium isotropic pressure [5]. The stress can be identified as minus the non-equilibrium part of the pressure tensor, $-(\mathbf{P} - p_o\mathbf{1})$. NEMD simulations of viscous flow are usually (but not always [6]) performed in an ensemble in which the velocity gradient tensor (the thermodynamic force) is the independent variable and the stress (the thermodynamic flux) is the dependent variable. The velocity gradient tensor occurs as a parameter in the equations of motion and the stress must be computed from the positions and momenta of the particles in the system. Therefore, we need an expression for the stress that can be calculated from the microscopic variables. Although this task may appear simple at first, there are many varieties of inter- and intra-molecular forces, different representations of the microscopic densities, and issues that arise in connection with periodic boundary conditions, that all seem to require special treatment in the derivation of the microscopic expression for the stress tensor. In this section we will attempt to give a unified and complete, but still relatively simple, discussion of these issues summarising information that is scattered throughout the literature.

Our discussion of the microscopic expression for the pressure tensor begins with definitions of the microscopic densities of mass, momentum and internal energy. For simplicity, we will only consider a single component fluid. Initially, we will assume that the mass of each atom or interaction site (for coarse-grained models that do not include explicit atomic detail) is localized at a point corresponding to the position of that mass element. This leads to a definition of the fluxes in the so-called *atomic*

representation. Later, we will also discuss the *molecular* representation of the fluxes.

The mass, momentum and internal energy densities in the atomic representation are given, respectively, by

$$\rho(\mathbf{r},t)=\sum_{i=1}^{N} m_i\delta(\mathbf{r}-\mathbf{r}_i), \tag{2.2}$$

$$\mathbf{J}(\mathbf{r},t)=\rho\mathbf{v}(\mathbf{r},t)=\sum_{i=1}^{N} m_i\mathbf{v}_i\delta(\mathbf{r}-\mathbf{r}_i), \tag{2.3}$$

$$\rho u(\mathbf{r},t)=\sum_{i=1}^{N} u_i\delta(\mathbf{r}-\mathbf{r}_i). \tag{2.4}$$

where m_i, $\mathbf{v}_i$ and u_i are the mass, velocity and internal energy of particle i. In these equations, the summations extend over the number of atoms N in the system. These equations also serve as microscopic definitions of the streaming velocity $\mathbf{v}$ and the local specific internal energy u. The mass density ρ, momentum density $\mathbf{J}$ and the internal energy density ρu are local, instantaneous quantities that depend on the initial microscopic state of the system $\mathbf{\Gamma}(0)$ in addition to the explicitly shown arguments of position and time. When these densities are averaged over an (equilibrium) ensemble of initial states, this dependence is removed and we obtain the usual hydrodynamic densities of non-equilibrium thermodynamics [6,7]. The microscopic and hydrodynamic densities of mass, momentum and internal energy obey the same set of balance equations, given by

$$\frac{\partial\rho}{\partial t}=-\nabla\cdot\mathbf{J}=-\nabla\cdot(\rho\mathbf{v}) \tag{2.5}$$

$$\frac{\partial(\rho\mathbf{v})}{\partial t}=-\nabla\cdot\mathbf{P}-\nabla\cdot(\rho\mathbf{v}\mathbf{v})+\rho\mathbf{F}^{\text{ext}} \tag{2.6}$$

$$\frac{\partial(\rho u)}{\partial t}=-\nabla\cdot\mathbf{J}_q-\nabla\cdot(\rho u\mathbf{v})-\mathbf{P}^{\mathrm{T}}:\nabla\mathbf{v} \tag{2.7}$$

where $\rho\mathbf{F}^{\text{ext}}$ is the local body force density due to external forces, which is expressed in terms of microscopic variables as

$$\rho\mathbf{F}^{\text{ext}}(\mathbf{r},t)=\sum_{i=1}^{N}\mathbf{F}_i^{\text{ext}}\delta(\mathbf{r}-\mathbf{r}_i) \tag{2.8}$$

and $\mathbf{F}_i^{\text{ext}}$ is the external force applied to particle i in the microscopic equations of motion.

The pressure tensor and the heat flux vector represent the diffusive fluxes of momentum and internal energy, respectively. By substituting the microscopic densities into the balance equations, we can obtain microscopic expressions for the fluxes. We will do this explicitly only for the pressure tensor, but the derivation of a microscopic expression for the heat flux vector is similar. The derivation is simplest in $\mathbf{k}$-space, so we first Fourier transform the momentum density balance equation, giving

$$\frac{\partial}{\partial t}[\widetilde{\rho\mathbf{v}}(\mathbf{k},t)]=i\mathbf{k}\cdot\tilde{\mathbf{P}}(\mathbf{k},t)+i\mathbf{k}\cdot[\widetilde{\rho\mathbf{v}\mathbf{v}}(\mathbf{k},t)]+\widetilde{\rho\mathbf{F}^{\text{ext}}}(\mathbf{k},t) \tag{2.9}$$

where we define the Fourier transform of any function $f(x)$ as

$$F\{f(x)\}=\tilde{f}(k)=\int_{-\infty}^{\infty}\mathrm{e}^{ikx}f(x)\mathrm{d}x \tag{2.10}$$

We now take the Fourier transform of the microscopic expression for the momentum density and evaluate the partial derivative with respect to time:

$$\frac{\partial}{\partial t}[\widetilde{\rho\mathbf{v}}(\mathbf{k},t)]=\frac{\partial}{\partial t}\sum_{i=1}^{N}m_i\mathbf{v}_i\mathrm{e}^{i\mathbf{k}\cdot\mathbf{r}_i}=\sum_{i=1}^{N}m_i(\dot{\mathbf{v}}_i+i\mathbf{k}\cdot\mathbf{v}_i\mathbf{v}_i)\mathrm{e}^{i\mathbf{k}\cdot\mathbf{r}_i}. \tag{2.11}$$

The equations of motion in their most general Newtonian form are

$$m_i\dot{\mathbf{v}}_i=\mathbf{F}_i \tag{2.12}$$

where $\mathbf{F}_i$ is the total force on atom i, including intermolecular forces, constraint forces and any synthetic (i.e. not naturally-occurring) forces added to the equations of motion to maintain a constant temperature or generate non-equilibrium perturbations. For the present discussion, we will restrict our attention to forces that can be expressed in the form:

$$\mathbf{F}_i=\mathbf{F}_i^{\phi}+\mathbf{F}_i^{\mathrm{C}}+\mathbf{F}_i^{\text{ext}} \tag{2.13}$$

where the first term represents forces due to atomic potentials (which may include Lennard–Jones, bond stretching and bending, dihedral or others), the second term represents internal constraint forces (e.g. bond length and bond angle constraints) and the third term represents external forces, which may be applied via the equations of motion. The first term of equation (2.11) can be written as

$$\sum_{i=1}^{N}\mathbf{F}_i\mathrm{e}^{i\mathbf{k}\cdot\mathbf{r}_i}=\sum_{i=1}^{N}\left(\mathbf{F}_i^{\phi}+\mathbf{F}_i^{\mathrm{C}}+\mathbf{F}_i^{\text{ext}}\right)\mathrm{e}^{i\mathbf{k}\cdot\mathbf{r}_i} \tag{2.14}$$

The term involving the external force is equal to the corresponding body force term on the right hand side of the momentum conservation equation, and does not contribute to the expression for the pressure tensor. The other two terms will be considered in turn. The term due to interatomic potential forces (e.g. Lennard–Jones and dihedral potentials) will become

$$\begin{aligned}\sum_{i=1}^{N}\mathbf{F}_i^{\phi}\mathrm{e}^{i\mathbf{k}\cdot\mathbf{r}_i}&=\sum_{i=1}^{N}\mathbf{F}_i^{\phi}\left(1+i\mathbf{k}\cdot\mathbf{r}_i+\frac{1}{2}(i\mathbf{k}\cdot\mathbf{r}_i)^2+\cdots\right)\\&=i\mathbf{k}\cdot\sum_{i=1}^{N}\mathbf{r}_i\left(1+\frac{1}{2}i\mathbf{k}\cdot\mathbf{r}_i+\cdots\right)\mathbf{F}_i^{\phi}\\&=i\mathbf{k}\cdot\sum_{i=1}^{N}\mathbf{r}_i\mathbf{F}_i^{\phi}+O(k^2)\end{aligned} \tag{2.15}$$

where we have used the fact that the sum of any type of internal force over the whole system is zero. Similarly, we can write

$$\sum_{i=1}^{N} \mathbf{F}_i^{\mathrm{C}} e^{i\mathbf{k}\cdot\mathbf{r}_i} = i\mathbf{k}\cdot\sum_{i=1}^{N} \mathbf{r}_i \mathbf{F}_i^{C} + O(k^2) \tag{2.16}$$

for the internal constraint forces (e.g. molecular bond length and bond angle constraint forces).

Now we consider the convective term in the momentum conservation equation. It is convenient to introduce the peculiar velocity here, by the definition

$$\mathbf{c}_i = \mathbf{v}_i - \mathbf{v}(\mathbf{r}_i) \tag{2.17}$$

where $\mathbf{v}_i$ is the velocity of particle i relative to the laboratory frame, $\mathbf{v}(\mathbf{r}_i)$ is the streaming velocity at the position of atom i and we will assume that the equations of motion ensure that the sum of the peculiar momenta remains equal to zero for all time, $\sum_{i=1}^{N} m_i \mathbf{c}_i = 0$. For flowing molecular fluids, the correct determination of the atomic peculiar velocity is a non-trivial exercise, because internal motions such as rotation may possess a systematic or streaming component. We will discuss this issue in more detail later.

The definition of the peculiar velocity allows us to write

$$\sum_{i=1}^{N} m_i \mathbf{v}_i \mathbf{v}_i e^{i\mathbf{k}\cdot\mathbf{r}_i} = \sum_{i=1}^{N} m_i [\mathbf{c}_i + \mathbf{v}(\mathbf{r}_i)][\mathbf{c}_i + \mathbf{v}(\mathbf{r}_i)] \times e^{i\mathbf{k}\cdot\mathbf{r}_i}. \tag{2.18}$$

If we assume that the streaming velocity is given as a function of position and time, substitute the microscopic expression for the momentum density into the convective term of the momentum balance equation and use the properties of the delta function when taking the Fourier transform, we can show that

$$\begin{aligned}
\widetilde{\rho\mathbf{v}\mathbf{v}}(\mathbf{k},t) &= F\{(\rho\mathbf{v})\mathbf{v}\} \\
&= F\left\{\left[\sum_{i=1}^{N} m_i \mathbf{v}_i \delta(\mathbf{r}-\mathbf{r}_i)\right]\mathbf{v}(\mathbf{r},t)\right\} \\
&= \sum_{i=1}^{N} m_i \mathbf{v}_i \mathbf{v}(\mathbf{r}_i,t) e^{i\mathbf{k}\cdot\mathbf{r}_i} \\
&= \sum_{i=1}^{N} m_i [\mathbf{c}_i + \mathbf{v}(\mathbf{r}_i,t)]\mathbf{v}(\mathbf{r}_i,t) e^{i\mathbf{k}\cdot\mathbf{r}_i} \\
&= \sum_{i=1}^{N} m_i [\mathbf{c}_i \mathbf{v}(\mathbf{r}_i,t) + \mathbf{v}(\mathbf{r}_i,t)\mathbf{v}(\mathbf{r}_i,t)] e^{i\mathbf{k}\cdot\mathbf{r}_i}
\end{aligned} \tag{2.19}$$

Similarly,

$$\begin{aligned}
\widetilde{\rho\mathbf{v}\mathbf{v}}(\mathbf{k},t) &= F\{\mathbf{v}(\rho\mathbf{v})\} \\
&= \sum_{i=1}^{N} m_i [\mathbf{v}(\mathbf{r}_i,t)\mathbf{c}_i + \mathbf{v}(\mathbf{r}_i,t)\mathbf{v}(\mathbf{r}_i,t)] e^{i\mathbf{k}\cdot\mathbf{r}_i}
\end{aligned} \tag{2.20}$$

and

$$\widetilde{\rho\mathbf{v}\mathbf{v}}(\mathbf{k},t) = F\{\rho(\mathbf{v}\mathbf{v})\} = \sum_{i=1}^{N} m_i \mathbf{v}(\mathbf{r}_i,t)\mathbf{v}(\mathbf{r}_i,t) e^{i\mathbf{k}\cdot\mathbf{r}_i} \tag{2.21}$$

giving

$$\sum_{i=1}^{N} m_i \mathbf{v}(\mathbf{r}_i,t)\mathbf{c}_i e^{i\mathbf{k}\cdot\mathbf{r}_i} = \sum_{i=1}^{N} m_i \mathbf{c}_i \mathbf{v}(\mathbf{r}_i,t) e^{i\mathbf{k}\cdot\mathbf{r}_i} = 0 \tag{2.22}$$

Combining these results and expanding the exponential to lowest order in wavevector, we obtain

$$\begin{aligned}
\sum_{i=1}^{N} m_i \mathbf{v}_i \mathbf{v}_i e^{i\mathbf{k}\cdot\mathbf{r}_i} &= i\mathbf{k}\cdot\sum_{i=1}^{N} m_i \mathbf{v}_i \mathbf{v}_i + O(k^2) \\
&= i\mathbf{k}\cdot\sum_{i=1}^{N} m_i [\mathbf{c}_i \mathbf{c}_i + \mathbf{v}(\mathbf{r}_i)\mathbf{v}(\mathbf{r}_i)] \\
&\quad + O(k^2)
\end{aligned} \tag{2.23}$$

Substituting these results into the momentum balance equation and collecting terms to first order in wavevector, we obtain

$$\begin{aligned}
i\mathbf{k}\cdot\tilde{\mathbf{P}}(\mathbf{k},t) &= \frac{\partial}{\partial t}[\widetilde{\rho\mathbf{v}}(\mathbf{k},t)] - i\mathbf{k}\cdot[\widetilde{\rho\mathbf{v}\mathbf{v}}(\mathbf{k},t)] - \widetilde{\rho\mathbf{F}^{\mathrm{ext}}}(\mathbf{k},t) \\
&= i\mathbf{k}\cdot\left(\sum_{i=1}^{N} m_i \mathbf{c}_i \mathbf{c}_i + \sum_{i=1}^{N} \mathbf{r}_i \mathbf{F}_i^{\phi} + \sum_{i=1}^{N} \mathbf{r}_i \mathbf{F}_i^{\mathrm{C}}\right) \\
&\quad + O(k^2)
\end{aligned} \tag{2.24}$$

In real space, this equation relates the divergence of the local, instantaneous pressure tensor to the divergence of a microscopic quantity. It also provides us with an expression, to within an arbitrary divergenceless quantity, for the zero wavevector pressure tensor itself,

$$\begin{aligned}
\tilde{\mathbf{P}}(\mathbf{k}=0,t) &= V\mathbf{P}(t) \\
&= \sum_{i=1}^{N} m_i \mathbf{c}_i \mathbf{c}_i + \sum_{i=1}^{N} \mathbf{r}_i \mathbf{F}_i^{\phi} + \sum_{i=1}^{N} \mathbf{r}_i \mathbf{F}_i^{\mathrm{C}}
\end{aligned} \tag{2.25}$$

where V is the system volume. The arbitrary divergenceless quantity is usually chosen to be equal to zero, as we have done here, giving a pressure tensor that is consistent with thermodynamics. Different choices of the divergenceless quantity that may be added to the pressure tensor are analogous to the choice of gauge in electrodynamics [8]. For a simple atomic fluid with two-body central forces between atoms and no internal constraint forces, the forces can be written as

$$\mathbf{F}_i^{\phi} = \sum_j \mathbf{F}_{ij}^{\phi} = -\sum_j \frac{\partial \phi(r_{ij})}{\partial \mathbf{r}_i} = \sum_j \frac{\partial \phi(r_{ij})}{\partial r_{ij}} \frac{\mathbf{r}_{ij}}{r_{ij}}$$

where $\mathbf{r}_{ij}$ is defined as $\mathbf{r}_{ij} = \mathbf{r}_j - \mathbf{r}_i$. Since $\mathbf{F}_{ij} = -\mathbf{F}_{ji}$, we then have the usual expression for the volume-averaged

instantaneous pressure tensor in a simple atomic fluid:

$$V\mathbf{P}(t) = \sum_{i=1}^{N} m_i \mathbf{c}_i \mathbf{c}_i - \frac{1}{2}\sum_{j\neq i}^{N}\sum_{i=1}^{N} \mathbf{r}_{ij}\mathbf{F}_{ij}^{\phi} \qquad (2.26)$$

If the derivation is carried out without making the small wavevector approximation, the expression for the wavevector dependent pressure tensor for a simple atomic fluid with only two-body central forces becomes

$$\mathbf{P}(\mathbf{k},t) = \sum_{i=1}^{N} m_i \mathbf{c}_i \mathbf{c}_i e^{i\mathbf{k}\cdot\mathbf{r}_i} - \frac{1}{2}\sum_{i=1}^{N}\sum_{j\neq i}^{N} \mathbf{r}_{ij}\mathbf{F}_{ij}\left(\frac{e^{i\mathbf{k}\cdot\mathbf{r}_{ij}}-1}{i\mathbf{k}\cdot\mathbf{r}_{ij}}\right)e^{i\mathbf{k}\cdot\mathbf{r}_i}, \qquad (2.27)$$

This expression must be used when non-zero wavevector components of the pressure tensor are evaluated, for example when we want to compute the wavevector dependent viscosity.

2.2 *Effect of periodic boundary conditions*

Let us now consider what effect periodic boundary conditions will have on the calculation of the pressure tensor. In the previous discussion, it has been assumed that the number of particles in the system and the volume are finite. Under these circumstances, it does not matter whether the potential part of the spatially averaged pressure tensor is computed using the expression

$$\mathbf{P}^{\phi}(t) = \frac{1}{V}\sum_{i=1}^{N1} \mathbf{r}_i \mathbf{F}_i^{\phi} \quad \text{or} \quad \mathbf{P}^{\phi}(t) = -\frac{1}{2V}\sum_{j\neq i}^{N}\sum_{i=1}^{N} \mathbf{r}_{ij}\mathbf{F}_{ij}^{\phi}.$$

However, under periodic boundary conditions, the total system volume is infinite. If we restrict the sum to particles within one periodic box, the volume is then finite, but the first expression will give incorrect results and the second is only correct if we use a special definition of the separation of a pair of interacting particles, i.e. the minimum image separation.

In computer simulations of homogeneous systems, we usually consider an infinite periodic system of particles constructed by replicating a set of particles in the primary simulation box over an infinite lattice. Once the initial positions and momenta have been allocated, each particle that is not in the primary box can be regarded as either a copy of a particle in the primary box, or as an independent particle with the same initial conditions and equations of motion. In principle, each primary particle should maintain its periodic relationship with every image of itself indefinitely. This is easily seen if we consider two different ways of solving the equations of motion. For simplicity, we will discuss a two-dimensional example, as illustrated in figure 1. Imagine that we start by positioning the particles on a lattice with four identical square unit cells in the primary simulation box. We make the

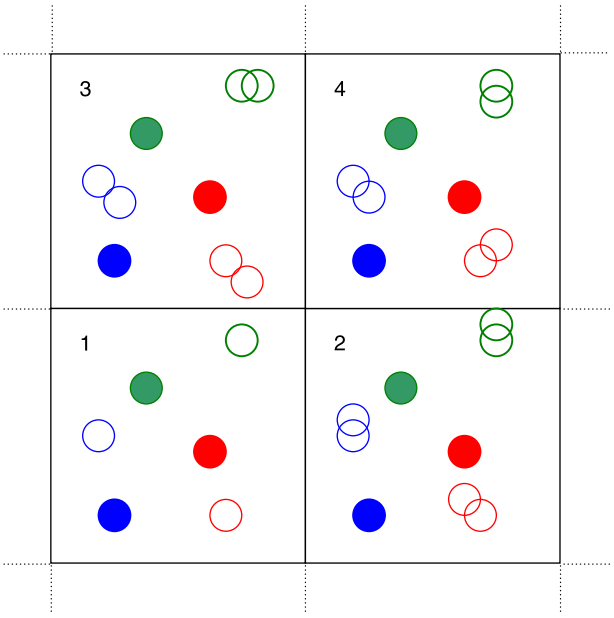

Figure 1. Filled circles represent the positions of particles and their periodic images at some time t_0. Unfilled circles represent the positions of the particles at some later time t. If box 1 is treated as the primary simulation box, and we solve the equations of motion numerically to obtain the positions of the particles at time t using periodic boundary conditions to determine the positions of the image particles in boxes 2–4, then the positions of the image particles at time t are given by the unfilled circles with full lines. If instead of this, a larger box consisting of boxes 1–4 is regarded as the primary simulation box and the equations of motion for all of the particles are solved numerically, then numerical error will result in a departure of particle trajectories from their exact periodic relationship indicated schematically by the circles with dashed lines. Only an exact analytical solution of the equations of motion would maintain the periodic relationships.

momentum of each image particle identical to that of the particle in the first cell, so that the simulation box contains four identical periodic copies of each particle, one in each cell. One way of solving the equations of motion would be to compute the new positions and momenta by explicitly solving the equations of motion for all particles in a primary simulation box consisting of all four unit cells and applying periodic boundary conditions to particles outside this box. The second is to only compute the positions and momenta of the particles in one of the unit cells (treating this unit cell as the primary simulation box), and apply periodic boundary conditions to particles outside this smaller box. If the solution of the equations of motion were perfect, both methods would give the same particle trajectories. In practice, at long times, the trajectories of the two systems would eventually diverge, due to numerical and discretization error and Lyapunov instability. Thus, we see that periodic boundary conditions can be regarded as a way of imposing exact periodicity on the solutions of the equations of motion for image particles.

To derive the form of the pressure tensor in an infinite periodic system, we begin with an expression for the momentum density. The momentum density at an arbitrary point $\mathbf{r}$ in a system of N particles replicated with a spatial

period L in all directions to infinity is given by

$$\mathbf{J}(\mathbf{r},t)=\rho\mathbf{v}(\mathbf{r},t)=\sum_{\boldsymbol{\nu}=-\infty}^{\infty}\sum_{i=1}^{N}m_i\mathbf{v}_{i\boldsymbol{\nu}}\delta(\mathbf{r}-\mathbf{r}_{i\boldsymbol{\nu}}) \tag{2.28}$$

where the sum over the integer vector $\boldsymbol{\nu}$ is an abbreviated notation representing a triple sum, one over each Cartesian component. If we Fourier transform the momentum density, substitute into the momentum density continuity equation and proceed with the derivation as before (assuming that only simple pair forces are present), we find

$$\begin{aligned}\mathbf{P}(\mathbf{k},t)=&\sum_{\boldsymbol{\nu}=-\infty}^{\infty}\sum_{i=1}^{N}m_i\mathbf{c}_i\mathbf{c}_i\mathrm{e}^{i\mathbf{k}\cdot r_{i\boldsymbol{\nu}}}\\&-\frac{1}{2}\sum_{\boldsymbol{\nu}=-\infty}^{\infty}\sum_{i=1}^{N}\sum_{\boldsymbol{\mu}=-\infty}^{\infty}\sum_{j=1}^{N}\mathbf{r}_{i\boldsymbol{\nu}j\boldsymbol{\mu}}\mathbf{F}_{i\boldsymbol{\nu}j\boldsymbol{\mu}}\\&\times\left(\frac{\mathrm{e}^{i\mathbf{k}\cdot\mathbf{r}_{i\boldsymbol{\nu}j\boldsymbol{\mu}}}-1}{i\mathbf{k}\cdot\mathbf{r}_{i\boldsymbol{\nu}j\boldsymbol{\mu}}}\right)\mathrm{e}^{i\mathbf{k}\cdot\mathbf{r}_{i\boldsymbol{\nu}}}\end{aligned} \tag{2.29}$$

where $\mathbf{F}_{i\boldsymbol{\nu}}$ is the total force on image $\boldsymbol{\nu}$ of particle i and $\mathbf{F}_{i\boldsymbol{\nu}j\boldsymbol{\mu}}$ is the force on $i\boldsymbol{\nu}$ due to $j\boldsymbol{\mu}$ and periodicity of the peculiar momenta has been assumed.

The potential part of the pressure tensor contains a quadruple summation over all pairs of periodic images of every pair of particles, but if the force is short ranged, we can use the well-known minimum image convention to simplify the expression to a double summation over the number of particles N in one periodic box. This becomes possible when the force is zero for particles of separation greater than or equal to $L/2$, because no more than one image of a particle j can then interact with a given image of particle i. In other words, for each value of $\boldsymbol{\nu}$ the force between the relevant images of particles i and j can only be non-zero for one value of $\boldsymbol{\mu}$, such that $\mathbf{F}_{i\boldsymbol{\nu}j\boldsymbol{\mu}}=\mathbf{F}_{ij}$ for $\boldsymbol{\mu}-\boldsymbol{\nu}=\mathbf{m}_{ij}$ and $\mathbf{F}_{i\boldsymbol{\nu}j\boldsymbol{\mu}}=0$ otherwise. The separation of the interacting images of particles i and j is called the minimum image distance, and it is defined as

$$\mathbf{r}_{i\boldsymbol{\nu}j\boldsymbol{\mu}}=\mathbf{r}_j+\boldsymbol{\nu}L-\mathbf{r}_i-\boldsymbol{\mu}L=\mathbf{r}_{ij}+\mathbf{m}_{ij}L=\mathbf{d}_{ij} \tag{2.30}$$

Thus, the summation over $\boldsymbol{\mu}$ reduces to a single term for each value of $\boldsymbol{\nu}$ and the expression for the pressure tensor becomes

$$\begin{aligned}\mathbf{P}(\mathbf{k},t)=\sum_{\boldsymbol{\nu}=-\infty}^{\infty}\Bigg[&\sum_{i=1}^{N}m_i\mathbf{c}_i\mathbf{c}_i\mathrm{e}^{i\mathbf{k}\cdot\mathbf{r}_{i\boldsymbol{\nu}}}\\&-\frac{1}{2}\sum_{i=1}^{N}\sum_{j\neq i}^{N}\mathbf{d}_{ij}\mathbf{F}_{ij}g(i\mathbf{k}\cdot\mathbf{d}_{ij})\mathrm{e}^{i\mathbf{k}\cdot\mathbf{r}_{i\boldsymbol{\nu}}}\Bigg]\end{aligned} \tag{2.31}$$

where

$$g(i\mathbf{k}\cdot\mathbf{d}_{ij})=\frac{\mathrm{e}^{i\mathbf{k}\cdot\mathbf{d}_{ij}}-1}{i\mathbf{k}\cdot\mathbf{d}_{ij}} \tag{2.32}$$

If we now recall that $\mathbf{r}_{i\boldsymbol{\nu}}=\mathbf{r}_i+\boldsymbol{\nu}L$ and use the identity

$$\sum_{\boldsymbol{\nu}=-\infty}^{\infty}\mathrm{e}^{i\mathbf{k}\cdot\boldsymbol{\nu}L}=\frac{2\pi}{L^3}\sum_{\mathbf{n}=-\infty}^{\infty}\delta(\mathbf{k}-\mathbf{k}_\mathbf{n}) \tag{2.33}$$

where $\mathbf{k}_\mathbf{n}=2\pi\mathbf{n}/L$, and the components of the vector $\mathbf{n}$ are integers, we see that the periodicity of the particle coordinates results in a discrete set of wavevectors. Thus, the usual expression for the wavevector dependent pressure tensor must be replaced by

$$\begin{aligned}\mathbf{P}(\mathbf{k},t)=\frac{2\pi}{L^3}\sum_{\mathbf{n}=-\infty}^{\infty}\Bigg[&\sum_{i=1}^{N}m_i\mathbf{c}_i\mathbf{c}_i\mathrm{e}^{i\mathbf{k}\cdot\mathbf{r}_i}\\&-\frac{1}{2}\sum_{i=1}^{N}\sum_{j\neq i}^{N}\mathbf{d}_{ij}\mathbf{F}_{ij}g(i\mathbf{k}\cdot\mathbf{d}_{ij})\mathrm{e}^{i\mathbf{k}\cdot\mathbf{r}_i}\Bigg]\delta(\mathbf{k}-\mathbf{k}_\mathbf{n})\end{aligned} \tag{2.34}$$

A periodic function with a Fourier series representation given by

$$A(\mathbf{r},t)=\sum_{\boldsymbol{\nu}=-\infty}^{\infty}\sum_{i=1}^{N}A_i\delta(\mathbf{r}-\mathbf{r}_{i\boldsymbol{\nu}})=\sum_{\mathbf{n}=-\infty}^{\infty}A_\mathbf{n}\mathrm{e}^{-i\mathbf{k}_\mathbf{n}\cdot\mathbf{r}} \tag{2.35}$$

can be Fourier transformed, giving

$$\begin{aligned}A(\mathbf{k},t)&=F\left\{\sum_{\mathbf{n}=-\infty}^{\infty}A_\mathbf{n}\mathrm{e}^{-i\mathbf{k}_\mathbf{n}\cdot\mathbf{r}}\right\}\\&=2\pi\sum_{\mathbf{n}=-\infty}^{\infty}A_\mathbf{n}\delta(\mathbf{k}-\mathbf{k}_\mathbf{n})\end{aligned} \tag{2.36}$$

where the Fourier coefficients are given by

$$A_\mathbf{n}=\frac{1}{L^3}\sum_i A_i\mathrm{e}^{i\mathbf{k}_\mathbf{n}\cdot\mathbf{r}_i} \tag{2.37}$$

Comparing equations (2.34) and (2.36), we see that the nth Fourier coefficient of the pressure tensor is

$$\begin{aligned}\mathbf{P}_\mathbf{n}(t)=\frac{1}{L^3}\Bigg[&\sum_{i=1}^{N}m_i\mathbf{c}_i\mathbf{c}_i\mathrm{e}^{i\mathbf{k}_\mathbf{n}\cdot\mathbf{r}_i}\\&-\frac{1}{2}\sum_{i=1}^{N}\sum_{j\neq i}^{N}\mathbf{d}_{ij}\mathbf{F}_{ij}g(i\mathbf{k}_\mathbf{n}\cdot\mathbf{d}_{ij})\mathrm{e}^{i\mathbf{k}_\mathbf{n}\cdot\mathbf{r}_i}\Bigg]\end{aligned} \tag{2.38}$$

The pressure that we actually compute in molecular dynamics simulations of homogeneous systems with periodic boundary conditions and the minimum image convention is then clearly seen to be the zeroth Fourier coefficient of a Fourier series expansion

$$\begin{aligned}\mathbf{P}(t)&=\mathbf{P}_0(t)\\&=\frac{1}{L^3}\left[\sum_{i=1}^{N}m_i\mathbf{c}_i\mathbf{c}_i-\frac{1}{2}\sum_{i=1}^{N}\sum_{j\neq i}^{N}\mathbf{d}_{ij}\mathbf{F}_{ij}\right]\end{aligned} \tag{2.39}$$

3. Homogeneous NEMD: algorithms

3.1 Atomic fluids

3.1.1 SLLOD equations for generalized flows. The problem of simulating homogeneous flows driven by boundaries in real physical systems (e.g. Couette or elongational flows) is that a microscopic simulation explicitly including the walls invariably induces density inhomogeneities into the fluid. If one is interested in nano-confined flow, then this is an acceptable simulation strategy since spatial inhomogeneity needs to be explicitly included in the simulation. However, if one is concerned with computing bulk properties, such as viscosities or heat fluxes, far removed from surface effects, then explicit use of boundaries is unacceptable because they induce strong inhomogeneities that make the extraction of meaningful bulk phase transport coefficients extremely difficult, if not impossible.

An alternative to using "solid" wall boundaries is to drive a flow via a suitable implementation of periodic boundary conditions. The most useful to date of these is the so-called Lees–Edwards boundary conditions [9] for planar shear flow (PSF). In such a scheme a simulation cell is replicated in all directions by periodic images. Atoms interact via their interatomic potential forces under Newton's second law, but no other external forces are explicitly imposed on them through the equations of motion. Unlike the case for standard equilibrium MD, the periodic image cells are translated with respect to the simulation cell by an amount $\pm L_y \dot{\gamma} t$, where L_y is the length of the cell in the y-direction, $\dot{\gamma}$ is the strain rate and t is the simulation time (figure 2). This translation of atoms as they move from top to bottom (or vice-versa) is what, in time, induces a linear streaming velocity profile for low Reynolds number flows. However, this approach has two serious shortcomings: first, there is no connection with response theory, so links to the statistical mechanics of transport (e.g. the Green–Kubo expressions for shear viscosity) are not possible; and second, it takes time for the effects of translation of atoms between boundaries to communicate throughout the fluid, and is approximately the time taken for sound to travel through the simulation cell. This means that a linear streaming velocity will not be imposed immediately, but will evolve only after a sufficiently long time. More importantly, it implies that time-dependent transport properties can not be studied using such a boundary-driven method.

It was because of the above shortcomings that the first of the homogeneous NEMD algorithms was invented, namely that based on the DOLLS Hamiltonian, proposed by Hoover *et al.* [10]. In this approach the effect of a boundary that drives the flow is replaced by a fictitious external field. The field itself is designed to guarantee that the required streaming velocity profile is maintained indefinitely. The DOLLS Hamiltonian is written as

$$H_{\text{dolls}}(\mathbf{r}^N, \mathbf{p}^N, t) = \phi(\mathbf{r}^N) + \sum_i \frac{\mathbf{p}_i^2}{2m_i} + \sum_i \mathbf{r}_i \cdot \nabla \mathbf{v} \cdot \mathbf{p}_i \Theta(t) \tag{3.1}$$

Here $\phi(\mathbf{r}^N)$ is the system potential energy due to interactions between all N atoms, $\mathbf{r}_i$ and $\mathbf{p}_i$ are the laboratory position and peculiar momentum of atom i, $\nabla \mathbf{v}$ is the gradient of the streaming velocity $\mathbf{v}$, and it is assumed that flow commences at time $t = 0$ ($\Theta(t)$ is the Heaviside step function). The peculiar momentum is just the thermal momentum relative to the streaming momentum of the fluid. This Hamiltonian generates the DOLLS equations of motion for the system,

$$\begin{aligned} \dot{\mathbf{r}}_i &= \frac{\mathbf{p}_i}{m_i} + \mathbf{r}_i \cdot \nabla \mathbf{v} \\ \dot{\mathbf{p}}_i &= \mathbf{F}_i^{\phi} - \nabla \mathbf{v} \cdot \mathbf{p}_i \end{aligned} \tag{3.2}$$

where $\mathbf{F}_i^{\phi}$ is the interatomic force on atom i due to all other atoms. Soon after the DOLLS equations of motion were proposed it was demonstrated by Evans and Morriss [11] that, while suitable for simulating flows in the linear response limit, they were unsuitable for generating physically realistic shear flow at higher field strengths. In fact, the errors in computed properties grow quadratically in strain rate and are clearly observable in the computed normal stress differences [12].

It was proposed by Evans and Morriss [12] and Ladd [13] (in the case of molecular fluids) that the correct set of equations could be written down as

$$\begin{aligned} \dot{\mathbf{r}}_i &= \frac{\mathbf{p}_i}{m_i} + \mathbf{r}_i \cdot \nabla \mathbf{v} \\ \dot{\mathbf{p}}_i &= \mathbf{F}_i^{\phi} - \mathbf{p}_i \cdot \nabla \mathbf{v} \end{aligned} \tag{3.3}$$

where now the only difference between equations (3.2) and (3.3) is that the last term in the DOLLS force equation is transposed, i.e. $\nabla \mathbf{v} \cdot \mathbf{p}_i \rightarrow \mathbf{p}_i \cdot \nabla \mathbf{v}$. Evans and Morriss [6], performed a number of definitive theoretical and simulation studies to prove that these equations of motion (which they termed "SLLOD" to indicate the transpose of DOLLS) did give the correct nonlinear response for shear flow. It was also clear that the SLLOD equations of motion could not be generated from a system Hamiltonian [14].

It is important to appreciate that the flow generated by the SLLOD algorithm is *not* driven by the boundaries of the simulation cell. The equations of motion and momentum conservation are sufficient to generate the correct velocity gradient. However, to prevent the periodic boundary conditions (pbcs) from interfering with particle trajectories the SLLOD equations of motion *must* be used in conjunction with suitably compatible pbcs. For PSF (often termed planar Couette flow (PCF) in the literature) a suitable pbc scheme is that proposed by Lees and Edwards [9]. Use of the SLLOD equations in conjunction with Lees–Edwards pbcs *guarantees* the generation of the desired velocity gradient for low Reynolds number flows. This is also true for planar elongational flows, except

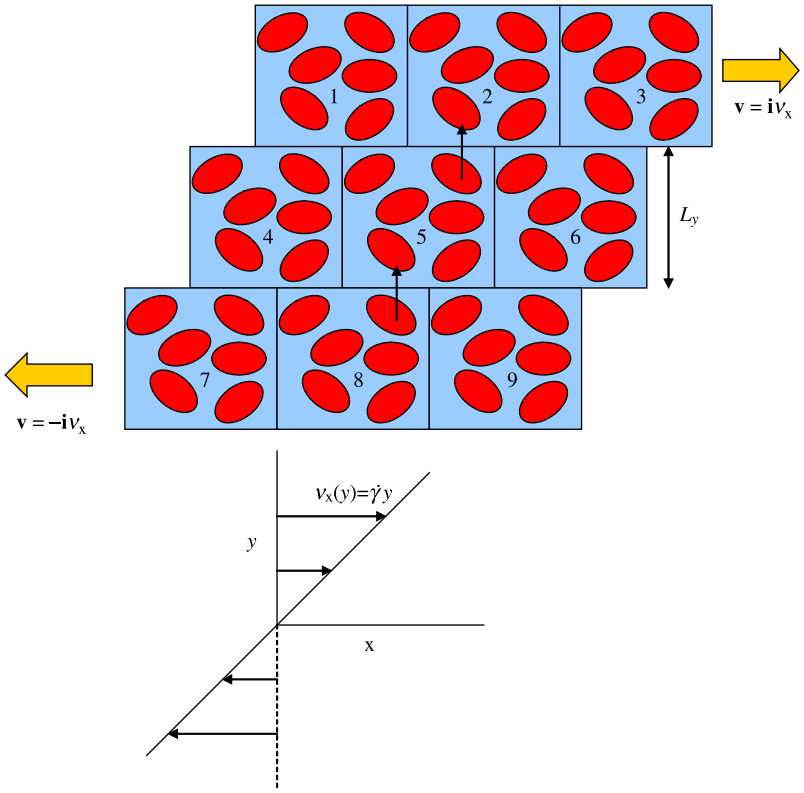

Figure 2. Representation in two dimensions of a simulation cell (cell number 5) surrounded by its periodic images (all other numbered image cells) undergoing PSF. The streaming velocity exists only in the x-direction and is linearly dependent on y, $\mathbf{v} = \mathbf{i}\dot{\gamma}y$. Image cells above and below the simulation cell are displaced by amounts $\pm L_y\dot{\gamma}t$. A molecule that moves out of the top of the simulation cell (from cell 5 into image cell 2) is displaced by an amount $-L_y\dot{\gamma}\Delta t$ (where Δt is the integration timestep) in the x-direction and $-L_y$ in the y-direction and is inserted into the bottom of the cell (from image cell 8 into cell 5). A similar but opposite translation occurs if a molecule moves out of the bottom of the simulation cell. Molecules that move out of the left or right faces are simply translated by $\pm L_x$, respectively, as is the case with usual equilibrium periodic boundary conditions.

now one must use the so-called Kraynik–Reinelt (KR) boundary conditions [15], suitably implemented for NEMD simulations [16–19]. Indeed it is true for *any* generalized homogeneous, divergenceless flow as long as suitably compatible boundary conditions are used [6]. The compatibility between equations of motion and boundary conditions is essential to ensure that the boundaries themselves do not perturb the system and hence invalidate the use of response theory.

The SLLOD algorithm thus succeeds in transforming a boundary driven flow into one that is driven solely by a fictitious external field. It has been demonstrated [6] that in fact SLLOD generates the correct nonlinear response for shear flow and is equivalent to a system with an initial local equilibrium distribution function, with a superposed linear streaming velocity profile, that is propagated in time with Newton's equations of motion [6,20,21]. Apart from the statistical mechanical rigor of the SLLOD equations of motion for both time-independent and time-dependent flows, they are also of great value because nonlinear response theory can be implemented (table 1). This has the practical benefit of allowing the extraction of transport properties under field strengths much weaker than can normally be used for direct averaging of NEMD fluxes via use of the transient-time correlation function formalism [6,22–30]. As previously indicated, boundary driven algorithms can not make use of response theory due to the absence of an appropriate mechanical driving force.

We have recently presented a simple, direct derivation of the SLLOD equations of motion for generalized homogeneous flows [14]. This derivation serves as a proof of the validity of the SLLOD algorithm for generalized flows (such as planar shear and elongational flows) and was performed partly in response to recent claims in the literature that SLLOD is incorrect for elongational flow [31–34]. Here we do not reproduce our derivation, but rather sketch the proof as follows. Interested readers can refer to the detailed derivation [14].

Noting that the time dependence of the zero-wavevector component of the momentum density is determined only by the sum of all external forces acting on a system of particles, one writes the equation of motion for the zero-wavevector component of the momentum density as

$$\frac{\mathrm{d}}{\mathrm{d}t}\sum_i m_i\mathbf{v}_i = \sum_i \mathbf{F}_i^{\mathrm{ext}} \tag{3.4}$$

where m_i is the mass of particle i, $\mathbf{v}_i$ is its laboratory frame velocity and $\mathbf{F}_i^{\mathrm{ext}}$ is the external force on particle i. One now defines the peculiar (thermal) velocity $\mathbf{c}_i$ for particle i to be

$$\mathbf{v}_i = \mathbf{c}_i + \mathbf{r}_i\cdot\nabla\mathbf{v}\Theta(t) \tag{3.5}$$

where we note that for a homogeneous velocity gradient the streaming velocity at any point in the fluid can be written as $\mathbf{v}(\mathbf{r}_i) = \mathbf{r}_i \cdot \nabla \mathbf{v}$. Substitution of equation (3.5) into equation (3.4) and requiring that the sum of the thermal momentum and its derivative are zero, i.e. $\sum_i m_i \mathbf{c}_i = 0, (\mathrm{d}/\mathrm{d}t)\sum_i m_i \mathbf{c}_i = 0$ gives

$$\sum_i \mathbf{F}_i^{\text{ext}} = \sum_i (m_i \mathbf{r}_i \cdot \nabla \mathbf{v} \cdot \nabla \mathbf{v} \Theta(t) + m_i \mathbf{r}_i \cdot \nabla \mathbf{v} \delta(t)) \tag{3.6}$$

Now if we assume that the external force is the same function of the particle positions for each particle, we have

$$\mathbf{F}_i^{\text{ext}} = g(\mathbf{r}_i) \tag{3.7}$$

or

$$\mathbf{F}_i^{\text{ext}} - g(\mathbf{r}_i) = 0 \tag{3.8}$$

for every particle. The external force acting on each particle to generate the correct zero-wavevector momentum density is therefore,

$$\mathbf{F}_i^{\text{ext}} = m_i \mathbf{r}_i \cdot \nabla \mathbf{v} \delta(t) + m_i \mathbf{r}_i \cdot \nabla \mathbf{v} \cdot \nabla \mathbf{v} \Theta(t) \tag{3.9}$$

Any zero-wavevector flow is thus generated by a sum of *two* components acting on every particle, *i*. The first is an impulse force at time $t = 0$ at the instant the field is switched on. The second term is zero before the application of the field and a constant multiplied by the particle's laboratory position at $t > 0$. For shear flow the second term is zero indicating that only the initial impulse is necessary for sustaining an indefinite zero-wavevector momentum current. For elongational flow the first and second terms are both non-zero. The fact that the second term is non-zero for *all* times (unlike the case for shear flow, in which a force exists only at $t = 0$ and is zero for all time afterwards) implies that elongation, unlike shear, involves an accelerating fluid streaming velocity. This will be made clearer shortly.

In order to obtain the SLLOD equations of motion we write Newton's equation of motion as

$$\mathbf{F}_i = m_i \frac{\mathrm{d}\mathbf{v}_i}{\mathrm{d}t} = \mathbf{F}_i^{\phi} + \mathbf{F}_i^{\text{ext}} \tag{3.10}$$

Equation (3.5), which expresses the total velocity as a sum of thermal and streaming components, is just the first line of the SLLOD equations of motion, equation (3.3). Substitution of equation (3.5) into equation (3.10) and performing the necessary algebra (noting that the external force $\mathbf{F}_i^{\text{ext}}$ is given by equation (3.9)) gives the equation of motion for the peculiar momenta (2nd line of equation (3.3))

$$m_i \dot{\mathbf{c}}_i = \mathbf{F}_i^{\phi} - m_i \mathbf{c}_i \cdot \nabla \mathbf{v} \Theta(t) \tag{3.11}$$

where we note that $\mathbf{p}_i \equiv m_i \mathbf{c}_i$. From this derivation it is immediately clear that the SLLOD equations of motion are equivalent to Newton's equations of motion including an external force. In actual NEMD simulations it is convenient to solve the two first order differential equations (equation (3.3)) rather than the second order differential equation implicit in equation (3.10) because positions and momenta are both obtained to the same order in time.

It is instructive at this point to demonstrate the compatibility of the SLLOD algorithm with periodic boundary conditions and homogeneity of the stress tensor. We do this by first writing down the momentum continuity equation, which is valid for any flow arbitrarily far from equilibrium,

$$\rho(\mathbf{r}, t) \frac{\mathrm{d}\mathbf{v}(\mathbf{r}, t)}{\mathrm{d}t} = -\nabla \cdot \mathbf{P}(\mathbf{r}, t) + \rho(\mathbf{r}, t) \mathbf{F}^{\text{ext}} \tag{3.12}$$

where ρ is the fluid density and $\mathbf{P}$ is the pressure tensor. For the case of homogeneous planar elongational flow, in which we have stretching in the *x*-direction, contraction in the *y*-direction, and no flow in *z*, we can express the components of the streaming velocity as

$$\mathbf{v}(\mathbf{r}, t) = \dot{\varepsilon}(x, -y, 0) \tag{3.13}$$

where $\dot{\varepsilon}$ is the elongation strain rate. The acceleration of the fluid at any point $\mathbf{r}$ and time t for this flow is thus

$$\begin{aligned} \frac{\mathrm{d}\mathbf{v}(\mathbf{r}, t)}{\mathrm{d}t} &= \dot{\varepsilon}(\dot{x}, -\dot{y}, 0) = \dot{\varepsilon}(v_x, -v_y, 0) \\ &= \dot{\varepsilon}^2(x, y, 0) \neq 0 \end{aligned} \tag{3.14}$$

Thus, from equation (3.12) it is clear that if there is no external force acting on the fluid then $\nabla \cdot \mathbf{P} \neq 0$. This contradicts the assumption of homogeneity. Therefore, homogeneous elongational flow can *only* be simulated with the inclusion of a non-zero external force.

In the case of shear flow, we have as the only non-zero flow velocity component

$$v_x(y) = \dot{\gamma} y \tag{3.15}$$

where $\dot{\gamma}$ is the shear strain rate, so

$$\mathbf{v}(\mathbf{r}, t) = (\dot{\gamma} y, 0, 0) \tag{3.16}$$

Therefore,

$$\frac{\mathrm{d}\mathbf{v}(\mathbf{r}, t)}{\mathrm{d}t} = (\dot{\gamma}\dot{y}, 0, 0) = (\dot{\gamma} v_y, 0, 0) = 0 \tag{3.17}$$

since $v_y = 0$. Thus, unlike elongational flow, there is *no* acceleration for shear flow anywhere in the fluid, which implies that it *can* be sustained in the zero-wavevector limit by an initial impulse at $t = 0$. This is just the realization of Newton's first law of motion at times $t > 0$ (at time $t = 0$, Newton's second law applies of course, as seen in equation (3.9)).

One could just as well drive such systems with Lees–Edwards (in the case of shear flow) or KR (in the case of planar elongational flow) boundary conditions and solve Newton's equations without an external driving field, which, as already discussed, will generate either steady shear or elongational flows. The disadvantage is that in the absence of appropriate terms in the equations of motion the application of either Lees–Edwards or KR boundary conditions lead to perturbations of the particle trajectories.

Since these perturbations do not appear in the equations of motion the link with response theory is lost. This link is vital because response theory is the only rigorous way of determining the validity of the equations of motion. For SLLOD dynamics, response theory has been proven to yield excellent comparisons with direct NEMD averaging for shear and elongation stresses [6,12,22–30,35].

3.1.2 Compatible periodic boundary conditions. In this section we cover the implementation of suitable periodic boundary conditions that are compatible with the SLLOD equations of motions for generalized homogeneous flows. There is one governing principle, which dictates how the boundaries must evolve in time, namely they must be compatible with the imposed streaming velocity profile. To see this clearly, we first write down the strain rate tensor as

$$\nabla \mathbf{v} = \begin{pmatrix} \frac{\partial v_x}{\partial x} & \frac{\partial v_y}{\partial x} & \frac{\partial v_z}{\partial x} \\ \frac{\partial v_x}{\partial y} & \frac{\partial v_y}{\partial y} & \frac{\partial v_z}{\partial y} \\ \frac{\partial v_x}{\partial z} & \frac{\partial v_y}{\partial z} & \frac{\partial v_z}{\partial z} \end{pmatrix} \tag{3.18}$$

The SLLOD equation of motion for particle velocities (equation (3.3)) is

$$\dot{\mathbf{r}}_i = \frac{\mathbf{p}_i}{m_i} + \mathbf{r}_i \cdot \nabla \mathbf{v} \tag{3.19}$$

This equation states that the total laboratory velocity (not the peculiar velocity, which is defined by the first line in equation (3.3)) is a superposition of the streaming velocity at particle i's position ($\mathbf{r}_i \cdot \nabla \mathbf{v}$) and the thermal velocity ($\mathbf{p}_i/m_i$) *relative* to the streaming velocity. The evolution of the boundaries (or indeed of any point not subject to thermal motion) is governed by the same equation of motion, except that there is no contribution to a thermal velocity for the boundaries, i.e.

$$\dot{\mathbf{L}}_k(t) = \mathbf{L}_k(t) \cdot \nabla \mathbf{v} \tag{3.20}$$

where $\mathbf{L}_k(t) = (L_{kx}(t), L_{ky}(t), L_{kz}(t))$ are the initially orthogonal set of primitive lattice vectors (cell or box vectors) that define the axes of the boundaries for $k = 1, 2, 3$, and we have explicitly included the time dependence for clarity (figure 3).

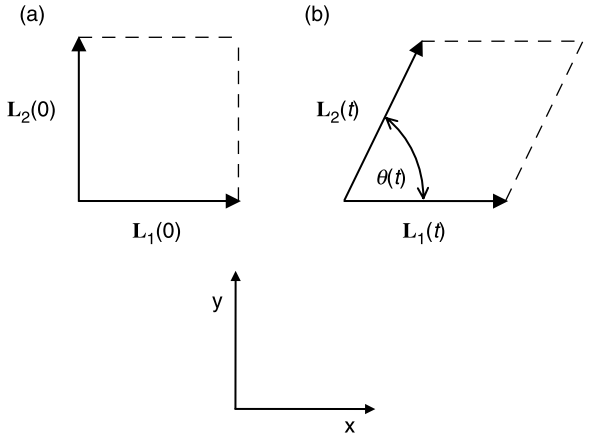

Figure 3. 2-dimensional representation of primitive cell lattice vectors, $\mathbf{L}_1$ and $\mathbf{L}_2$, (a) $t = 0$; (b) $t > 0$. As $t \to \infty$ it is clear that $\theta(t) \to 0$ and $|\mathbf{L}_2| \to \infty$, whereas $\mathbf{L}_1$ remains unchanged.

Thus the spatial evolution of the boundaries is solved by integrating equation (3.20).

3.1.2.1 Shear flow

For shear flow in which the fluid flows in the x-direction with a velocity gradient ($\dot{\gamma}$) in the y-direction (figure 2), this reduces to

$$\begin{aligned} \mathrm{d}L_{kx}(t) &= L_{ky}(t)\dot{\gamma}\mathrm{d}t \\ \mathrm{d}L_{ky}(t) &= 0 \\ \mathrm{d}L_{kz}(t) &= 0 \end{aligned} \tag{3.21}$$

The second and third lines in equation (3.21) imply that the box vectors in the y and z directions do not change in time, i.e. $L_{ky}(t) = L_{ky}(t = 0) \equiv L_{ky}$ (similarly for L_{kz}). For a simulation of length t_s (starting from $t = 0$), we find that the boundaries of the simulation box in the x-direction grow and are displaced linearly in time as

$$L_{kx}(t_s) = L_{ky}\dot{\gamma}t_s \tag{3.22}$$

This evolution of L_{kx} is depicted in figure 3, in which the two initially orthogonal vectors are depicted as $\mathbf{L}_1$ and $\mathbf{L}_2$. In this figure it is seen that an initially square simulation box (drawn in two-dimensions but equally valid arguments apply for a three-dimensional cube) is deformed in the x-direction (figure 3(b)). If atoms leave the left/right faces of the box, they are returned into the box through the right/left faces. If they move through the top/bottom faces, they are returned to the bottom/top faces, but displaced in the x-direction by an amount $\mp L_{2y}\dot{\gamma}\Delta t$, where Δt is the simulation timestep. If $\mathbf{L}_1$ is parallel to the x-axis at $t = 0$, it is clear from equation (3.21) that $\mathbf{L}_1$ is the same for all times afterwards. Since $\mathbf{L}_2$ is orthogonal to $\mathbf{L}_1$ at $t = 0$ (hence parallel to the y-axis at $t = 0$), equation (3.21) tells us that it will evolve for $t > 0$. Denoting $\theta(t)$ as the angle between $\mathbf{L}_1$ and $\mathbf{L}_2$, then simple geometry gives $\theta(t_s) = \arctan(1/\dot{\gamma}t_s)$. Clearly the situation becomes untenable as $t \to \infty$ because $\theta(t) \to 0$ and $|\mathbf{L}_2|$, (i.e. L_{2x}) $\to \infty$. Computationally this is very inefficient as one deals with bigger and bigger numbers in the implementation of the equations of motion, in which the $\mathbf{r}_i$ can now become very large in magnitude, even though the $\mathbf{p}_i$ do not. Fortunately there are two simple geometrical operations that save the simulator from this problem. These two operations can be implemented in two different but equivalent algorithms for the application of periodic boundary conditions. The first of these is to let the simulation box deform until it reaches some angle, $\theta(t)$, at which time the box is transformed back into the original square (cubic) shape. In this way transformations occur relatively infrequently and box side lengths do not get too large. An implementation of this algorithm has been performed for $\theta(t) = \pi/4$, and a slight modification allows the box to be transformed back to an initial angle of $-\pi/4$, thus halving again the number of transformations [36]. The second, equivalent, method is to just use the Lees–Edwards "sliding brick" implementation of pbcs. As already discussed, image boxes above and below the

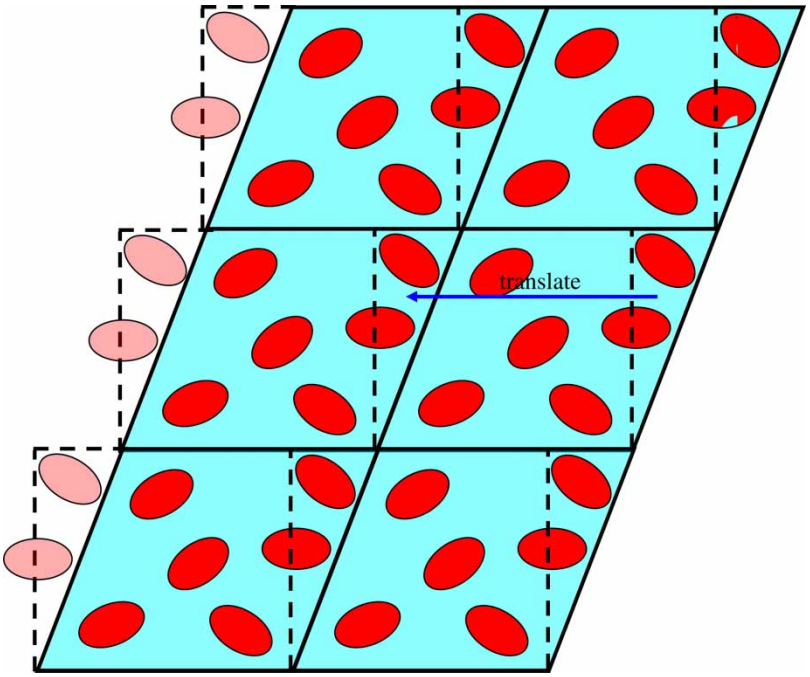

Figure 4. Equivalence of Lagrangian-rhomboid (LR) and sliding-brick (SB) periodic boundary conditions. SB boundaries are constructed from LR boundaries by slicing the triangular regions shown and translating by L_x to create cubes. Stacking LR cells or SB cells on top of each other results in two systems that are entirely equivalent, in that the relative distances between all molecules remains the same. Hence all thermodynamic properties are also equivalent for both systems.

simulation box are displaced relative to it by $\mp L_{2y}\dot{\gamma}\Delta t$, respectively. The equivalence of both schemes is depicted in figure 4. Both schemes are similarly efficient computationally, though the former is more useful for implementation in parallel computing environments [36,37]. It is of note that both schemes are actually non-autonomous in nature, i.e. the boundary conditions are explicitly time dependent. For sufficiently large systems this time dependence is in fact unnoticeable and poses no problem in the computation of time independent properties of thermodynamic systems far from equilibrium.

3.1.2.2 Elongational flow

An analogous scheme for the implementation of non-autonomous pbcs for elongational flow exists and is based upon the so-called KR boundary conditions. Kraynik and Reinelt [15], demonstrated that several types of lattice structures are reproducible under planar extensional flow. One such structure is the cubic lattice. Todd and Daivis [17] and, independently, Baranyai and Cummings [16], showed that this reproducibility can be successfully utilized as periodic boundary conditions for NEMD simulations of indefinite planar elongational flow. In a later paper Todd and Daivis [18], developed an efficient scheme of pbcs that is analogous to both the sliding brick and deforming box schemes used for shear.

A typical simulation box for implementation with KR pbcs is shown in figure 5. While the primitive lattice vectors $\mathbf{L}_1$ and $\mathbf{L}_2$ are again orthogonal, they are now no longer parallel to the x- and y-axes, which themselves are defined as the directions of expansion and contraction, respectively. For planar elongation under this geometrical configuration, the strain rate tensor (equation (3.18)) reduces to

$$\nabla\mathbf{v} = \begin{pmatrix} \dot{\varepsilon} & 0 & 0 \\ 0 & -\dot{\varepsilon} & 0 \\ 0 & 0 & 0 \end{pmatrix} \tag{3.23}$$

Equation (3.20), therefore, becomes

$$\begin{aligned} \mathrm{d}L_{kx}(t) &= L_{kx}(t)\dot{\varepsilon}\mathrm{d}t \\ \mathrm{d}L_{ky}(t) &= -L_{ky}(t)\dot{\varepsilon}\mathrm{d}t \\ \mathrm{d}L_{kz}(t) &= 0 \end{aligned} \tag{3.24}$$

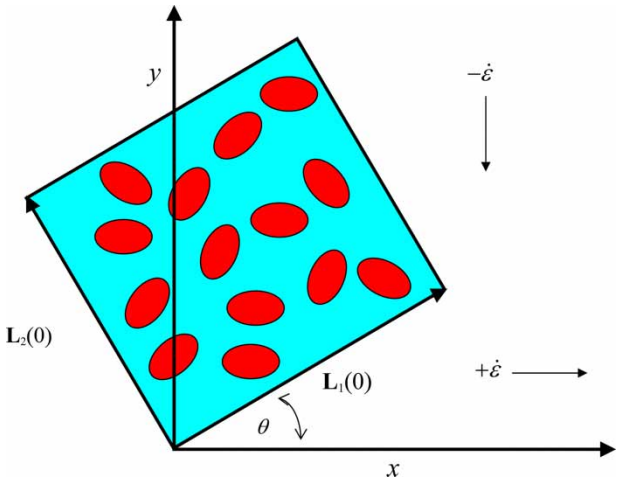

Figure 5. Initial orientation of a simulation cell utilizing KR boundary conditions [15,17,18]. The x- and y-axes define the directions of expansion and contraction, respectively, with an elongational strain rate $\dot{\varepsilon}$. The simulation cell is oriented at an angle θ with respect to the x-axis.

which, when solved, leads to the exponentially growing/contracting evolution of lattice vectors for planar elongation,

$$\begin{aligned} L_{kx}(t) &= L_{kx}(0)\exp(\dot{\varepsilon}t) \\ L_{ky}(t) &= L_{ky}(0)\exp(-\dot{\varepsilon}t) \\ L_{kz}(t) &= L_{kz}(0) \end{aligned} \tag{3.25}$$

The simulation box thus deforms (stretching in x and contracting in y) until such time that the total strain equals the periodic strain amplitude, ε_p, and the box is mapped back into the original shape, as depicted in figure 6. This mapping preserves all relative distances and ensures there are no discontinuities in computed thermodynamic properties. The derivation of the KR scheme is quite involved and not intuitive. A far more intuitive approach was taken by Hunt and Todd [38], in which the equivalence of the KR scheme and the famous Arnold cat map of dynamical systems theory was demonstrated. The cat map derivation is far simpler and easier to understand, and readers are referred to references [38,39] for further details. Figure 6 depicts this mapping scheme.

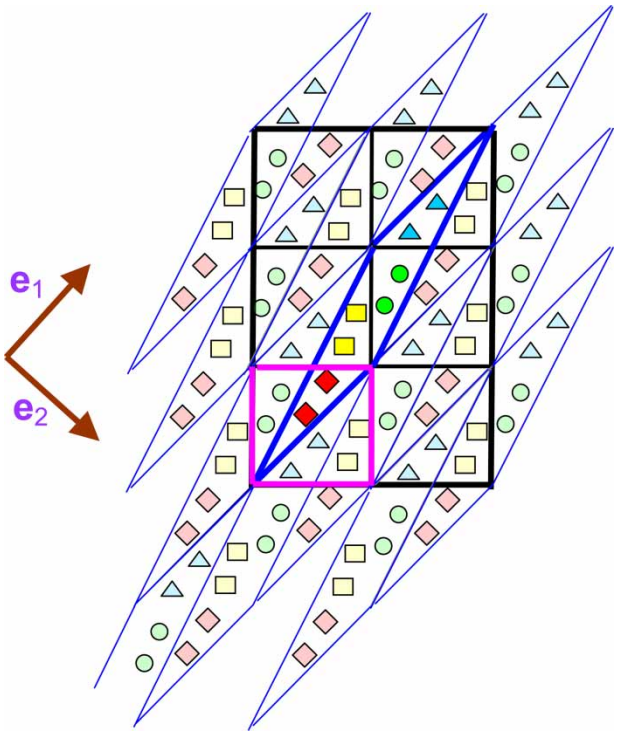

Figure 6. Schematic representation of the KR (or equivalently, the Arnold cat map) simulation cell and periodic boundary conditions. At $t = 0$ the simulation cell is square (the bottom left box, depicted in cyan colour). An elongation field is applied for $t \geq 0$, with direction and magnitude given by the eigenvectors $\mathbf{e}_1$ (direction of expansion, x-axis) and $\mathbf{e}_2$ (direction of compression, y-axis). As time progresses the square box deforms into a parallelogram. At a time corresponding to a strain given by $\varepsilon = \varepsilon_p$ (the Hencky strain amplitude, or equivalently in the cat map scheme, the positive Lyapunov exponent of the mapping operation) the cell is stretched to its maximum extent, depicted by the thick blue boundaries. At this time the cell is mapped back onto the original square, and all molecules are likewise mapped back onto the square. The mapping preserves all relative distances between molecules (each molecule is depicted by coloured shapes). Thus, the system of parallelogram KR/cat map cell and its replicated periodic images (depicted by thin blue boundaries and semi-transparent molecules) is identical to the system of the mapped square cell and its replicated periodic images (depicted by thick black boundaries and exactly the same semi-transparent molecules). The parallelograms and squares and their associated molecules extend infinitely in space, though only a few are drawn for the purposes of illustration (colour in online version).

The implementation of pbcs in the reference frame shown in figure 6 is not efficient. Efficiency can be improved significantly by performing a rotation of the simulation box about the origin and performing all necessary pbc operations (computation of minimum image distances and translation of particles as they cross boundaries) in the rotated frame. It is important to appreciate that no particle dynamics takes place in this rotated frame, only pbc operations that are dynamics-independent. Once pbc operations are performed, the box is rotated back to its original orientation and the simulation continues for the next time-step, and so on indefinitely. This scheme is illustrated in figure 7.

Let $\mathbf{r}_i$ be the position vector of atom i at time t in the simulation box and $\mathbf{r}'_i$ be its rotated (transformed) position vector. $\mathbf{r}'_i$ and $\mathbf{r}_i$ are related to each other via a transformation matrix $\mathbf{M}(t)$ such that

$$\mathbf{r}'_i = \mathbf{M}(t)\mathbf{r}_i \tag{3.26}$$

where the transformation matrix is

$$\mathbf{M}(t) = \begin{pmatrix} \cos\phi(t) & \sin\phi(t) & 0 \\ -\sin\phi(t) & \cos\phi(t) & 0 \\ 0 & 0 & 0 \end{pmatrix} \tag{3.27}$$

and $\phi(t)$ is the angle between $\mathbf{L}_1$ and the x-axis. After minimum image distances and pbcs are applied in the rotated frame the periodically imaged particles $P(\mathbf{r}_i)$ are inverse-rotated back into the original simulation frame

$$P(\mathbf{r}_i) = \mathbf{M}^{-1}(t)P'(\mathbf{r}'_i) \tag{3.28}$$

where

$$\mathbf{M}^{-1}(t) = \begin{pmatrix} \cos\phi(t) & -\sin\phi(t) & 0 \\ \sin\phi(t) & \cos\phi(t) & 0 \\ 0 & 0 & 0 \end{pmatrix} \tag{3.29}$$

and $P'(\mathbf{r}'_i)$ is the periodically imaged particle i in the $\mathbf{r}'$ frame. Once again dynamics are applied, where now the time has advanced to $t + \Delta t$, and the procedure is repeated. It is simple to show that the angle ϕ evolves as

$$\begin{aligned} \phi(t) &= \arctan(L_{1y}(t)/L_{1x}(t)) \\ &= \arctan(L_{1y}(0)/L_{1x}(0))\exp(-2\dot{\varepsilon}t) \end{aligned} \tag{3.30}$$

However, once the strain is equivalent to ε_p the entire simulation box is mapped back into the original shape, i.e. $\mathbf{L}_k(nt_p) \rightarrow \mathbf{L}_k(0)$, where t_p is the time that corresponds to a strain of ε_p and n is a positive integer. ε_p is itself computed from the positive Lyapunov exponent [39] which, via the cat map formalism, is easily determined by solving the eigenvalue equation for the mapping operation [38]. It is

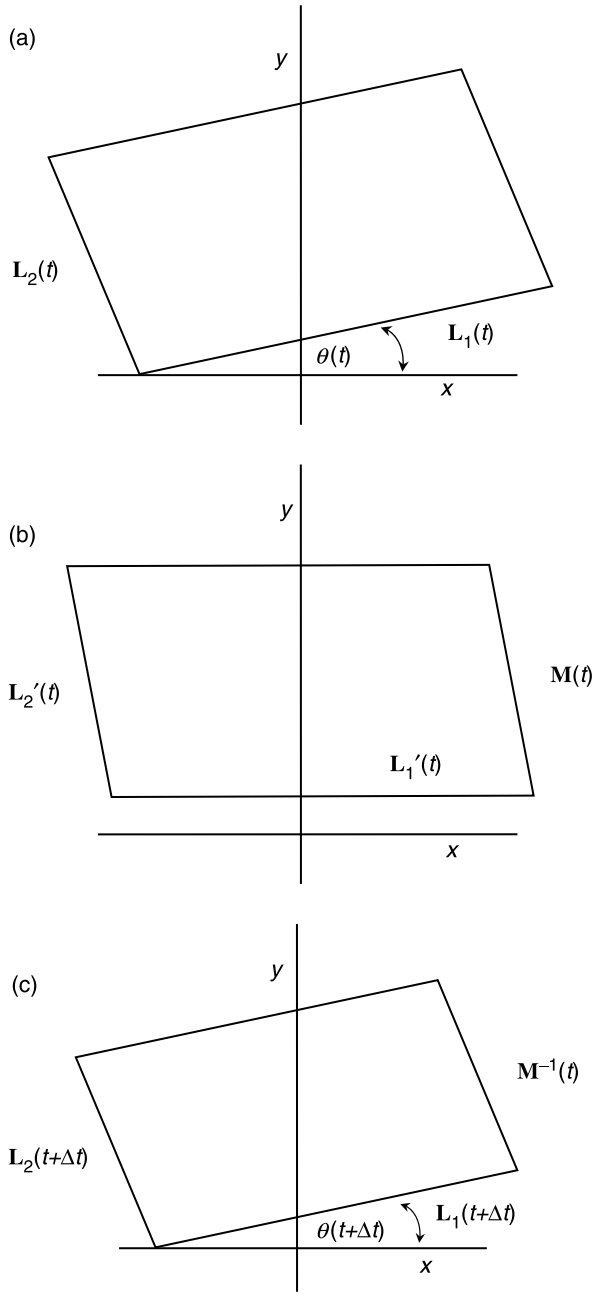

Figure 7. Schematic diagram for application of pbcs and minimum image distance computations for elongational flow. In (a) the simulation has been running for time t. The vectors $\mathbf{L}_1$ and $\mathbf{L}_2$ define the boundaries of the cell. Expansion occurs in the x-direction, contraction in the y-direction, and the cell is oriented at an angle $\theta(t)$ with respect to $\mathbf{L}_1$. (b) The cell is now rotated by $\theta(t)$ with respect to the x-axis, pbcs and minimum image distances are computed in this reference frame but no particle dynamics takes place. This is accomplished via the transformation operation $\mathbf{M}(t)$ given by equations (3.26) and (3.27). (c) Once pbcs and minimum image distances have been computed, the cell is rotated by $-\theta(t)$ back to the configuration in (a) and dynamics proceeds for an incremental timestep Δt. The inverse rotation is accomplished by the operation $\mathbf{M}^{-1}(t)$, given by equations (3.28) and (3.29). Steps (b) and (c) are then repeated on this new configuration, and so on until the end of the simulation. Note that at times corresponding to $t = n\tau_p$, where n is an integer, the fully extended KR cell is mapped back into the original square cell, as described in figure 6.

this mapping operation that allows for indefinite simulation times and is analogous to the mapping of a shear cell back into the original shape for any particular desired value of $\theta(t)$ (see section 3.1.2.1). Note that there are in principle an infinite number of initial orientations of the simulation cell (i.e. infinitely many possible $\phi(0)$), but in practice one chooses values of $\phi(0)$ that ensure the minimum extension of the simulation cell at $t = nt_p$ must be $\ll 2r_c$, where r_c is the interaction potential cut-off radius. This ensures that there is no violation of the minimum image convention.

As there are two equivalent schemes for implementation of pbcs in shear (sliding brick and deforming cube) so too are there two equivalent schemes for elongation [18]. These schemes are implemented in the rotated reference frame, and are shown in figure 8. In the deformed box (or Lagrangian rhomboid (LR)) scheme particles that move out of the left/right sides are translated back into the right/left sides by an amount $\pm L_{1x}'(t)$. Particles that move out of the top/bottom are imaged back into the bottom/top but displaced by $\pm L_{2x}'$ in the x-direction and $\mp L_{2y}'$ in the y-direction. Equivalently, the particles can move out of boundaries defined by the dashed lines in figure 8. In this case, known as the deforming brick (DB) scheme, the cell is a rectangular brick that deforms in time. The translation of particles in and out of box sides is treated in exactly the same way, except that it is slightly simpler because the box boundaries are parallel to the y-axis. The Fortran code for the implementation of both these schemes is given in our earlier work [18].

3.1.2.3 Periodic boundary conditions for arbitrary parallelepiped boxes

When we apply periodic boundary conditions to the particle position vectors $\mathbf{r}_i$ or to interparticle separation vectors to determine the minimum image separation of a pair of particles, it is convenient to use a method that applies generally, regardless of whether the flow is an elongational, shear, or bulk (isotropic) deformational flow. The method described here is a general method suitable for this purpose.

The essential idea behind this method is that we express the particle position as a linear combination of the box vectors $\mathbf{L}_1$, $\mathbf{L}_2$, and $\mathbf{L}_3$, which need not be orthogonal (figure 9):

$$\mathbf{r}_i = a_i\mathbf{L}_1 + b_i\mathbf{L}_2 + c_i\mathbf{L}_3 \tag{3.31}$$

The values of a_i, b_i, and c_i, will be real numbers and their fractional parts will be the coefficients of vectors $\mathbf{L}_1$, $\mathbf{L}_2$, and $\mathbf{L}_3$ that locate the image particle in the primary simulation box. The value of a_i is determined by finding the scalar product of both sides of equation (3.31) with a vector that is perpendicular to both $\mathbf{L}_2$, and $\mathbf{L}_3$, i.e.

$$\mathbf{r}_i\cdot\mathbf{L}_2\times\mathbf{L}_3 = a_i\mathbf{L}_1\cdot\mathbf{L}_2\times\mathbf{L}_3 \tag{3.32}$$

giving

$$a_i = \frac{\mathbf{r}_i\cdot\mathbf{L}_2\times\mathbf{L}_3}{\mathbf{L}_1\cdot\mathbf{L}_2\times\mathbf{L}_3} = \frac{\mathbf{r}_i\cdot\mathbf{L}_2\times\mathbf{L}_3}{V} \tag{3.33}$$

where it is assumed that the box vectors are defined in such a way that the volume $V = \mathbf{L}_1\cdot\mathbf{L}_2\times\mathbf{L}_3$ is positive.

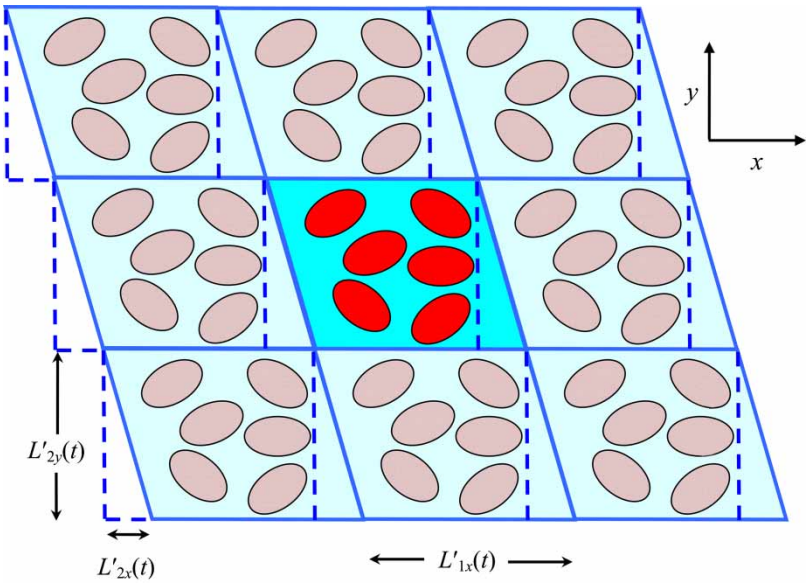

Figure 8. Schematic diagram of LR and DB periodic boundary conditions. The simulation cell is the central box with molecules, surrounded by an infinite number of periodic image cells. The LR boundaries are outlined in thick solid blue lines, whereas the DB boundaries are dashed. The equivalence of the two schemes is easily seen by cutting the triangular shaped region in the simulation cell, translating it by $-L'_{1x}(t)$ and then replicating the "brick" infinitely in space.

Similarly, we find that b_i, and c_i are given by

$$b_i = \frac{\mathbf{r}_i \cdot \mathbf{L}_3 \times \mathbf{L}_1}{\mathbf{L}_2 \cdot \mathbf{L}_3 \times \mathbf{L}_1} \quad c_i = \frac{\mathbf{r}_i \cdot \mathbf{L}_2 \times \mathbf{L}_3}{\mathbf{L}_3 \cdot \mathbf{L}_1 \times \mathbf{L}_2} \tag{3.34}$$

Thus, the position vector of the image of particle i that is located in the primary simulation box is given by

$$\mathbf{r}'_i = \mathbf{r}_i - [\text{nint}(a_i - 0.5)]\mathbf{L}_1 + [\text{nint}(b_i - 0.5)]\mathbf{L}_2 + [\text{nint}(c_i - 0.5)]\mathbf{L}_3 \tag{3.35}$$

where nint(x) represents the nearest integer to x.

3.1.3 Conservation of momentum for shear and elongational flows. The SLLOD equations of motion identically conserve the total peculiar momentum of the system under any generalized homogeneous flow. For shear flow, the governing force equation (from equation (3.3)) is

$$\begin{aligned} \dot{p}_{ix} &= F^{\phi}_{ix} - \dot{\gamma} p_{iy} \\ \dot{p}_{iy} &= F^{\phi}_{iy} \\ \dot{p}_{iz} &= F^{\phi}_{iz} \end{aligned} \tag{3.36}$$

Denoting $P_\alpha(t) \equiv \sum_i p_{\alpha i}$, where α is any of x, y, z, and noting by Newton's third law that $\sum_i F^{\phi}_{\alpha i} = 0$ (identically), we have

$$\begin{aligned} \dot{P}_x(t) &= -\dot{\gamma} P_y(t) \\ \dot{P}_y(t) &= 0 \\ \dot{P}_z(t) &= 0 \end{aligned} \tag{3.37}$$

The second and third equations above imply that $P_y(t) = P_y(0) = 0$ and $P_z(t) = P_z(0) = 0$, because the initial peculiar momenta are set to zero as demanded by SLLOD. This then implies that $P_x(t) = P_x(0) = 0$. This is the exact result for SLLOD and the result that would be achieved if computers had infinite numerical precision. However, in practice computers have only finite numerical precision which means that none of $P_\alpha(0)$ are identically zero. There is always some round off error, which means the values of $P_\alpha(0)$ are very small (depending on the floating point precision of the processing chip used) but non-zero. Therefore, assuming a small but non-zero $P_\alpha(0)$ we have from the first line of equation (3.37)

$$P_x(t) = P_x(0) - \dot{\gamma} P_y(0) t \tag{3.38}$$

Thus the numerical error in the total momentum in the x-direction grows linearly in time. Because $P_\alpha(0)$ is very small, and because the growth in the sum of momenta is

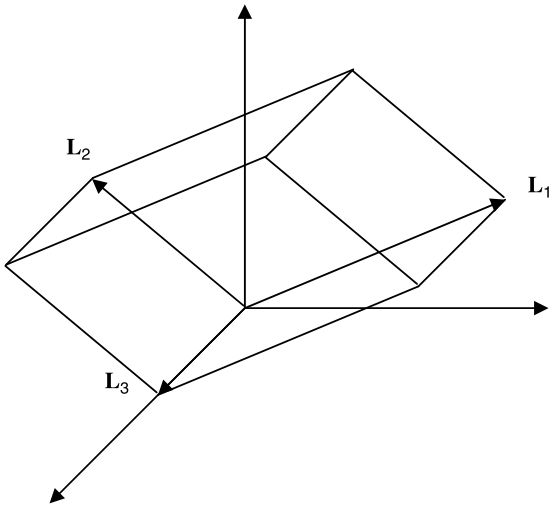

Figure 9. Simulation box constructed from non-orthogonal box vectors.

linear in time, in practice no NEMD simulation of planar shear has ever been significantly affected by lack of momentum conservation. One would need to run a calculation for trillions of timesteps before any problems could be detected. As an example, consider an NEMD simulation with $P_x(0) \sim P_y(0) \sim 10^{-12}$ (typically). If $\dot{\gamma} = 0.5$ and $\Delta t = 10^{-3}$ (all units are in reduced form) then it will take two hundred trillion (2×10^{14}) timesteps for $P_x(t)$ to reach a value of 0.1 where stability problems will be catastrophic. There has never been an NEMD simulation of this duration to date.

It is important to appreciate that this lack of conservation is not due to the SLLOD dynamics. It is solely a feature of finite precision numerics and is unavoidable. In fact, the analysis performed above is itself a simplification of the true picture. In practice one simulates NEMD systems not with adiabatic equations (as the currently written SLLOD equations are), but coupled with a thermostat to extract dissipated heat. Therefore, another term $-\alpha \mathbf{p}_i$ (where α is the thermostat multiplier, not to be confused with the Cartesian coordinate index α used above) is added on the right hand side of the second equation in equation (3.3), which makes such a simple analysis impossible (thermostats will be considered in greater detail in sections 3.1.4 and 3.2.5). Furthermore, again due to finite precision numerics, $\sum_i F_{i\alpha}^{\phi}$ is not identically zero. However, this tends to be a very small effect and can be fairly safely neglected in the above analysis [19].

Consider now the scenario for planar elongational flow. The governing adiabatic SLLOD equation is

$$\begin{aligned} \dot{p}_{ix} &= F_{ix}^{\phi} - \dot{\varepsilon} p_{ix} \\ \dot{p}_{iy} &= F_{iy}^{\phi} + \dot{\varepsilon} p_{iy} \\ \dot{p}_{iz} &= F_{iz}^{\phi} \end{aligned} \tag{3.39}$$

Using the same notation as above and assuming finite precision numerics we find

$$\begin{aligned} P_x(t) &= P_x(0) \exp(-\dot{\varepsilon} t) \\ P_y(t) &= P_y(0) \exp(\dot{\varepsilon} t) \\ P_z(t) &= P_z(0) \end{aligned} \tag{3.40}$$

Identically (i.e. with infinite numerical precision) we have $P_\alpha(t) = 0$, in which case momentum is again exactly conserved. But with finite precision numerics it is clear that errors in the total peculiar momentum will grow exponentially in the contracting direction. Because this growth is exponential it leads to problems in the system stability after only a few thousand timesteps, depending on the value of $\dot{\varepsilon}$. Following from the example of momentum non-conservation in shear flow above, consider now a comparable NEMD system under planar elongation. Again we have $P_y(0) \sim 10^{-12}$ and $\dot{\varepsilon} = 0.5$. Now to reach a value of $P_y(t) = 0.1$ only requires around 50,000 timesteps, where again $\Delta t = 10^{-3}$. This exponential growth was clearly reported and explained in reference [19]. Also shown in that work is $P_x(t)$, which is forced to converge to zero at all times. It is instructive also to observe that this numerical problem is intimately related to dynamical systems theory and chaos, and can in fact be directly related to the Arnold cat map which, as noted above, is equivalent to the KR scheme of boundary conditions but which gives greater physical insight into the nature of the flow [38,39].

Fortunately the solution to this numerical problem is quite simple. For example, for a single component atomic system, after the calculation of the momenta at each timestep one can subtract the average y-component of momentum from the y-momentum of each particle

$$p_{yi} \rightarrow p_{yi} - P_y(t)/N \tag{3.41}$$

This perturbation is very small and actually does not affect the particle dynamics in any meaningful way [40], but does guarantee that momentum is conserved at all times. Alternatively, one could apply either a constraint or proportional feedback [19].

Recently, it has been claimed [31] that this divergence in the total momentum for elongational flow is symptomatic of an inherent flaw in the SLLOD algorithm. By use of the g-SLLOD equations of motion these authors show that for elongational flow the momentum grows linearly in time, as it does with shear. They then claim that this is physically more realistic. We disagree, and our arguments are documented in some detail in a recent publication [14]. It is reasonable from the macroscopic nature of the flow (i.e. from the streamlines of the flow themselves) that numerical errors in elongational flow should evolve exponentially in time, whereas errors for shear flow evolve linearly. As shear involves linear streamlines there is no non-zero Lyapunov exponent associated with the mapping scheme for periodic boundary conditions (i.e. the macroscopic flow is not chaotic, even though the microscopic flow is [39]). That errors in total momenta grow linearly is one consequence of the non-chaotic nature of the macroscopic flow field. Elongation, on the other hand, has hyperbolic streamlines and non-zero Lyapunov exponents associated with the KR/cat-map mapping scheme, taking on values of $\pm\lambda$ [38–40], where $\lambda \in \mathbb{R}$. The macroscopic flow is, therefore, chaotic by definition and *must* involve the exponential divergence of neighbouring values of the total system momentum. Furthermore, the introduction of the additional term $-m_i \mathbf{r}_i \cdot \nabla \mathbf{v} \cdot \nabla \mathbf{v}$ into the force equation for g-SLLOD does not actually solve the so-called problem. It merely transforms an exponential growth of numerical errors into a linear growth of those same errors! If the simulation were run for long enough the same stability problems experienced in elongational flow under SLLOD dynamics would also be experienced for elongational flow under g-SLLOD dynamics (indeed, it would also be experienced for shear, where we note that SLLOD and g-SLLOD are equivalent for this flow geometry). The root of the problem remains unchanged, nor can it ever be changed without computers and algorithms that have infinite

numerical precision. A linear growth in numerical error is unphysical for elongational flow and incompatible with the requirements of a hyperbolic, accelerating, inherently chaotic streaming velocity profile.

3.1.4 Thermostats for atomic fluids. Work done by stresses will result in viscous heating. This is true whether the source of the work is an external field (such as is the case for SLLOD) or the boundaries (such as shear flow generated solely by moving boundaries, e.g. Lees–Edwards pbcs without the application of the SLLOD equations). As energy is dissipated in the system its temperature rises. To maintain the system at a thermodynamic steady-state this excess heat must be removed. This is normally accomplished by the use of appropriately formulated thermostats. Over the years various thermostats have been devised, but for NEMD systems the two most favoured are the Gaussian isokinetic thermostat [41] and the Nosé–Hoover thermostat [42–44]. Recently, the so-called configurational thermostat [45–50] has also been shown to be advantageous in certain circumstances. It has been shown that both Gaussian and Nosé–Hoover thermostats give identical steady-state averages of material properties [51,52] and have equivalent nonlinear responses [53]. It has also been demonstrated that material properties computed via artificially thermostatted systems undergoing SLLOD dynamics are identical to those computed in systems that attempt to more faithfully model nature. For example, Liem *et al.* [54] conducted a careful comparison between a homogeneous shearing system under SLLOD thermostatted dynamics and a wall-driven PSF system, in which a liquid was sandwiched between solid walls and the walls allowed to move with equal and opposite constant velocities. By keeping the confinement length large they were able to generate a system that was essentially homogeneous in the central part of the channel. Computations of viscosity and pressure at equivalent thermodynamic state points were in excellent agreement with corresponding values computed via SLLOD dynamics. Padilla and Toxvaerd also performed a similar study [55] in which thermostatted shear flow was investigated for atomic and molecular fluids. They concluded that shear rates should be sufficiently low so that the rate of production of viscous heat is not significantly greater than the characteristic rate of heat transport through the system. Indeed a similar conclusion was also reached by Liem *et al.* [54]. The conclusions reached by these studies demonstrate that as long as one is careful in the implementation of a suitably formulated thermostat and one is working within reasonable rates of energy dissipation, then the synthetic SLLOD algorithm can be trusted to provide accurate values for the transport properties of fluids that may not be currently possible to measure experimentally. In what follows we briefly review the Gaussian, Nosé–Hoover and configurational thermostats for atomic fluid systems and pay particular attention to their correct implementation. Molecular thermostats will be discussed later in section 3.2.5.

Thermodynamic constraints are nonholonomic by nature and non-integrable. Peculiar kinetic energy constraints are one type of nonholonomic constraint that can be used to fix the temperature of a system. In general, for a system under the influence of an external field and constrained by a Gaussian thermostat, the equations of motion can be written as

$$\begin{aligned}\dot{\mathbf{r}}_i &= \frac{\mathbf{p}_i}{m_i} + \mathbf{C}_i\cdot\mathbf{F}^{\text{ext}}(t)\\ \dot{\mathbf{p}}_i &= \mathbf{F}_i^{\phi} + \mathbf{D}_i\cdot\mathbf{F}^{\text{ext}}(t) - \alpha\mathbf{p}_i\end{aligned} \tag{3.42}$$

Here $\mathbf{C}_i$ and $\mathbf{D}_i$ are vector phase variables that express the coupling of the field to the system, $\mathbf{F}^{\text{ext}}(t)$ is an external generalized tensorial force, α is the thermostat multiplier and the other variables are as previously defined. The equation for the thermostat multiplier α can be straightforwardly derived from Gauss' principle of least constraint [6]. In doing so, it must be assumed that $\mathbf{p}_i$ are relative to the streaming velocity of the fluid (i.e. $\mathbf{p}_i \equiv m_i(\mathbf{v}_i - \mathbf{v}(\mathbf{r}_i))$, where $\mathbf{v}_i$ is the laboratory frame velocity of particle i and $\mathbf{v}(\mathbf{r}_i)$ is the fluid streaming velocity at $\mathbf{r}_i$), that the sum of these peculiar (i.e. thermal) momenta are identically zero (see the discussion in section 3.1.3 above) and that the total internal energy is given by the sum of the total peculiar kinetic energy and the total interatomic potential energy. The thermostat multiplier is in turn shown to be

$$\alpha = \frac{1}{\left(\sum_i \frac{\mathbf{p}_i^2}{m_i}\right)}\left[\sum_i \frac{\mathbf{p}_i}{m_i}\cdot\mathbf{F}_i^{\phi} + \sum_i \frac{\mathbf{p}_i}{m_i}\cdot\mathbf{D}_i\cdot\mathbf{F}^{\text{ext}}(t)\right] \tag{3.43}$$

In the case of the SLLOD equations of motion with no time dependence in the strain rate tensor equations (3.42) and (3.43), reduce to

$$\begin{aligned}\dot{\mathbf{r}}_i &= \frac{\mathbf{p}_i}{m_i} + \mathbf{r}_i\cdot\nabla\mathbf{v}\\ \dot{\mathbf{p}}_i &= \mathbf{F}_i^{\phi} + \mathbf{p}_i\cdot\nabla\mathbf{v} - \alpha\mathbf{p}_i\end{aligned} \tag{3.44}$$

and

$$\alpha = \frac{\sum_i \frac{\mathbf{p}_i}{m_i}\cdot\left(\mathbf{F}_i^{\phi} - \mathbf{p}_i.\nabla\mathbf{v}\right)}{\sum_i \frac{\mathbf{p}_i^2}{m_i}} \tag{3.45}$$

Note, however, that a time-dependent velocity gradient tensor $\nabla\mathbf{v}(t)$ is completely compatible with SLLOD and has in fact been used to study time-periodic shear [25–28,56,57] and elongational flows [30,58,59].

Equations (3.42) and (3.43) will keep the temperature fixed to its desired target value *instantaneously*. A more physically intuitive way of seeing this is to write the total peculiar kinetic energy ($\sum_i \mathbf{p}_i^2/2m_i$, which *defines* the

kinetic temperature as

$$T_K(t) \equiv \frac{1}{(\mathrm{d}N - N_\mathrm{c})k_\mathrm{B}} \sum_i \frac{\mathbf{p}_i^2}{m_i} \tag{3.46}$$

where d is the dimensionality of the system, N is the number of particles, N_c is the number of constraints on the system (including constraints for conserved quantities) and k_B is the Boltzmann constant. Taking the time derivative of this expression, substituting $\dot{\mathbf{p}}_i$ in the generalized equations of motion, equation (3.42), and setting the resulting expression equal to zero (since $\dot{T}_K(t) = 0, \forall t$) gives equation (3.43).

Gaussian constraints do suffer from one undesirable feature, namely that in the limit as $t \to \infty$ the constrained quantity (in this case the temperature) may drift away from its target value. This is true either at equilibrium or under non-equilibrium conditions. A solution to this problem is straightforward [60] and involves adding a proportional feedback term into the force equation (second equation in equation (3.42)) via a slightly modified thermostat multiplier, i.e.

$$\alpha \to \alpha + \alpha' \left[\frac{\left(\sum_i \mathbf{p}_i^2/m_i - (\mathrm{d}N - N_\mathrm{c})k_\mathrm{B}T \right)}{(\mathrm{d}N - N_\mathrm{c})k_\mathrm{B}T} \right] \tag{3.47}$$

where α is a weighting term chosen such that it is large enough to correct for numerical drift, but not too large so that the equations of motion do not become stiff. Typical values range between 0.1 and 10. The term in square brackets represents the proportion of deviation between the actual kinetic temperature and the desired target temperature T. If the kinetic temperature and target temperature are identical the second term in equation (3.47) is zero and no feedback is applied. If they are not the same (as is the case in practice), then the amount of feedback added into the constraint term is directly proportional to the deviation.

The Gaussian thermostat generates the so-called isokinetic ensemble. At equilibrium this ensemble is characterized by the distribution function

$$f_T(\mathbf{\Gamma}) = \frac{\exp\left[-\beta\phi(\mathbf{\Gamma})\right]\delta(K(\mathbf{\Gamma}) - K(\mathbf{\Gamma}_0))}{\int \mathrm{d}\mathbf{\Gamma} \exp[-\beta\phi(\mathbf{\Gamma})]\delta(K(\mathbf{\Gamma}) - K(\mathbf{\Gamma}_0))} \tag{3.48}$$

where $\beta = 1/k_\mathrm{B}T$, $\mathbf{\Gamma}$ is the phase-space variable ($\mathbf{\Gamma} = (\mathbf{r}_1, \mathbf{r}_2, \ldots, \mathbf{r}_N; \mathbf{p}_1, \mathbf{p}_2, \ldots, \mathbf{p}_N)$) and K is the kinetic energy. The streaming motion of a point in phase space is characterized by a non-zero time derivative $\mathrm{d}f_T/\mathrm{d}t$ and is associated with the compression of phase space. In the thermodynamic limit a system that evolves under the equilibrium equations of motion with a Gaussian thermostat will preserve an initial canonical distribution [6].

Bright *et al.* [61] show that there are an infinite number of ways of thermostatting a system, namely by fixing the sum of any of the momenta raised to an arbitrary power, i.e. $\sum_i |p_i|^{\mu+1} = c$, where c is a constant (see also Sarman *et al.* [62]). Interestingly, they find that only one unique value of μ, namely $\mu = 1$, minimizes the phase space compression. This value of μ corresponds to the traditional Gaussian isokinetic thermostat. It is also the only value of μ for which the conjugate pairing rule [63,64] remains valid. All other $\mu \neq 1$ thermostats actually perform work on the system and only a $\mu = 1$ thermostat allows for an equilibrium state. See also references [53] and [62] for related work.

In 1984 Nosé developed his now famous integral feedback thermostat and associated equations of motion [43,44] that preserve an initial canonical distribution for all time and for all system sizes. This approach was made more useful for simulations by Hoover [42], and the resulting thermostat has been known thereafter as the Nosé–Hoover thermostat. The form of the equations of motion is essentially the same as equation (3.42) except now the thermostat multiplier is not a simple function of positions and momenta (as is the case for Gaussian constraints) but instead is obtained by solving an additional equation of motion. For a system under the influence of an external field, the Nosé–Hoover equations of motion are thus

$$\begin{aligned} \dot{\mathbf{r}}_i &= \frac{\mathbf{p}_i}{m_i} + \mathbf{C}_i \cdot \mathbf{F}^\mathrm{ext}(t) \\ \dot{\mathbf{p}}_i &= \mathbf{F}_i^\phi + \mathbf{D}_i \cdot \mathbf{F}^\mathrm{ext}(t) - \zeta \mathbf{p}_i \\ \dot{\zeta} &= \frac{1}{Q}\left[\sum_i \frac{\mathbf{p}_i^2}{m_i} - N_f k_\mathrm{B} T \right] \end{aligned} \tag{3.49}$$

Here ζ is the Nosé–Hoover thermostat multiplier, and the target temperature T is related to the target kinetic energy K_0 by $T = 2K_0/N_f k_\mathrm{B}$, where N_f is the number of degrees of freedom. Q is a parameter associated with an additional degree of freedom coupled to an external heat reservoir and should be chosen to correctly determine the average kinetic energy and its fluctuations [65,66]. This additional degree of freedom is what essentially scales the particle velocities to the desired kinetic temperature. For the SLLOD equations of motion, $\mathbf{C}_i = \mathbf{r}_i$, $\mathbf{D}_i = \mathbf{p}_i$ and $\mathbf{F}^\mathrm{ext} = \nabla\mathbf{v}$. The field-free Nosé–Hoover equations of motion generate an equilibrium distribution that is canonical in the extended phase space

$$f_\mathrm{c}(\mathbf{\Gamma}, \zeta) = \frac{\exp\left[-\beta\left(U + \frac{1}{2}Q\zeta^2\right)\right]}{\int \mathrm{d}\mathbf{\Gamma}\, \mathrm{d}\zeta \exp\left[-\beta\left(U + \frac{1}{2}Q\zeta^2\right)\right]} \tag{3.50}$$

After Nosé's initial work it was shown that the Nosé–Hoover thermostat does not generate ergodicity in the system it is being applied to if the system is small or stiff [42,67]. While various attempts at resolving this issue have been attempted, the simplest and most workable solution was proposed by Martyna *et al.* [68]. In this formulation one imposes not one but a chain of thermostat variables. Thus the thermostat momenta are themselves thermostatted with thermostats, which are again thermostatted with thermostats, etc. until a chain of M thermostats is formed. The extended phase space (including both N particles plus M chains) is thus increased somewhat which allows greater accessibility of the available $\mathbf{\Gamma}$ phase space.

The method has been successfully applied to systems ranging from protein dynamics to Car-Parrinello systems. However, Holian *et al.* [66] have demonstrated that Nosé–Hoover chain (NHC) thermostats do not preserve the target temperature for systems far from equilibrium. Brańka [69] proposed a solution to this problem by slightly modifying the NHC equations of motion for the M thermostat multipliers. While the method fixes the problem with temperature control and does give values of phase variables (viscosities, pressures and autocorrelation functions) that agree with conventional Nosé–Hoover and Gaussian thermostats, the methodology as yet appears somewhat arbitrary and lacks a rigorous statistical mechanical basis. Brańka *et al.* [70] have proposed generalized Nose–Hoover (gNH) equations, which differ to the original equations in that the thermostat multiplier in the second line of equation (3.49) changes from ζ to ζ^{2n-1}, where n is an integer (corresponding to an additional factor of $1/n$ in the thermostat "kinetic energy" term of the extended system Hamiltonian). The gNH thermostat allows for enhancement of ergodicity for small and stiff systems, retains its canonical form and reproduces the target temperature for a system under SLLOD dynamics, but again the choice of introducing a system Hamiltonian with a $1/n$ term to scale the thermostat kinetic energy seems somewhat arbitrary.

Both the Gaussian and Nosé–Hoover thermostats are kinetic thermostats that are typically implemented to thermostat thermal momenta *relative* to the zero-wavevector momentum current. The most common application of these thermostats for NEMD simulations of homogeneous systems is under SLLOD dynamics, in which the thermostat *assumes* a linear streaming velocity profile. This is true for both shear ($\mathbf{v} = \mathbf{i}\dot{\gamma}y$) and elongational flows ($\mathbf{v} = \dot{\varepsilon}(\mathbf{i}x - \mathbf{j}y)$). For low shear rates and low Reynolds numbers this assumption is justified. For higher flow rates this assumption can no longer be trusted. For a system under PSF at high rates of strain the streaming velocity profile is no longer linear but rather develops an S-shaped profile. The thermostat, however, is designed in such a way that it interprets any deviations away from linearity as excess thermal energy. It therefore, tries to correct for this "deviation" by removing what it interprets as this excess thermal energy. This in turn forces the streaming velocity back to a linear profile, even though it should not by rights be linear! The end result of this is an enhanced ordering effect, in which the liquid structure (even for a simple atomic liquid) displays accentuated alignment with respect to the velocity streamlines. This effect was first observed by Erpenbeck [71] and was initially thought to be a new "string" phase of matter. However, this was soon demonstrated to be caused entirely by the thermostat [72,73].

Thermostats that assume a fixed, unchanging streaming velocity profile are termed *profile-biased thermostats* (PBT). They are the most widely used thermostats. However, in circumstances in which one cannot assume an unchanging streaming velocity profile (e.g. for high strain rates where secondary flows may exist, or inhomogeneous systems) such thermostats are entirely inappropriate. Under such conditions one should use equations of motion that make no assumption on the form of the streaming velocity profile. Thermostats with this characteristic are termed *profile-unbiased thermostats* (PUT). Both PBTs and PUTs can be formulated in either the Gaussian or Nosé–Hoover schemes.

One can in fact re-cast the SLLOD equations (or any other type of defining equations of motion) for a PUT. In the case of an atomic fluid these equations become

$$\dot{\mathbf{r}}_i = \mathbf{v}_i, \quad m_i\dot{\mathbf{v}}_i = \mathbf{F}_i - \alpha m_i(\mathbf{v}_i - \mathbf{v}(\mathbf{r}_i, t)) \tag{3.51}$$

where $\mathbf{F}_i$ is the total force on particle i, given as $\mathbf{F}_i = \mathbf{F}_i^{\phi} + \mathbf{F}_i^{\text{ext}}$. The streaming velocity must now be computed "on the fly" at each timestep. This can be done by using the definition of the momentum density

$$\mathbf{J}(\mathbf{r}, t) \equiv \rho(\mathbf{r}, t)\mathbf{v}(\mathbf{r}, t) \tag{3.52}$$

and therefore

$$\mathbf{v}(\mathbf{r}, t) = \frac{\langle \mathbf{J}(\mathbf{r}, t)\rangle}{\langle \rho(\mathbf{r}, t)\rangle} \tag{3.53}$$

The momentum density itself can be defined microscopically as

$$\rho(\mathbf{r}, t)\mathbf{v}(\mathbf{r}, t) = \mathbf{v}(\mathbf{r}, t)\sum_i m_i\delta(\mathbf{r}_i - \mathbf{r}) \tag{3.54}$$

where the mass density is given as $\rho(\mathbf{r}, t) = \sum_i m_i\delta(\mathbf{r}_i - \mathbf{r})$. Equation (3.54) can be equivalently expressed as

$$\rho(\mathbf{r}, t)\mathbf{v}(\mathbf{r}, t) = \sum_i m_i\mathbf{v}_i\delta(\mathbf{r}_i - \mathbf{r}) \tag{3.55}$$

Substitution of this latter form of the momentum density into equation (3.53) gives

$$\mathbf{v}(\mathbf{r}, t) = \frac{\left\langle \sum_i m_i\mathbf{v}_i\delta(\mathbf{r}_i - \mathbf{r})\right\rangle}{\left\langle \sum_i m_i\delta(\mathbf{r}_i - \mathbf{r})\right\rangle} \tag{3.56}$$

In practice one does not evaluate the delta functions in equation (3.56) but rather constructs bins of finite volume ΔV. Thus, equation (3.56) is more usefully expressed as

$$\mathbf{v}(\mathbf{r}_{\text{bin}}, t) = \frac{\left\langle \sum_{i\in\text{bin}} m_i\mathbf{v}_i\right\rangle}{\left\langle \sum_{i\in\text{bin}} m_i\right\rangle} \tag{3.57}$$

$\mathbf{r}_{\text{bin}}$ is a coarse-grained "position" centred at the location $\mathbf{r}_{\text{bin},0}$ with volume ΔV. Unless the streaming velocity is allowed to fluctuate in all directions, a partially biased thermostat is obtained and artifacts such as the string phase are observed [74,75]. Equations (3.52)–(3.57) could all be equivalently cast in terms of number density rather than mass density if all atoms have the same mass. The resulting streaming velocity profile is of course identical using either definition.

Once the streaming velocity is computed at any number of bins its value at *any* location $\mathbf{r}_i$ can be determined by least-squares fitting. Note now that least squares fitting itself requires the user to supply a functional form for the streaming velocity. This requires caution and some cross-checking to ensure that the assumed functional form for the streaming velocity does in fact accurately represent it. For example, in the case of high Reynolds number PSF, an S-shaped velocity profile could be fit by an odd polynomial of order n. The fit should then be compared directly with $\mathbf{v}(\mathbf{r}, t)$ computed in bins via equation (3.57).

It is instructive to write out equation (3.51) explicitly for planar shear and planar elongational flows. The general form for the SLLOD equations of motion *in the laboratory frame* is

$$\begin{aligned}\dot{\mathbf{r}}_i &= \mathbf{v}_i \\ m_i\dot{\mathbf{v}}_i &= \mathbf{F}_i^{\phi} + m_i\mathbf{r}_i\cdot\nabla\mathbf{v}\delta(t) \\ &\quad + m_i\mathbf{r}_i\cdot\nabla\mathbf{v}(\mathbf{r},t)\cdot\nabla\mathbf{v}(\mathbf{r},t)\Theta(t) - \alpha m_i(\mathbf{v}_i - \mathbf{v}(\mathbf{r}_i,t))\end{aligned} \tag{3.58}$$

For PSF the term $m_i\mathbf{r}_i\cdot\nabla\mathbf{v}(\mathbf{r},t)\cdot\nabla\mathbf{v}(\mathbf{r},t)$ is zero, so the equations reduce to

$$\begin{aligned}\dot{\mathbf{r}}_i &= \mathbf{v}_i \\ m_i\dot{\mathbf{v}}_i &= \mathbf{F}_i^{\phi} + m_i\mathbf{r}_i\cdot\nabla\mathbf{v}\delta(t) - \alpha m_i(\mathbf{v}_i - \mathbf{v}(\mathbf{r}_i,t))\end{aligned} \tag{3.59}$$

In the low Reynolds number flow regime where PBTs are valid, for times greater than zero this equation could be validly expressed as

$$\begin{aligned}\dot{\mathbf{r}}_i &= \mathbf{v}_i \\ m_i\dot{\mathbf{v}}_i &= \mathbf{F}_i^{\phi} - \alpha m_i(\mathbf{v}_i - \mathbf{i}\dot{\gamma}y_i)\end{aligned} \tag{3.60}$$

For planar elongation at times greater than zero, equation (3.58) becomes

$$\begin{aligned}\dot{\mathbf{r}}_i &= \mathbf{v}_i \\ m_i\dot{\mathbf{v}}_i &= \mathbf{F}_i^{\phi} + m_i\dot{\varepsilon}^2(\mathbf{i}x_i + \mathbf{j}y_i) \\ &\quad - \alpha m_i(\mathbf{v}_i - \mathbf{v}(\mathbf{r}_i,t))\end{aligned} \tag{3.61}$$

which again in the low Reynolds number regime can be accurately expressed as

$$\begin{aligned}\dot{\mathbf{r}}_i &= \mathbf{v}_i \\ m_i\dot{\mathbf{v}}_i &= \mathbf{F}_i^{\phi} + m_i\dot{\varepsilon}^2(\mathbf{i}x_i + \mathbf{j}y_i) \\ &\quad - \alpha m_i(\mathbf{v}_i - \dot{\varepsilon}[\mathbf{i}x_i - \mathbf{j}y_i])\end{aligned} \tag{3.62}$$

The second term for the forces in equation (3.62) represents the contribution from the external field that must exist for the SLLOD equations to drive a steady-state elongational flow (see discussion in section 3.1.1 and equation (3.9)). This term does not exist for shear flow because, as discussed in section 3.1.1, shear flow in an infinite system does not require an external force at $t > 0$ to sustain the flow. The only force exerted for shear flow is at $t = 0$, in which an initial impulse force is applied.

An examination of equations (3.58)–(3.62) reveals another important and subtle point. Consider the shear flow described by equation (3.59), and ask the question: what drives the flow at $t > 0$? Writing the SLLOD equations in this form (required for formulation with a PUT) seems to give the impression that nothing is driving the flow! This is because the streaming velocity only appears in the thermostat term but nowhere else, unlike the usual form of the SLLOD equations (equation (3.44)). If one were to write the adiabatic form of equation (3.60) then no thermostat term would exist and the equations would be nothing but Newton's equations with no external force at $t > 0$. How therefore, could a flow exist? However, in an actual simulation one first superposes an initial linear streaming velocity profile on all particle thermal velocities at $t = 0$ and demand that peculiar momentum is conserved. Equation (3.60) is nothing more than Newton's equations of motion at all times $t > 0$, with an additional thermostat constraint force. This is in complete harmony with the discussion in section 3.1.1, in which it was shown that the adiabatic SLLOD equations of motion for shear flow are equivalent to Newton's equations of motion. The initial impulse term in equation (3.59) is generated at $t = 0$ in a simulation by superposing the linear streaming velocity profile onto all particle thermal velocities. For all times $t > 0$ the flow velocity is self-sustaining (by Newton's equations of motion alone) and can be computed instantaneously as described above, and fed back into equation (3.59) as $\mathbf{v}(\mathbf{r}_i, t)$. It is only useful in that it allows for the computation of the thermal momenta (hence kinetic temperature, pressure tensor and heat flux vector) but in itself has no thermodynamic significance.

For elongational flow (equation (3.61)) it is clear that the initial superposition of linear velocity profiles in the x- and y-directions can not in itself sustain the flow indefinitely. In this case an additional force $m_i\mathbf{r}_i\cdot\nabla\mathbf{v}(\mathbf{r},t)\cdot\nabla\mathbf{v}(\mathbf{r},t)$ needs to exist at all times to sustain the flow for $t > 0$. The impulse term in equation (3.9) again manifests itself in an actual simulation as a superpositioning of linear streaming velocities in x and y onto the particles' thermal momenta. At times $t > 0$ the flow is sustained indefinitely by the additional external force $m_i\dot{\varepsilon}^2(\mathbf{i}x_i + \mathbf{j}y_i)$. Without it the flow would decay exponentially in time. This is again completely compatible with the discussion in section 3.1.1. These observations gleaned from re-casting the SLLOD equations in a form suitable for implementation with a PUT (i.e. cast in terms of laboratory momenta rather than the standard peculiar momenta) provide a useful perspective from which to critically examine the SLLOD equations and understand how they work. A convincing simulation study that demonstrates how SLLOD works for a system under planar shear has also recently been performed by Delhommelle *et al.* [76]. This study clearly shows that for planar shear SLLOD is equivalent to (a) superposing a linear streaming velocity profile onto canonically

(or isokinetically) distributed thermal momenta at $t = 0$, and (b) propagating this initial distribution forward in time by Newton's equations alone.

All the kinetic thermostats described above, as well as others not considered in this review, rely upon one crucial property: knowledge of an accurate streaming velocity profile. There are serious consequences if $\mathbf{v}(\mathbf{r}, t)$ is incorrectly assumed. The thermostat term in the force equation of motion itself can induce an additional perturbation in the system if $\mathbf{v}(\mathbf{r}, t)$ is incorrect. Evans and Morriss [73] have shown that in the case of shear flow under SLLOD dynamics coupled with a kinetic thermostat α, the momentum continuity equation has the form

$$\frac{\partial \mathbf{J}(\mathbf{r},t)}{\partial t} = -\nabla\cdot(\mathbf{P} + \rho(\mathbf{r},t)\mathbf{v}(\mathbf{r},t)\mathbf{v}(\mathbf{r},t)) - \frac{\alpha}{m}(\mathbf{J}(\mathbf{r},t) - \rho(\mathbf{r},t)\mathbf{v}_{\mathrm{PSF}}(\mathbf{r},t)) \tag{3.63}$$

where $\mathbf{J}(\mathbf{r}, t)$ is the momentum density, $\mathbf{P}(\mathbf{r}, t)$ is the pressure tensor, $\mathbf{v}_{\mathrm{PSF}}(\mathbf{r}, t)$ is the *assumed* linear streaming velocity for PSF and the analysis is performed with an atomic fluid of particles each of mass m. It is clear that only if the momentum density is identically $\mathbf{J}(\mathbf{r}, t) = \rho(\mathbf{r}, t)\mathbf{v}_{\mathrm{PSF}}(\mathbf{r}, t) = \mathbf{i}m\dot{\gamma}y\ \forall \mathbf{r}, t$ will the contribution to the stress due to the thermostat be identically zero at all times and all locations. If however $\mathbf{J}(\mathbf{r}, t) \neq \mathbf{i}m\dot{\gamma}y$ anywhere or at any time, then an additional stress will be induced in the system. This stress is purely artificial and undesirable. It has been seen to cause "string" phases in computer simulations of shear flow [71], which are an ordering of particles preferentially in the direction of the velocity streamlines at high rates of strain where a linear velocity profile can not be assumed. These strings were demonstrated to be artifacts by employing a suitably formulated PUT [73]. Similar problems, as well as some new ones, occur for molecular systems if the thermostatting is not handled correctly. These issues will be discussed later in sections 3.2.4 and 3.2.5.

Other types of thermostats have been devised over the years, but the Gaussian and Nosé–Hoover (both in their profile-biased and profile-unbiased forms) are the only kinetic thermostats that have found favour in NEMD simulations. However, recently the configurational thermostat (based on thermostatting the configurational temperature) has been a valuable inclusion. The configurational temperature (T_c) is determined only from the configurational component of the system's full phase-space, and is given as [45]

$$\frac{1}{k_B T_c} = \left\langle \frac{\sum_i \nabla_i^2 \phi}{\left|\sum_i \nabla_i \phi\right|^2} \right\rangle \tag{3.64}$$

for sufficiently large N. Because the system is thermostatted to a configurational quantity involving only particle positions but not momenta, the thermostat term now operates on the equation of motion that governs the evolution of particle positions and, for the SLLOD equations, can be written as [46]

$$\begin{aligned} \dot{\mathbf{r}}_i &= \frac{\mathbf{p}_i}{m_i} + \mathbf{r}_i\cdot\nabla\mathbf{v} + \frac{s}{T}\frac{\partial T_c}{\partial \mathbf{r}_i} \\ \dot{\mathbf{p}}_i &= \mathbf{F}_i^{\phi} + \mathbf{p}_i\cdot\nabla\mathbf{v} \\ \dot{s} &= -Q\frac{(T_c - T)}{T} \end{aligned} \tag{3.65}$$

Here T is the target temperature, s is an additional degree of freedom coupling the heat reservoir to the system and Q is a damping factor.

The above equations of motion are formulated with a Nosé–Hoover feedback scheme rather than a Gaussian formalism due to the relative simplicity of the former implementation and the complexity of the latter for this particular thermostat. The advantage of using a configurational thermostat for an NEMD system is that one does not need to worry about how to compute the streaming velocity profile. As the thermostat acts only on particle positions without reference to the streaming velocity, one can be assured of no artifacts such as string phases, etc. It also simplifies the coding by not requiring binned velocity profiles or least squares fits in the case of PUTs (see above). Detailed studies by Delhommelle, Evans and colleagues have addressed many of the advantages of using configurational thermostats for atomic and molecular systems under PSF, including the elimination of string phases, and readers are referred to these papers for further details [46,48,49,72,76–78].

A recent development in the formulation of configurational thermostats was made by Braga and Travis [79]. They have derived a new form of the configurational temperature thermostat also based on the Nosé–Hoover equations of motion. Their thermostat is an improvement on the one proposed by Delhommelle and Evans [46] in that it does not contain a term proportional to the spatial gradient of the temperature, which can lead to stiff equations of motion, and also because it generates the canonical ensemble. Their equations of motion for a system at equilibrium are

$$\begin{aligned} \dot{\mathbf{r}}_i &= \frac{\mathbf{p}_i}{m_i} - \zeta\frac{\partial \phi}{\partial \mathbf{r}_i} \\ \dot{\mathbf{p}}_i &= \mathbf{F}_i^{\phi} \\ \dot{\zeta} &= \frac{1}{Q_\zeta}\left[\sum_i \left(\frac{\partial \phi}{\partial \mathbf{r}_i}\right)^2 - k_B T \sum_i \frac{\partial^2 \phi}{\partial \mathbf{r}_i^2}\right] \end{aligned} \tag{3.66}$$

Their thermostat is shown to be more robust than that of Delhommelle and Evans and may be useful for systems involving large changes in temperature over small time scales, and possibly in NEMD simulations, though this has yet to be examined closely. They also demonstrate that the configurational thermostat is a special case of a general set of Nosé–Hoover equations developed by Kusnezov *et al.* [80]. Braga and Travis have also recently extended their method to the isobaric-isothermal ensemble [81].

The issue of exactly what a temperature is for systems far from equilibrium remains unresolved and so all thermostats, either kinetic or configurational, rely upon the standard thermodynamic (i.e. equilibrium) definition of temperature, i.e $1/T = (\partial S/\partial U)_V$.

3.1.5 Energy dissipation and other simulation ensembles. A number of alternative ensembles for NEMD computer simulation can be devised, such as isoenergetic, isothermal–isobaric, isobaric-isoenthalpic, constant stress, etc. Of these the two most useful ensembles for current applications are the isoenergetic and isothermal–isobaric ensembles, and we briefly discuss these in this section. For details on other ensembles see the book by Evans and Morriss [6].

One can generate a system under flow conditions at constant energy rather than constant temperature by applying an ergostat (rather than a thermostat) to the equations of motion. Running an NEMD simulation with an ergostat is useful in that it allows a check of energy conservation in much the same way as one should always check an equilibrium MD simulation for energy conservation. In order to devise an ergostat one first needs to consider the energy dissipation for a system undergoing SLLOD dynamics. For all forms of homogeneous flow (shear, elongation, etc) it is simple to show that the rate of energy dissipation for a thermostatted fluid is given by

$$\dot{U}(t) = -V\mathbf{P}^{\mathrm{T}}(t) : \nabla\mathbf{v} - \alpha\sum_i \frac{\mathbf{p}_i^2}{m_i} \tag{3.67}$$

To prove this, one writes the total system internal energy as $U(t) = \sum_i(\mathbf{p}_i^2/2m_i) + \sum_i \phi_i$, takes the time derivative and substitutes the equations of motion for the variables $\dot{\mathbf{r}}_i$ and $\dot{\mathbf{p}}_i$ (see for instance equation (3.101) for the adiabatic SLLOD equations). Here, $\mathbf{P}$ is the pressure tensor given as [7]

$$\mathbf{P}(t) = \frac{1}{V}\left[\sum_i \frac{\mathbf{p}_i(t)\mathbf{p}_i(t)}{m_i} - \frac{1}{2}\sum_{i,j}\mathbf{r}_{ij}(t)\mathbf{F}_{ij}(t)\right] \tag{3.68}$$

and V is the system volume. For an unthermostatted fluid the second term in equation (3.67) is zero and one obtains the expected thermodynamic result [5]. For PSF this is $\dot{U}^{\mathrm{ad}}(t) = -P_{yx}\dot{\gamma}V$ whereas for planar elongation it is $\dot{U}^{\mathrm{ad}}(t) = -(P_{xx} - P_{yy})\dot{\varepsilon}V$, where the superscript "*ad*" implies this is the adiabatic solution. For constant temperature simulations in the steady-state, the *average* rate of viscous heat dissipation is equal to the average rate of energy extraction by the thermostat, i.e.

$$\langle -V\mathbf{P}^{\mathrm{T}}(t) : \nabla\mathbf{v}\rangle = \left\langle \alpha\sum_i \frac{\mathbf{p}_i^2}{m_i}\right\rangle \tag{3.69}$$

This is very useful because one can compute the shear or elongational viscosities in two ways: firstly via the hydrodynamic constitutive relations

$$\eta_S = -\langle P_{yx}\rangle/\dot{\gamma} \tag{3.70}$$

for shear and

$$\eta_{\mathrm{E}} = -\langle P_{xx} - P_{yy}\rangle/4\dot{\varepsilon} \tag{3.71}$$

for planar elongation, and secondly by making use of the equivalence of viscous dissipation and extraction of dissipated heat by the thermostat in the steady-state (equation (3.69)). Substitution of equations (3.70) and (3.71) into equation (3.69) gives the second method of computing the viscosities as

$$\eta_{\mathrm{S}} = \frac{\left\langle \alpha\sum_i \frac{\mathbf{p}_i^2}{m_i}\right\rangle}{V\dot{\gamma}^2} \tag{3.72}$$

for shear and

$$\eta_{\mathrm{E}} = \frac{\left\langle \alpha\sum_i \frac{\mathbf{p}_i^2}{m_i}\right\rangle}{4V\dot{\varepsilon}^2} \tag{3.73}$$

for planar elongation.

Now, instead of keeping the temperature fixed at all times, let the internal energy be fixed instantaneously. In this case the left hand side of equation (3.67) is zero, which leads to the result

$$\alpha_U = -\frac{V\dot{\gamma}P_{yx}}{\sum_i \frac{\mathbf{p}_i^2}{m_i}} \tag{3.74}$$

for shear and

$$\alpha_U = -\frac{V\dot{\varepsilon}(P_{xx} - P_{yy})}{\sum_i \frac{\mathbf{p}_i^2}{m_i}} \tag{3.75}$$

for planar elongation, where now the subscript "U" indicates the multiplier is an ergostat that constrains the total system internal energy to be a constant of the motion (see also the discussion in section 3.2.4).

Equations (3.72)–(3.75) serve as useful checks that the computer program for an NEMD simulation is behaving correctly. While ergostatically constrained systems are a useful simulation tool for checking the reliability of NEMD code, they are not particularly useful for physical applications of interest to most researchers. Apart from the isothermal–isochoric (*NVT*) ensemble the next most physically significant ensemble is the isothermal–isobaric (*NpT*) ensemble, in which both the temperature and isotropic pressure are constrained. Constant pressure simulations under shear were first performed by Evans and Morriss [11,82], later extended by Daivis and Evans for molecular systems [83], and were accomplished by coupling the system to an extended degree of freedom associated with the volume of the simulation box. Thus, the volume, rather than the pressure, is allowed to fluctuate. One can implement constant pressure simulations in either the Gaussian or Nosé–Hoover forms [6]. The barostat is more easily implemented with a Nosé–Hoover feedback scheme which implies that the instantaneous pressure will fluctuate about its mean (target) value. For a thermostatted system, the

isothermal–isobaric SLLOD equations of motion are

$$\begin{aligned}\dot{\mathbf{r}}_i &= \frac{\mathbf{p}_i}{m_i} + \mathbf{r}_i\cdot\nabla\mathbf{v} + \dot{\varepsilon}\mathbf{r}_i \\ \dot{\mathbf{p}}_i &= \mathbf{F}_i^{\phi} - \mathbf{p}_i\cdot\nabla\mathbf{v} - \alpha\mathbf{p}_i - \dot{\varepsilon}\mathbf{p}_i \\ \dot{V} &= 3\dot{\varepsilon}V\end{aligned} \tag{3.76}$$

Now there are additional constraints imposed on both the $\dot{\mathbf{r}}_i$ and $\dot{\mathbf{p}}_i$ equations (to account for the fact that pressure has both configurational and kinetic contributions), with $\dot{\varepsilon}$ the new barostat multiplier which is the rate of dilation that depends on the difference between the instantaneous and target pressures. This dilation rate is obtained by solving the additional differential equation

$$\ddot{\varepsilon} = \frac{(p - p_0)V}{QNk_{\mathrm{B}}T} \tag{3.77}$$

where p is the instantaneous pressure ($p = 1/3Tr(\mathbf{P})$), p_0 is the desired pressure and Q is a damping factor for which the optimal value will depend on the type of system studied. Thus there are a total of $6N + 2$ differential equations to solve: $3N$ for the atomic positions, $3N$ for the peculiar momenta, one for the system volume and one for the dilation rate.

Care must be taken in coupling the system to a barostat because the pressure can oscillate about the mean value with a period dependent on the value of Q. The choice of the value of Q should take into account two requirements. First, in order to ensure that the thermodynamic properties computed from the phase space trajectories are independent of these oscillations, one must ensure that the simulations are sufficiently long, considerably longer than the wavelength of the oscillations. This can be accomplished by a combination of sufficiently long simulation times and sufficiently small values of Q. Next, Q should be chosen such that the period of oscillation is large compared to the characteristic decay time of dynamical correlation functions (e.g. the velocity autocorrelation function). This ensures that oscillations are decoupled from the particle dynamics. In practice, trial and error is required to find the right balance that satisfies all the above requirements.

For systems in which it is important to allow the shape of the simulation box to vary (e.g. solids) an implementation of *NPT* dynamics has been published by Melchionna *et al.* [84].

To date, implementations of the isothermal–isobaric ensemble for NEMD systems have been performed and published on shearing fluids. Implementation for elongating polymer melts has been published [85], but in this study the pressure was kept constant by fixing the system density rather than by application of equations (3.76) and (3.77). Work soon to be published will discuss how to implement these equations for steady planar elongational flow [86]. Furthermore, implementations of the method for systems using configurational thermostats have been described by Delhommelle and Evans [77] and Braga and Travis [81].

3.2 Molecular fluids

3.2.1 Molecular representation of the pressure tensor. Although equation (2.3) is a valid representation for the momentum density, it may not provide as much physical insight as a representation that explicitly accounts for the existence of molecules. In this section, we show how the molecular representation of the densities and fluxes can be obtained from the atomic representation, using the momentum density and the pressure tensor as an example.

The atomic representation of the mass and momentum densities for a molecular fluid can be written as

$$\rho(\mathbf{r}, t) = \sum_{i=1}^{N_{\mathrm{m}}}\sum_{\alpha=1}^{N_{\mathrm{s}}} m_{i\alpha}\delta(\mathbf{r} - \mathbf{r}_{i\alpha}) \tag{3.78}$$

and

$$\mathbf{J}(\mathbf{r}, t) = \rho\mathbf{v}(\mathbf{r}, t) = \sum_{i=1}^{N_{\mathrm{m}}}\sum_{\alpha=1}^{N_{\mathrm{s}}} m_{i\alpha}\mathbf{v}_{i\alpha}\delta(\mathbf{r} - \mathbf{r}_{i\alpha}) \tag{3.79}$$

where the inner summation extends over the number of atoms (or interaction sites) N_{s} in a molecule and the outer summation extends over the number of molecules N_{m} in the system. In general, N_{s} could depend on the molecule index i for a multicomponent system, but for simplicity, we will assume that this is not the case. The Fourier transforms of the mass and momentum densities are

$$\tilde{\rho}(\mathbf{k}, t) = \sum_{i=1}^{N_{\mathrm{m}}}\sum_{\alpha=1}^{N_{\mathrm{s}}} m_{i\alpha}e^{i\mathbf{k}\cdot\mathbf{r}_{i\alpha}} \tag{3.80}$$

and

$$\tilde{\mathbf{J}}(\mathbf{k}, t) = \sum_{i=1}^{N_{\mathrm{m}}}\sum_{\alpha=1}^{N_{\mathrm{s}}} m_{i\alpha}\mathbf{v}_{i\alpha}\mathrm{e}^{i\mathbf{k}\cdot\mathbf{r}_{i\alpha}} \tag{3.81}$$

Now it is convenient to introduce the position of site α of molecule i relative to the centre of mass of molecule i by the definition $\mathbf{R}_{i\alpha} = \mathbf{r}_{i\alpha} - \mathbf{r}_i$, where the centre of mass of molecule i is defined by

$$\mathbf{r}_i = \frac{\sum_{\alpha=1}^{N_{\mathrm{s}}} m_{i\alpha}\mathbf{r}_{i\alpha}}{m_i} \tag{3.82}$$

and $m_i = \sum_{\alpha=1}^{N_{\mathrm{s}}} m_{i\alpha}$ is the mass of molecule i. This means that the Fourier transform of the atomic mass density can be written as

$$\begin{aligned}\tilde{\rho}(\mathbf{k}, t) &= \sum_{i=1}^{N_{\mathrm{m}}}\sum_{\alpha=1}^{N_{\mathrm{s}}} m_{i\alpha}\mathrm{e}^{i\mathbf{k}\cdot(\mathbf{r}_i + \mathbf{R}_{i\alpha})} \\ &= \sum_{i=1}^{N_{\mathrm{m}}}\sum_{\alpha=1}^{N_{\mathrm{s}}} m_{i\alpha}\mathrm{e}^{i\mathbf{k}\cdot\mathbf{R}_{i\alpha}}\mathrm{e}^{i\mathbf{k}\cdot\mathbf{r}_i} \\ &= \sum_{i=1}^{N_{\mathrm{m}}}\sum_{\alpha=1}^{N_{\mathrm{s}}} m_{i\alpha}\left(1 + i\mathbf{k}\cdot\mathbf{R}_{i\alpha} + \frac{1}{2}[i\mathbf{k}\cdot\mathbf{R}_{i\alpha}]^2 + \cdots\right)\mathrm{e}^{i\mathbf{k}\cdot\mathbf{r}_i} \\ &= \tilde{\rho}^{(M)}(\mathbf{k}, t) + i\mathbf{k}\cdot\sum_{i=1}^{N_{\mathrm{m}}}\sum_{\alpha=1}^{N_{\mathrm{s}}} m_{i\alpha}\mathbf{R}_{i\alpha}\mathrm{e}^{i\mathbf{k}\cdot\mathbf{r}_i} + \frac{1}{2}i\mathbf{k}i\mathbf{k} \\ &\quad : \sum_{i=1}^{N_{\mathrm{m}}}\sum_{\alpha=1}^{N_{\mathrm{s}}} m_{i\alpha}\mathbf{R}_{i\alpha}\mathbf{R}_{i\alpha}\mathrm{e}^{i\mathbf{k}\cdot\mathbf{r}_i} + \cdots\end{aligned} \tag{3.83}$$

in which we define the Fourier transformed mass density in the molecular representation as $\tilde{\rho}^{(M)}(\mathbf{k},t) = \sum_{i=1}^{N_m} m_i e^{i\mathbf{k}\cdot\mathbf{r}_i}$. The local molecular mass density in real space is clearly just $\rho^{(M)}(\mathbf{r},t) = \sum_{i=1}^{N_m} m_i \delta(\mathbf{r}-\mathbf{r}_i)$, which localizes the entire mass of each molecule at the position of the molecular centre of mass. The second term on the right hand side of equation (3.83) is equal to zero because $\sum_{\alpha=1}^{N_s} m_{i\alpha}\mathbf{R}_{i\alpha} = 0$. The third term, sometimes called the mass dispersion tensor [87] is related to the local moment of inertia density, which can be shown by writing

$$\begin{aligned}\sum_{\alpha=1}^{N_s} m_{i\alpha}\mathbf{R}_{i\alpha}\mathbf{R}_{i\alpha} &= \sum_{\alpha=1}^{N_s} m_{i\alpha}R_{i\alpha}^2\mathbf{1} \\ &\quad - \left[\sum_{\alpha=1}^{N_s}\left(m_{i\alpha}R_{i\alpha}^2\mathbf{1} - m_{i\alpha}\mathbf{R}_{i\alpha}\mathbf{R}_{i\alpha}\right)\right] \\ &= \sum_{\alpha=1}^{N_s} m_{i\alpha}R_{i\alpha}^2\mathbf{1} - \mathbf{I}_i = m_i R_{g,i}^2\mathbf{1} - \mathbf{I}_i \end{aligned} \tag{3.84}$$

where $\mathbf{1}$ is the unit tensor and $\mathbf{I}_i$ is the instantaneous moment of inertia tensor of molecule i, and $R_{g,i}^2$ is the instantaneous squared radius of gyration about the centre of mass of molecule i, as defined in polymer science [88].

Following a similar procedure to expand the atomic momentum density about the molecular centre of mass, we find

$$\begin{aligned}\tilde{\mathbf{J}}(\mathbf{k},t) &= \sum_{i=1}^{N_m}\sum_{\alpha=1}^{N_s} m_{i\alpha}\mathbf{v}_{i\alpha}(1 + i\mathbf{k}\cdot\mathbf{R}_{i\alpha} + \cdots)e^{i\mathbf{k}\cdot\mathbf{r}_i} \\ &= \sum_{i=1}^{N_m} m_i\mathbf{v}_i e^{i\mathbf{k}\cdot\mathbf{r}_i} + i\mathbf{k}\cdot\sum_{i=1}^{N_m}\sum_{\alpha=1}^{N_s} m_{i\alpha}\mathbf{R}_{i\alpha}\mathbf{v}_{i\alpha}e^{i\mathbf{k}\cdot\mathbf{r}_i} + \cdots \\ &= \tilde{\mathbf{J}}^{(M)}(\mathbf{k},t) + i\mathbf{k}\cdot\sum_{i=1}^{N_m}\sum_{\alpha=1}^{N_s} m_{i\alpha}\mathbf{R}_{i\alpha}\mathbf{v}_{i\alpha}e^{i\mathbf{k}\cdot\mathbf{r}_i} + \cdots \end{aligned} \tag{3.85}$$

where $\sum_{\alpha=1}^{N_s} m_{i\alpha}\mathbf{v}_{i\alpha} = m_i\mathbf{v}_i$ is the momentum of the centre of mass of molecule i and $\tilde{\mathbf{J}}^{(M)}(\mathbf{k},t)$ is the Fourier transform of the momentum density in the molecular representation. The second term of equation (3.85) can be simplified by defining the velocity of site α of molecule i relative to the velocity of the molecular centre of mass as $\mathbf{V}_{i\alpha} = \mathbf{v}_{i\alpha} - \mathbf{v}_i$ and recalling that $\sum_{\alpha=1}^{N_s} m_{i\alpha}\mathbf{R}_{i\alpha} = 0$, giving

$$\tilde{\mathbf{J}}(k,t) = \tilde{\mathbf{J}}^{(M)}(\mathbf{k},t) + i\mathbf{k}\cdot\sum_{i=1}^{N_m}\sum_{\alpha=1}^{N_s} m_{i\alpha}\mathbf{R}_{i\alpha}\mathbf{V}_{i\alpha}e^{i\mathbf{k}\cdot\mathbf{r}_i} + \cdots \tag{3.86}$$

to first order in $i\mathbf{k}\cdot\mathbf{R}_{i\alpha}$. This can be simplified further by separating the last term into symmetric and antisymmetric parts, i.e.

$$\begin{aligned}\mathbf{R}_{i\alpha}\mathbf{V}_{i\alpha} &= \frac{1}{2}(\mathbf{R}_{i\alpha}\mathbf{V}_{i\alpha} + \mathbf{V}_{i\alpha}\mathbf{R}_{i\alpha}) + \frac{1}{2}(\mathbf{R}_{i\alpha}\mathbf{V}_{i\alpha} - \mathbf{V}_{i\alpha}\mathbf{R}_{i\alpha}) \\ &= (\mathbf{R}_{i\alpha}\mathbf{V}_{i\alpha})^s + (\mathbf{R}_{i\alpha}\mathbf{V}_{i\alpha})^a \end{aligned} \tag{3.87}$$

The symmetric part can be written in terms of the time derivative of the mass dispersion tensor [87] (also known as the mass-weighted orientational order parameter [89]). Adopting the terminology of Olmsted and Snider (with minor differences), we define the mass dispersion tensor in such a way that its Fourier transform is

$$\tilde{\mathbf{M}}(\mathbf{k},t) = \sum_{i=1}^{N_m}\sum_{\alpha=1}^{N_s} m_{i\alpha}\mathbf{R}_{i\alpha}\mathbf{R}_{i\alpha}e^{i\mathbf{k}\cdot\mathbf{r}_i} \tag{3.88}$$

As mentioned earlier, this is closely related to the local moment of inertia density. The time derivative of the mass dispersion tensor is

$$\begin{aligned}\dot{\tilde{\mathbf{M}}}(k,t) &= \sum_{i=1}^{N_m}\sum_{\alpha=1}^{N_s} m_{i\alpha}(\mathbf{R}_{i\alpha}\mathbf{V}_{i\alpha} + \mathbf{V}_{i\alpha}\mathbf{R}_{i\alpha})e^{i\mathbf{k}\cdot\mathbf{r}_i} \\ &\quad + i\mathbf{k}\cdot\sum_{i=1}^{N_m}\sum_{\alpha=1}^{N_s} m_{i\alpha}\mathbf{v}_i\mathbf{R}_{i\alpha}\mathbf{R}_{i\alpha}e^{i\mathbf{k}\cdot\mathbf{r}_i} \end{aligned} \tag{3.89}$$

The second term, representing the flux of the mass dispersion tensor, is of higher order in wavevector and we will assume that it can be neglected.

The antisymmetric part of a second rank tensor $\mathbf{A}^a = 1/2(\mathbf{A} - \mathbf{A}^{\mathrm{T}})$ is related to its pseudovector dual $\mathbf{A}^d$, by $\mathbf{A}^a = \boldsymbol{\varepsilon}\cdot\mathbf{A}^d$, where $\boldsymbol{\varepsilon}$ is the completely antisymmetric, isotropic third rank tensor ($\varepsilon_{ijk} = +1$ for indices ijk equal to cyclic permutations of 123, -1 for all other permutations of these indices, and 0 when two or more of the indices are equal). The cross product of two vectors can also be written in terms of the isotropic third rank tensor as $\mathbf{a}\times\mathbf{b} = -\boldsymbol{\varepsilon} : \mathbf{ab}$. If the tensor $\mathbf{A}$ can be represented as a dyadic, $\mathbf{A} = \mathbf{ab}$, $\mathbf{A}^d$ can also be written as $\mathbf{A}^d = (1/2)(\mathbf{a}\times\mathbf{b})$. Using these results, we obtain

$$\begin{aligned}i\mathbf{k}\cdot(\mathbf{R}_{i\alpha}\mathbf{V}_{i\alpha})^a &= i\mathbf{k}\cdot[\boldsymbol{\varepsilon}\cdot(\mathbf{R}_{i\alpha}\mathbf{V}_{i\alpha})^d] \\ &= -i\mathbf{k}\times(\mathbf{R}_{i\alpha}\mathbf{V}_{i\alpha})^d \\ &= -\frac{1}{2}i\mathbf{k}\times(\mathbf{R}_{i\alpha}\times\mathbf{V}_{i\alpha}) \end{aligned} \tag{3.90}$$

Note that this can also be obtained more simply by using the vector identity $\mathbf{a}\times(\mathbf{b}\times\mathbf{c}) = (\mathbf{a}\cdot\mathbf{c})\mathbf{b} - (\mathbf{a}\cdot\mathbf{b})\mathbf{c} = \mathbf{a}\cdot(\mathbf{cb} - \mathbf{bc})$. These can then be combined to obtain the result

$$\tilde{\mathbf{J}}(\mathbf{k},t) = \tilde{\mathbf{J}}^{(M)}(\mathbf{k},t) + \frac{1}{2}i\mathbf{k}\cdot\dot{\tilde{\mathbf{M}}}(\mathbf{k},t) - \frac{1}{2}i\mathbf{k}\times\tilde{\mathbf{S}}(\mathbf{k},t) \tag{3.91}$$

where

$$\tilde{\mathbf{S}}(\mathbf{k},t) = \sum_{i=1}^{N_m}\sum_{\alpha=1}^{N_s} m_{i\alpha}\mathbf{R}_{i\alpha}\times\mathbf{V}_{i\alpha}e^{i\mathbf{k}\cdot\mathbf{r}_i} \tag{3.92}$$

is the Fourier transform of the local density of spin angular momentum. This shows that the total momentum density can be broken into three parts with definite physical interpretations in the molecular picture. The first part is the flux of molecular centre of mass momentum, the second is a flux of momentum due to the change in the mass dispersion tensor, and the third is the momentum flux due to molecular rotation about the centre of mass.

The molecular picture is seen to be useful mainly due to the way that it allows us to construct a clear physical interpretation of molecular transport processes. This is particularly beneficial in situations where molecular rotation needs to be considered explicitly, for example in the construction of thermostats for molecular fluids, which we will discuss later.

The spatially averaged, instantaneous pressure tensor for a system of particles with two-body central forces is given by the zero wavevector limit of equation (2.27). Rewriting this in terms of molecular centre of mass positions and velocities, we have

$$\begin{aligned} V\mathbf{P}(t) &= \sum_{i=1}^{N_\mathrm{m}}\sum_{\alpha=1}^{N_\mathrm{s}} m_{i\alpha}\mathbf{c}_{i\alpha}\mathbf{c}_{i\alpha} - \frac{1}{2}\sum_{i=1}^{N_\mathrm{m}}\sum_{\alpha=1}^{N_\mathrm{s}}\sum_{j=1}^{N_\mathrm{m}}\sum_{\beta=1}^{N_\mathrm{s}} \mathbf{r}_{i\alpha j\beta}\mathbf{F}_{i\alpha j\beta} \\ &= \sum_{i=1}^{N_\mathrm{m}}\sum_{\alpha=1}^{N_\mathrm{s}} m_{i\alpha}(\mathbf{c}_i + \mathbf{C}_{i\alpha})(\mathbf{c}_i + \mathbf{C}_{i\alpha}) \\ &\quad - \frac{1}{2}\sum_{i=1}^{N_\mathrm{m}}\sum_{\alpha=1}^{N_\mathrm{s}}\sum_{j=1}^{N_\mathrm{m}}\sum_{\beta=1}^{N_\mathrm{s}} (\mathbf{r}_{ij} + \mathbf{R}_{j\beta} - \mathbf{R}_{i\alpha})\mathbf{F}_{i\alpha j\beta} \\ &= V\mathbf{P}^{(M)}(t) + \sum_{i=1}^{N_\mathrm{m}}\sum_{\alpha=1}^{N_\mathrm{s}} m_{i\alpha}\mathbf{C}_{i\alpha}\mathbf{C}_{i\alpha} + \sum_{i=1}^{N_\mathrm{m}}\sum_{\alpha=1}^{N_\mathrm{s}} \mathbf{R}_{i\alpha}\mathbf{F}_{i\alpha} \end{aligned} \tag{3.93}$$

where we have defined $\mathbf{C}_{i\alpha} = \mathbf{c}_{i\alpha} - \mathbf{c}_i$, with $\mathbf{c}_{i\alpha} = \mathbf{v}_{i\alpha} - \mathbf{v}(\mathbf{r}_{i\alpha})$ and $\mathbf{c}_i = \mathbf{v}_i - \mathbf{v}(\mathbf{r}_i)$ and it is assumed that terms $j\beta = i\alpha$ are omitted from the quadruple sum. The zero-wavevector molecular pressure tensor for molecules consisting of atoms with only two-body central forces is given by

$$V\mathbf{P}^{(M)}(t) = \sum_{i=1}^{N_\mathrm{m}} m_i\mathbf{c}_i\mathbf{c}_i - \frac{1}{2}\sum_{i=1}^{N_\mathrm{m}}\sum_{j=1}^{N_\mathrm{m}} \mathbf{r}_{ij}\mathbf{F}_{ij}. \tag{3.94}$$

Note that this need not be instantaneously symmetric, even though the atomic pressure tensor is. The difference between the atomic and molecular pressure tensors can be expressed as follows.

$$\begin{aligned} &V\mathbf{P}(t) - V\mathbf{P}^{(M)}(t) \\ &= \sum_{i=1}^{N_\mathrm{m}}\sum_{\alpha=1}^{N_\mathrm{s}} m_{i\alpha}\mathbf{C}_{i\alpha}\mathbf{C}_{i\alpha} + \sum_{i=1}^{N_\mathrm{m}}\sum_{\alpha=1}^{N_\mathrm{s}} \mathbf{R}_{i\alpha}\mathbf{F}_{i\alpha} \\ &= \sum_{i=1}^{N_\mathrm{m}}\sum_{\alpha=1}^{N_\mathrm{s}} m_{i\alpha}\mathbf{C}_{i\alpha}\mathbf{C}_{i\alpha} + \sum_{i=1}^{N_\mathrm{m}}\sum_{\alpha=1}^{N_\mathrm{s}} (\mathbf{R}_{i\alpha}\mathbf{F}_{i\alpha})^s \\ &\quad + \sum_{i=1}^{N_\mathrm{m}}\sum_{\alpha=1}^{N_\mathrm{s}} (\mathbf{R}_{i\alpha}\mathbf{F}_{i\alpha})^a \\ &= \frac{1}{2}V\ddot{\mathbf{M}}(t) - V\mathbf{P}^{(M)a}(t) \end{aligned} \tag{3.95}$$

where

$$\begin{aligned} \frac{1}{2}V\ddot{\mathbf{M}}(t) &= \sum_{i=1}^{N_\mathrm{m}}\sum_{\alpha=1}^{N_\mathrm{s}} m_{i\alpha}\mathbf{C}_{i\alpha}\mathbf{C}_{i\alpha} \\ &\quad + \sum_{i=1}^{N_\mathrm{m}}\sum_{\alpha=1}^{N_\mathrm{s}} (\mathbf{R}_{i\alpha}\mathbf{F}_{i\alpha})^s \end{aligned} \tag{3.96}$$

and

$$\begin{aligned} V\mathbf{P}^{(M)a}(t) &= \sum_{i=1}^{N_\mathrm{m}}\sum_{\alpha=1}^{N_\mathrm{s}} (\mathbf{R}_{i\alpha}\mathbf{F}_{i\alpha})^a \\ &= \frac{1}{2}\sum_{i=1}^{N_\mathrm{m}} (\mathbf{r}_i\mathbf{F}_i - \mathbf{F}_i\mathbf{r}_i) \end{aligned} \tag{3.97}$$

Note that the antisymmetric part of the molecular pressure tensor arises solely from the potential part, because the kinetic part is inherently symmetric.

Several studies have shown that the time averaged value of the antisymmetric part of the molecular pressure tensor in a shearing steady state is zero [89–92]. This means that the steady state viscometric functions can equally well be evaluated from either the molecular or atomic pressure tensor. However, the molecular formalism has some advantages over the atomic formalism. One important advantage is that the molecular stress tensor varies more slowly with time than the atomic stress tensor, particularly when high frequency bond length vibrations are present. This means that evaluation of the viscosity from the integral of the stress autocorrelation function is numerically easier to perform when the molecular stress tensor is used [93]. Another important advantage of using the molecular stress tensor is that its antisymmetric part can be used to determine whether any torques are being applied to the system, either intentionally, through a fictitious spin force [94] or unintentionally through an incorrectly formulated thermostat [95].

3.2.2 Molecular SLLOD. The SLLOD algorithm for atomic fluids can be directly applied to molecular fluids without modification, provided that all of the relevant forces are included. In fact, this is the most commonly implemented form of the equations of motion for NEMD simulations of molecular fluids, including polymeric fluids. In the atomic SLLOD algorithm, the streaming term in the equations of motion is applied at the position of each atom in a molecule, i.e.

$$\dot{\mathbf{r}}_{i\alpha} = \frac{\mathbf{p}_{i\alpha}}{m_{i\alpha}} + \mathbf{r}_{i\alpha}\cdot\nabla\mathbf{v}, \quad \dot{\mathbf{p}}_{i\alpha} = \mathbf{F}_{i\alpha} - \mathbf{p}_{i\alpha}\cdot\nabla\mathbf{v} \tag{3.98}$$

The molecular SLLOD algorithm differs in the point at which the streaming velocity is evaluated:

$$\dot{\mathbf{r}}_{i\alpha} = \frac{\mathbf{p}_{i\alpha}}{m_{i\alpha}} + \mathbf{r}_i\cdot\nabla\mathbf{v}, \quad \dot{\mathbf{p}}_{i\alpha} = \mathbf{F}_{i\alpha} - \left(\frac{m_{i\alpha}}{m_i}\right)\mathbf{p}_i\cdot\nabla\mathbf{v} \tag{3.99}$$

where $\mathbf{F}_{i\alpha}$ includes all intermolecular forces due to potential energy functions, constraints etc., $m_{i\alpha}$ is the mass of site α of molecule i and m_i is the mass of molecule i.

The molecular version of the SLLOD equations of motion was originally proposed by Ladd [13]. Edberg, Morriss and Evans [96] showed that although the transient responses of a system to the molecular and atomic SLLOD equations of motion are different, they produce identical averages in the steady state. In particular, both forms of the equations of motion generate a steady state in which the antisymmetric part of the time averaged molecular pressure tensor is zero when a correctly formulated thermostat is applied [97].

Later, when we consider molecular thermostats, we will see that an additional complication arises from the difference between the atomic and molecular forms of the SLLOD equations of motion. The first equation of equation (3.99) acts as a *definition* of the peculiar momentum of site α of molecule i. This peculiar momentum is used to calculate the pressure, temperature and other properties. The molecular pressure tensor and temperature will be correctly calculated, but, as equation (3.91) shows, the local atomic momentum density (and therefore, the atomic streaming velocity) differs from the molecular momentum density due to terms that account for molecular rotation and deformation. In other words, the assumption that the streaming velocity at site α of molecule i is given by the perfectly linear expression $\mathbf{v}(\mathbf{r}_{i\alpha}) = \mathbf{r}_{i\alpha}\cdot\nabla\mathbf{v}$ cannot possibly be correct when it is applied to atoms within a molecule, because nearby bonded sites of a molecule cannot be separated from each other by an indefinite amount by the velocity gradient in the same way that independent atoms can. Instead, molecular rotation and limited deformation occur. On the other hand, the molecular centre of mass streaming velocity does not suffer from this problem, making it a more attractive quantity for the calculation of the molecular peculiar velocity, which can then be used to compute and control the molecular pressure, temperature and other properties. Thus, the main advantage of the molecular SLLOD equations of motion is that they provide us with a definition of the molecular centre of mass peculiar momentum that does not rely on assumptions about the systematic internal molecular motions associated with flow, such as molecular rotation and deformation. It is worth noting here that irrotational flows such as elongation should be less strongly affected by these problems due to the absence of shear-induced molecular rotation. Of course, a molecular thermostat introduces its own problems. In a system consisting of a very small number of extremely long molecules, only a few degrees of freedom will be thermostatted. This may lead to severe non-equipartitioning of energy at high deformation rates. In such cases, the configurational thermostat introduced by Braga and Travis [79] may have distinct advantages.

3.2.3 Energy balance in molecular fluids. The total internal energy of the particles in an isolated, finite system is given by

$$U = \sum_i u_i = \sum_i \left(\frac{\mathbf{p}_i^2}{2m_i} + \frac{1}{2}\sum_j \phi_{ij} \right) \tag{3.100}$$

The time derivative of the internal energy is

$$\begin{aligned} \frac{\mathrm{d}U}{\mathrm{d}t} &= \sum_i \frac{\mathbf{p}_i}{m_i}\cdot\dot{\mathbf{p}}_i + \frac{1}{2}\sum_i\sum_j \left(\dot{\mathbf{r}}_i\cdot\frac{\partial\phi_{ij}}{\partial\mathbf{r}_i} + \dot{\mathbf{r}}_j\cdot\frac{\partial\phi_{ij}}{\partial\mathbf{r}_j} \right) \\ &= \sum_i \frac{\mathbf{p}_i}{m_i}\cdot\dot{\mathbf{p}}_i - \sum_i \dot{\mathbf{r}}_i\cdot\mathbf{F}_i \\ &= \sum_i \frac{\mathbf{p}_i}{m_i}\cdot(\mathbf{F}_i - \mathbf{p}_i\cdot\nabla\mathbf{v}) - \sum_i \left(\frac{\mathbf{p}_i}{m_i} + \mathbf{r}_i\cdot\nabla\mathbf{v} \right)\cdot\mathbf{F}_i \\ &= -\sum_i \left(\frac{\mathbf{p}_i\mathbf{p}_i}{m_i} + \mathbf{F}_i\mathbf{r}_i \right) : \nabla\mathbf{v} = -V\mathbf{P}^{\mathrm{T}} : \nabla\mathbf{v} \end{aligned} \tag{3.101}$$

where we have used the SLLOD equations of motion, equation (3.98) and the pressure tensor, equation (2.25) (both simplified to the case of a simple atomic fluid). This result shows that the total internal energy increases in exactly the way described by the internal energy balance equation (2.7).

The expression for the pressure tensor used in equation (3.101) is not strictly valid for an infinite periodic system. The correct expression, equation (2.39), depends on the minimum image separation of interacting images of particles i and j, rather than the absolute position of each particle. If the whole derivation is performed starting from the expression for the internal energy of an infinite periodic system, and the minimum image convention is used in the same way as in the derivation of equation (2.39), then the correct result is obtained. In fact, there are several features of simulations in homogeneous periodic systems that need to be carefully taken into account when applying the balance equations. Firstly, the local heat flux vector has a time averaged value of zero everywhere in the system, even when a velocity gradient produces viscous heating. The periodicity of the heat flux vector ensures that the net heat absorbed by conduction through the periodic boundaries of the simulation box is exactly zero at all times, since the flux entering through one face is always exactly matched by the flux leaving through the opposite face. By the divergence theorem, this is equivalent to saying that the integral of the divergence of the heat flux vector over the volume of the periodic simulation box is zero. Similarly, if we consider only simulations of systems that are at equilibrium or in flows with spatially uniform, divergenceless velocity gradient tensors, the densities of mass, momentum and internal energy could be expected to remain uniform (in the absence of unusual flow instabilities) and the integrals over the whole simulation box of the convective terms in the balance equations are also then equal to zero. This means that the change in the total internal energy of the simulation box is entirely due to the thermodynamic work term, as given by equation (3.101). Fortunately, the

net result of these subtle differences between a finite, isolated system and an infinite, periodic system is only a very minor change: the potential part of the expression for the pressure tensor in periodic boundary conditions must contain the minimum image particle separations rather than the absolute particle positions, as previously stated.

3.2.4 Momentum and internal energy balance in the presence of a homogeneous thermostat. The thermostat term in the equations of motion for homogeneous flow effectively removes heat from the system, making it possible to generate a steady state with constant time averaged values of the static thermodynamic properties such as the pressure and internal energy and the relevant fluxes. The equations of motion for an atomic system with a deterministic thermostat are given by equation (3.44). The details of the vast number of thermostats that have been proposed were discussed in section 3.1.4 and have been thoroughly reviewed in previous publications [79,81,95,97,98]. However, two subjects that have received far less attention are the detailed analysis of the place of the thermostat in the balance equations for momentum and internal energy, and the subtle issues surrounding the formulation of thermostats for molecular fluids. These will be the topics of our discussion in this section.

We will only consider the simplest deterministic thermostat, the Gaussian isokinetic thermostat, in our discussion. This choice is not intended to imply that this thermostatting mechanism is superior to others. Rather, we have chosen it because it enables us to study the main issues of interest, energy balance and the thermostatting of molecular fluids, using a simple and familiar model.

The effect of the thermostat on the momentum balance equation will be considered first. Physically, it seems best to regard the thermostat term in the atomic equations of motion as an internal force because, as we will soon see, it cannot contribute to the acceleration of the centre of mass of the system. However, it remains distinct from interatomic constraint forces such as the bond length or bond angle constraints, which must be included in the atomic pressure tensor. Therefore, we add a term to account for the thermostat in addition to the external body force term, $\rho\mathbf{F}^{\mathrm{ext}}$ in equation (2.6). Macroscopically, we then have

$$\frac{\partial(\rho\mathbf{v})}{\partial t} = -\nabla\cdot\mathbf{P} - \nabla\cdot(\rho\mathbf{v}\mathbf{v}) + \rho\mathbf{F}^{\mathrm{ext}} + \rho\mathbf{T} \tag{3.102}$$

where $\rho\mathbf{T} = \rho(\mathbf{r}, t)\mathbf{T}(\mathbf{r}, t)$ is the local force density due to the thermostat term in the equations of motion. The microscopic expression for this force density is easily obtained by considering the effect of the additional term in the equations of motion on the microscopic expression for the rate of change of the momentum density. Once again, this is most easily calculated after Fourier transformation:

$$\begin{aligned}\frac{\partial(\widetilde{\rho\mathbf{v}})}{\partial t} &= \frac{\partial}{\partial t}\sum_i m_i\mathbf{v}_i e^{i\mathbf{k}\cdot\mathbf{r}_i} \\ &= \sum_i m_i\dot{\mathbf{v}}_i e^{i\mathbf{k}\cdot\mathbf{r}} + i\mathbf{k}\cdot\sum_i m_i\mathbf{v}_i\mathbf{v}_i e^{i\mathbf{k}\cdot\mathbf{r}_i} \\ &= i\mathbf{k}\cdot\tilde{\mathbf{P}}(\mathbf{k}, t) + i\mathbf{k}\cdot[\widetilde{\rho\mathbf{v}\mathbf{v}}(\mathbf{k}, t)] \\ &\quad + \widetilde{\rho\mathbf{F}^{\mathrm{ext}}}(\mathbf{k}, t) - \alpha\sum_i m_i\mathbf{c}_i e^{i\mathbf{k}\cdot\mathbf{r}_i}\end{aligned} \tag{3.103}$$

This shows that the microscopic expression for the density of the force due to the thermostat is

$$\rho(\mathbf{r}, t)\mathbf{T}(\mathbf{r}, t) = -\alpha\sum_i m_i\mathbf{c}_i\delta(\mathbf{r} - \mathbf{r}_i) \tag{3.104}$$

The integral of this quantity over the whole volume is equal to zero, because the peculiar velocity is defined in such a way that the sum of the peculiar momenta is zero at all times. Equivalently, in a periodic system, the zeroth Fourier component of the force exerted on the system by the thermostat is zero. This assumes the streaming velocity used to define the peculiar velocity has been evaluated correctly, e.g. using a PUT (see section 3.1.4).

The effect of the thermostat on the internal energy is taken into account by adding a term to the internal energy balance equation,

$$\frac{\partial(\rho u)}{\partial t} = -\nabla\cdot\mathbf{J}_q - \nabla\cdot(\rho u\mathbf{v}) - \mathbf{P}^{\mathrm{T}} : \nabla\mathbf{v} + R \tag{3.105}$$

where R represents the density of the rate at which internal energy is added to the system by the homogeneous thermostat in the equations of motion. By substituting the equations of motion into the Fourier transform of the left hand side of equation (3.105), we find that the Fourier transform of R is

$$\tilde{R} = -\alpha\sum_i m_i\mathbf{c}_i^2 e^{i\mathbf{k}\cdot\mathbf{r}_i} \tag{3.106}$$

The zeroth Fourier component of this quantity for a periodic system gives us the total rate of change of the internal energy of the particles in the primary simulation box due to the thermostat. In a spatially homogeneous system in which work is done by stresses, we can keep the internal energy constant by applying the condition that

$$\frac{\mathrm{d}U}{\mathrm{d}t} = \int\frac{\partial(\rho u)}{\partial t}\mathrm{d}\mathbf{r} = -V\mathbf{P}^{\mathrm{T}} : \nabla\mathbf{v} + VR = 0 \tag{3.107}$$

which, when combined with equation (3.106), provides us with the expression for α that is required to keep the internal energy constant (see also section 3.1.5):

$$\alpha = -\frac{V\mathbf{P}^{\mathrm{T}} : \nabla\mathbf{v}}{\sum_i m_i\mathbf{c}_i^2} \tag{3.108}$$

3.2.5 Temperature and thermostats for molecular fluids. The equipartition theorem ensures that the temperatures of all degrees of freedom are equal at equilibrium. It is

well known that this is not the case for systems that are far from equilibrium, even for simple atomic fluids. For example, the shear rate dependence of the differences between the temperatures calculated from the x, y and z components of the peculiar momentum in a shearing atomic fluid have been shown to be significant at extremely high shear rates by Baranyai [99]. This is linked to a greater question regarding the validity of our usual thermodynamic definition of temperature, $T = (\partial U/\partial S)_V$ for systems far from equilibrium. In fact, the existence of a non-equilibrium temperature has itself been questioned and the issue is far from being resolved [100]. The zeroth law of thermodynamics, which deals with the definition of thermal equilibrium and the existence of a unique temperature, has been shown to be invalid for an atomic system in a strong, spatially varying strain rate field [101]. From a purely pragmatic point of view, it is convenient to assume that temperature does exist in far from equilibrium systems, although, any chosen means of calculating it may no longer be unique, and we must accept that the thermodynamic meaning of such a quantity is questionable when we consider systems far from equilibrium. The kinetic temperature, which has its basis in the equipartition theorem, the ideal gas equation of state and kinetic theory, is defined for an atomic system through the relationship

$$\langle K \rangle = \left\langle \sum_i \frac{1}{2} m_i \mathbf{c}_i^2 \right\rangle = \frac{N_f k_B T}{2} \tag{3.109}$$

where N_f is the number of independent degrees of freedom contributing to the peculiar kinetic energy. For a system in which all of the momenta are independent, this would be equal to $3N$ where N is the number of atoms. In the presence of constraints, this must be modified, because the number of degrees of freedom is reduced by one for every constraint on the momenta. This means that in a molecular dynamics simulation in which the equations of motion include no explicit constraints, only the three components of the total momentum are fixed and $N_f = 3N - 3$. If a Gaussian thermostat is used to additionally fix the total peculiar kinetic energy, we have $N_f = 3N - 4$. For an equilibrium constant energy simulation of a system of molecules with N_c internal constraints per molecule, the number of degrees of freedom that should be used to calculate the atomic temperature is $N_f = N_m(3N_s - N_c) - 3$, where N_m is the number of molecules and N_s is the number of sites per molecule. The kinetic temperature has an attractive interpretation as the residual (or random) part of the kinetic energy that results from a least squares estimation of the streaming velocity from the velocities of the individual atoms [6].

Another measure of temperature that can be used in molecular systems is the kinetic temperature of the molecular centre of mass degrees of freedom. In this case, the temperature is obtained from the centre of mass peculiar kinetic energy of each molecule using equation (3.109) again, but with $\mathbf{c}_i$ now representing the molecular centre of mass peculiar velocity instead of the atomic peculiar velocity, m_i representing the mass of molecule i and the sum now extending over all molecules. The number of degrees of freedom for the calculation of the molecular centre of mass kinetic temperature in a system with fixed total momentum and a constrained value of the total molecular peculiar kinetic energy is $N_f = 3N_m - 4$, where N_m is the number of molecules in the system. The molecular and atomic temperatures have identical average values at equilibrium, but far from equilibrium these two temperatures differ. In steady PSF, the difference is proportional to the strain rate squared and the atomic temperature is higher than the molecular temperature [96] when the molecular centre of mass degrees of freedom are thermostatted. This occurs because the relaxation time for the heat generated by viscous flow processes to flow from the internal molecular degrees of freedom to the thermostatted centre of mass translational degrees of freedom is significant.

All calculations of the kinetic temperature assume that the relevant (atomic or molecular) peculiar velocity has been correctly computed. The SLLOD equations of motion provide us with a definition of the peculiar velocity, but there is a difference between the peculiar velocities that we obtain from the atomic (equation (3.98)) and molecular (equation (3.99)) forms of the equations of motion. Is this difference significant? This question has been examined by Travis *et al.* [95,97,98], and the brief answer is that a significant difference does exist, and that an incorrectly formulated thermostat can produce misleading results. In particular, enhanced orientational ordering and non-zero values of the antisymmetric part of the molecular stress tensor in a shearing steady state can result from the use of an incorrectly formulated atomic thermostat. Travis *et al.* [95,97,98] have shown that when the antisymmetric part of the molecular stress tensor is non-zero in a steady state, it indicates that a torque is being applied to the molecules. If this is done unintentionally by applying an incorrectly formulated thermostat, errors result.

It is easily shown that if a thermostat is formulated using the molecular centre of mass kinetic temperature calculated from either the atomic or molecular SLLOD equations of motion, correct results are obtained. From the atomic SLLOD equations of motion, the peculiar momentum of the molecular centre of mass is given by summing over all sites on a given molecule

$$\begin{aligned} m_i \mathbf{c}_i &= \sum_\alpha m_{i\alpha} \dot{\mathbf{r}}_{i\alpha} - \sum_\alpha m_{i\alpha} \mathbf{r}_{i\alpha} \cdot \nabla \mathbf{v} \\ &= m_i \dot{\mathbf{r}}_i - m_i \mathbf{r}_i \cdot \nabla \mathbf{v} \end{aligned} \tag{3.110}$$

and similarly, from the molecular SLLOD equations of motion, we find

$$\begin{aligned} m_i \mathbf{c}_i &= \sum_\alpha m_{i\alpha} \dot{\mathbf{r}}_{i\alpha} - \sum_\alpha m_{i\alpha} \mathbf{r}_i \cdot \nabla \mathbf{v} \\ &= m_i \dot{\mathbf{r}}_i - m_i \mathbf{r}_i \cdot \nabla \mathbf{v} \end{aligned} \tag{3.111}$$

Thus, atomic SLLOD with a molecular thermostat (ASMT) is equivalent to molecular SLLOD with a

molecular thermostat (MSMT). However, in simulations where an atomic thermostat is formulated using the peculiar velocity defined by the atomic SLLOD equations of motion (ASAT), artifacts are generated.

The correct formulation of a thermostat that keeps the atomic kinetic temperature constant in a far from equilibrium molecular system requires that the streaming velocity at an atomic site of any molecule be computed accurately. Equation (3.91) shows that the difference between the momentum density at the centre of mass of a molecule and one of the atoms on that molecule can be used to calculate the difference in their streaming velocities. When this difference is properly taken into account, artefacts such as the enhanced orientational ordering and the non-zero antisymmetric part of the steady state molecular pressure tensor are eliminated [95,97,98].

The analysis of Travis *et al.* [95,97,98] showed that two issues must be addressed when formulating a homogeneous thermostat for a molecular liquid. The first issue, which is common to simple monatomic and polyatomic molecular fluids, is the determination of the correct form of the instantaneous velocity profile. At sufficiently high strain rates, the assumption of a stable, homogeneous velocity profile may not be valid, and the streaming velocity must be computed during the simulation. The calculated streaming velocity is then used in the thermostat term of the equations of motion. This type of thermostat is called a PUT. This was discussed in section 3.1.4. The second issue is unique to molecular fluids. A calculation of the streaming velocity of an atom that resides on a molecule with a non-zero average angular velocity superimposed on its centre of mass translational streaming motion must also take the rotational component into consideration when a thermostat is applied. Similarly, if there are any other systematic internal motions, such as an oscillatory molecular stretching, these should also be taken into consideration. This is clearly an extremely complicated task. The formulation of a rotationally unbiased atomic thermostat has only ever been successfully carried out for the relatively simple case of a fluid of rigid diatomic molecules [95,97,98].

The approach taken by Travis *et al.* [95,97,98] was as follows. First, it was assumed that the streaming velocity at site α of molecule i could be represented as

$$\begin{aligned}\mathbf{u}(\mathbf{r}_{i\alpha}) &= \mathbf{u}_T(\mathbf{r}_{i\alpha}) + \mathbf{u}_R(\theta_i, \phi_i) \\ &= \mathbf{u}_T(\mathbf{r}_i) + \boldsymbol{\omega}(\theta_i, \phi_i) \times \mathbf{R}_{i\alpha}\end{aligned} \tag{3.112}$$

where $\mathbf{u}_T(\mathbf{r}_i)$ represents the translational centre of mass streaming velocity of molecule i, and $\mathbf{u}_R(\theta_i, \phi_i)$ represents the angularly resolved average rotational streaming velocity of the fluid, assumed here to be independent of position. The introduction of an orientational dependence of the average angular velocity was found to be crucial. The average streaming velocity must be allowed to vary with the orientation of the molecule, specified by the angles (θ_i, ϕ_i), in order to eliminate spurious enhanced orientational ordering. Deviations of $\mathbf{u}_T(\mathbf{r}_i)$ from a strictly linear velocity profile were accounted for by expanding deviations from the linear velocity profile as a Fourier series, following the technique of Evans *et al.* [74].

The average streaming component of the angular velocity is conventionally defined by the equation

$$\mathbf{S} = \boldsymbol{\Theta} \cdot \boldsymbol{\omega} \tag{3.113}$$

where $\mathbf{S}$ is the total spin angular momentum of the system and $\boldsymbol{\Theta}$ is the total moment of inertia tensor for all molecules in the system [5]. It should be remarked that the numerical average of the angular velocity vectors of all molecules in the system, $\bar{\boldsymbol{\omega}}$, is different from the average angular velocity obtained by solving equation (3.113) and should not be regarded as a valid macroscopic definition of $\boldsymbol{\omega}$. In fact, for diatomic molecules, Travis *et al.* [95] have shown that in the limit of zero shear rate, the numerically averaged angular velocity is 2/3 of the streaming angular velocity. A simple physical interpretation of the difference between these two quantities is that while $\bar{\boldsymbol{\omega}}$ represents an unweighted average of molecular angular velocities, $\boldsymbol{\omega}$ represents a weighted average angular velocity that takes the molecular inertia tensor as the weighting factor. This is similar to the conventional definition of the translational streaming velocity as the mass-weighted average velocity (equation (3.56)).

Taking the orientation dependence of the streaming angular velocity into account, the angular velocity was expressed as a spherical harmonic expansion in which the expansion coefficients were determined at each timestep by the method of least squares. The value of the atomic streaming velocity was then determined for each atom using equation (3.112), and the equations of motion, given by

$$\begin{aligned}\dot{\mathbf{r}}_{i\alpha} &= \frac{\mathbf{p}_{i\alpha}}{m_{i\alpha}} + \mathbf{r}_i \cdot \nabla \mathbf{v} \\ \dot{\mathbf{p}}_{i\alpha} &= \mathbf{F}_{i\alpha} - \left(\frac{m_{i\alpha}}{m_i}\right)\mathbf{p}_i \cdot \nabla \mathbf{v} - \alpha^{(T)}[\mathbf{v}_i - \mathbf{v}(\mathbf{r}_i, t)] \\ &\quad - \alpha^{(R)}[\boldsymbol{\omega}_i - \boldsymbol{\omega}(\theta_i, \phi_i)] \\ \dot{\alpha}^{(T)} &= \xi[T(t) - T] \\ \dot{\alpha}^{(R)} &= \xi[T(t) - T]\end{aligned} \tag{3.114}$$

were integrated. Even with the simplest rotationally unbiased atomic thermostat (RUAT), which assumes that the translational streaming velocity is strictly linear but takes account of the molecular streaming velocity, the results showed a dramatic reduction in the antisymmetric part of the molecular pressure tensor, indicating that spurious thermostat-induced molecular torques were eliminated.

The extension of this approach to flexible molecules is expected to be very difficult, because no technique for the determination of the streaming components of internal motions have yet been devised. The recent development of

Table 1. Atomic fluids.

General theme	*Details investigated*	*Authors and year*	*References*
Viscous transport properties of simple fluids under shear	Homogeneous boundary driven algorithm for shear flow	Lees and Edwards (1972)	[9]
	Early field-driven NEMD simulations	Ashurst and Hoover (1975)	[102]
	NEMD simulation using the DOLLS tensor Hamiltonian; statistical mechanics basis	Hoover *et al.* (1980), Evans and Morriss (1984)	[10,11]
	SLLOD equations of motion replaces DOLLS for atomic fluids; use of thermostats in NEMD	Evans and Morriss (1984), Evans *et al.* (1983) (see also Evans and Morriss (1990))	[6,12,41]
	Calculation of non-equilibrium radial distribution functions	Hanley and Evans (1980), Evans *et al.* (1980)	[103,104]
	Simulations show $\eta \sim \dot{\gamma}^{1/2}, p \sim \dot{\gamma}^{3/2}, E \sim \dot{\gamma}^{3/2}$ for fluids near L–J triple point	Evans *et al.* (1981), (1984)	[105,106]
	Evidence of "string phase" reported for NEMD simulations of shearing fluid; shown to be artifact of incorrect thermostatting.	Erpenbeck (1984), Evans and Morriss (1986), Delhommelle *et al.* (2003), Delhommelle (2004)	[71–73,76,107]
	Quadratic dependence of η on $\dot{\gamma}$ suggested by simulation	Ryckaert *et al.* (1988)	[108]
	Number dependence of shear viscosity for 3D L–J fluid	Evans *et al.* (1989)	[109]
	Investigation of long-time tail for stress autocorrelation function: evidence for and against $t^{-3/2}$ tail	Evans (1980), Ferrario *et al.* (1991)	[110,111]
	Comparison of SLLOD with boundary driven Couette flow, shows good agreement for homogeneous flow	Liem *et al.* (1992), Todd *et al.* (1999)	[54,112]
	Simulation and theory for hard spheres under shear via SLLOD equations	Petravic *et al.* (1994), (1995), (2003)	[113–115]
	Strain rate and wavevector dependence of simple L-J fluid	Evans (1981); Travis *et al.* (1998), (1999)	[116–118]
	Comparison of theory with simulation for pair distribution functions of simple fluid under shear; development of non-equilibrium potentials	Kalyuzhnyi *et al.* (1999), Gan and Eu (1992)	[119–121]
	Strong evidence that strain rate dependence of pressure and energy is state-point dependent	Matin *et al.* (2000), Marcelli *et al.* (2001), Ge *et al.* (2001)	[122–125]
	Response theory (TTCF) to compute shear viscosity of L-J fluid over wide range of strain rates at triple point; viscosity data well fit to either Cross equation or $\dot{\gamma}^{1/2}$	Borzsák *et al.* (2002)	[35]
	Extracting shear viscosity via power dissipation	Holian (2002)	[126,127]
	Scaling behaviour of pressure, energy and viscosity for L–J fluid examined over wide range of state points; pressure, energy and viscosity found to scale as $\dot{\gamma}^{a}$, where a is a linear function of density and temperature	Ge *et al.* (2003), Todd (2005)	[128,129]
	Structural and rheological studies of simple fluids using configurational thermostats, thereby examining artifacts caused by assuming streaming velocity profiles; examination of jamming leading to shear thickening for colloidal systems	Delhommelle *et al.* (2004), (2005)	[130–132]
	Study of the effects of strain, stress relaxation and cooperative effects in non-equilibrium and equilibrium simple fluids	Petravic (2004)	[133,134]
Viscous transport properties of simple fluids under elongation	NEMD simulation of elongational flow by boundary driven method and by use of SLLOD equations	Heyes (1985), (1986), Evans and Heyes (1990)	[135–137]
	Shear and elongational viscosities simulated and compared with retarded motion expansion.	Pierleoni and Ryckaert (1991)	[138]
	Improvements in algorithms to simulate longer times	Baranyai and Cummings (1995), Todd and Daivis (1997), (1998)	[58,59,139]
	Exploitation of Kraynik-Reinelt boundary conditions for indefinite time elongation, and algorithmic improvements	Todd and Daivis (1998), (1999), (2000), Baranyai and Cummings (1999) (see also Kraynik and Reinelt (1992))	[15–19]

Table 1 – *Continued*

General theme	*Details investigated*	*Authors and year*	*References*
	Relationship of Kraynik-Reinelt boundary conditions to dynamical systems and simple re-derivation in terms of Arnold cat map	Hunt and Todd (2003)	[38]
	Microscopic chaos in elongational flow	Todd (2005), Frascoli *et al.* (2006)	[39,40]
	Derivation and validation of SLLOD algorithm for generalized homogeneous flows	Daivis and Todd (2006) (see also Edwards *et al.* (2006) for a response to this paper in defense of the GSLLOD/PSLLOD algorithm as well as Tuckerman *et al.* (1997), Evans *et al.* (1998) and Tuckerman *et al.* (1998))	[14,33,140–142]
	Constant pressure algorithm compatible with Kraynik-Reinelt boundary conditions	Frascoli and Todd (2006)	[86]
Phase behaviour	Chemical potential for non-equilibrium steady states	Baranyai and Cummings (1996), (1999)	[143,144]
	Methods to compute solid–liquid phase co-existence at equilibrium via NEMD methods	Baranyai and Cummings (1996), Butler and Harrowell (2002), (2003), Ge *et al.* (2003)	[143,145–147]
	Transport, structure and thermodynamics (including diffusion, viscosity and thermal conductivity coefficients) characterized in the vicinity of the liquid-solid phase transition.	Petravic (2004)	[148]
Many body potentials	Transport properties of argon and argon–krypton mixtures using 2- and 3- body potentials	Lee and Cummings (1993), (1994), Marcelli *et al.* (2001)	[124,149,150]
	Transport properties of xenon using 2- and 3- body potentials	Marcelli *et al.* (2001)	[151]
Glassy systems under shear	Transport properties of glassy shearing fluids and examination of fluctuation-dissipation relation	Barrat and Berthier (2000), Berthier *et al.* (2000), Berthier and Barrat (2002)	[152–154]
Non-equilibrium thermodynamics	Steady-state thermodynamics of shearing fluids	Evans and Hanley (1980), Daivis and Matin (2003), Taniguchi and Morriss (2004)	[155–157]
	Equilibrium entropy differences via NEMD; non-equilibrium entropy calculations	Baranyai and Evans (1991), Baranyai (1996)	[158–160]
	Equivalence of Norton and Thévenin ensembles	Evans (1993)	[161]
Algorithms not already described	Parallel algorithm for NEMD (shear flow)	Hansen and Evans (1994), Bhupathiraju *et al.* (1996)	[36,37]
	Multiple timestep SLLOD algorithm	Cui *et al.* (1996)	[162]
	Cell neighbour list method for NEMD (elongational flow)	Matin *et al.* (2003)	[163]
	Operator splitting integrators for isokinetic SLLOD	Pan *et al.* (2005)	[164]
	Alternative constraint method for NEMD	Galea and Attard (2002)	[3]
Studies of temperature for driven fluids	Thermodynamic equivalence of various thermostatted ensembles	Evans and Holian (1983), (1985), Evans and Sarman (1993)	[51–53]
	Fluctuations and anisotropy in temperature; directional dependence in kinetic energy of shearing fluids	Baranyai and Cummings (1995), (1997), Criado-Sancho *et al.* (2006)	[165–167]
	Demonstration of uniqueness of Gaussian isothermal thermostat, and that it minimizes phase space compression and change of particle accelerations	Sarman *et al.* (1994), Bright *et al.* (2005)	[61,62]
	Various definitions of temperature for non-equilibrium systems	Baranyai *et al.* (1992), Casas-Vázquez and Jou (1994), Morriss and Rondoni (1999), Baranyai (2000)	[99,101,168–170]
Thermal transport	Efficient NEMD thermal conductivity algorithms developed	Evans (1982), Gillan and Dixon (1983)	[171,172]
	Simulations of thermal conductivity of argon and comparison to experiment (Evans algorithm)	Evans (1986)	[173]

Table 1 – *Continued*

General theme	*Details investigated*	*Authors and year*	*References*
	Comparison of Evans and Gillan algorithms shows that while they are different, they both yield correct results in linear response region	MacGowan and Evans (1986)	[174]
	Specific heat of shearing fluids	Evans and Morriss (1987)	[175]
	Linear response theory for thermal conductivity tensor of shearing fluid	Evans (1991)	[176]
	Simulations of thermal conductivity of shearing fluid	Daivis and Evans (1993)	[177]
	Algorithm to compute thermal conductivity beyond linear regime—use of heat sources and sinks (non flowing systems)	Ashurst (1976), Tenenbaum *et al.* (1982), Baranyai (1996)	[178–180]
	Heat flux cross-couplings established between temperature gradient and gradient of strain rate tensor for shearing fluids	Baranyai *et al.* (1992), Casas-Vazquez and Jou (1994), Todd and Evans (1997), Cordero and Risso (1998), Ayton *et al.* (1999), Daivis and Coelho (2000)	[101,169,181–185]
Diffusion for shear and elongational flows	Calculation of self-diffusion tensor for simple fluid under shear	Cummings *et al.* (1991), Sarman *et al.* (1991)	[186,187]
	Mutual and self-diffusion tensors for fluids under strong shear	Sarman *et al.* (1992)	[188]
	NEMD simulations of the self-diffusion and velocity autocorrelation functions of fluids undergoing a variety of shear and elongational flows	Baranyai and Cummings (1995)	[189]
Microscopic chaos for shear flow and non-equilibrium distribution functions	Calculation of information dimension in shearing Couette flow demonstrates non-differentiable, fractal distribution function	Morriss (1987), (1988)	[190,191]
	Further evidence of fractal steady-state non-equilibrium distribution function from NEMD, etc.	Morriss (1989), Holian *et al.* (1989), Hoover and Posch (1998)	[192–194]
	On the nature of irreversible thermodynamic behaviour and underlying reversible equations of motion, including Fluctuation theorems and experimental verifications	Holian *et al.* (1987), Evans *et al.* (1993), Evans and Searles (1994), (1996), Gallavotti and Cohen (1995), Ayton *et al.* (2001), Mittag *et al.* (2002), Wang *et al.* (2002), Evans and Searles (2002), Mittag and Evans (2003), Williams *et al.* (2004), Reid *et al.* (2004), Carberry *et al.* (2004), Evans *et al.* (2005), Paneni *et al.* (2006), Williams *et al.* (2006)	[195–212]
	Computation of the Yamada-Kawasaki distribution function from NEMD simulation	Morriss and Evans (1988), Evans and Searles (1995)	[213,214]
	Computation of Lyapunov exponents for non-equilibrium system via NEMD simulation	Posch and Hoover (1988), (1989), Sarman *et al.* (1992), Dellago *et al.* (1996), Morriss *et al.* (1996), Searles *et al.* (1997)	[64,215–219]
	Viscosity from maximal Lyapunov exponents or escape rate formalism	Evans *et al.* (1990), Viscardy and Gaspard (2003)	[63,220]
	Entropy calculations for nonequilbrium states and relationship to fractal non-equilibrium distribution function	Evans (1989), Hoover (1998)	[221,222]
	The conjugate pairing rule	Morriss (1989), Evans *et al.* (1990), Sarman *et al.* (1992), Evans and Baranyai (1992), Dettmann and Morriss (1996), Searles *et al.* (1998), Morriss (2001), Panja and van Zon (2002), Frascoli *et al.* (2006)	[40,63,64,223–228]
Linear response theory	Adiabatic systems	Kubo (1957)	[229]
	Thermostatted systems	Morriss and Evans (1985), Evans and Morriss (1990) (and references therein)	[6,23]

Table 1 – *Continued*

General theme	*Details investigated*	*Authors and year*	*References*
Nonlinear response theory	Theory for adiabatic shear flow	Kubo (1957), Yamada and Kawasaki (1967), (1975), Kawasaki and Gunton (1973); see also Evans and Morriss (1990)	[6,20,21,229,230]
	Yamada-Kawasaki adiabatic response theory used to validate SLLOD algorithm for shear flow	Evans and Morriss (1984)	[12]
	Theory for thermostatted shear flow	Morriss and Evans (1985)	[23]
	Time-independent transient time correlation function (TTCF) method for shear flow	Morriss and Evans (1985), (1987), Evans and Morriss (1987), (1988), (1990)	[6,22–24,175]
	Coupling symmetry restrictions to response theory	Evans *et al.* (1992)	[231]
	Response theory for time-dependent fields, including TTCF method for shear flow	Evans (1985); Petravic and Evans (1997), (1998), Evans and Morriss (1990), Petravic (2005)	[6,25–28,56,57,232,233]
	Time-independent TTCF for generalized flows: application to elongational flow	Todd (1997)	[29]
	Time-dependent TTCF for generalized flows: application to oscillatory elongational flow	Todd (1998)	[30]
Books		Evans and Morriss (1990), Hoover (1991), (1999), Allen and Tildesley (1987), Rapaport (1995)	[6,234–238]

Table 2. Molecular fluids.

General theme	*Details investigated*	*Authors and year*	*References*
General algorithmic developments	SLLOD equations proposed for molecular systems	Ladd (1984)	[13]
	Application of Gaussian bond and temperature constraints for shear flow of linear chain molecules	Edberg *et al.* (1987) (see also Edberg *et al.* (1986))	[96,239] [60]
	Correction for numerical drift for Gaussian bond constraints	Baranyai and Evans (1990)	[240]
	Generalisation of constraint scheme for arbitrary molecular geometries	Morriss and Evans (1991)	[83]
	Constant pressure algorithm for molecular systems under shear	Daivis and Evans (1994)	
Atomic versus molecular representations of fluids	Differences and equivalences in computable properties depending on atomic or molecular representation; symmetric atomic pressure but antisymmetric molecular pressure established	Olmsted and Snider (1976), Marechal and Ryckaert (1983), Allen (1984)	[87,89, 92,241]
	Equivalence of atomic and molecular stress correlation functions to compute shear viscosity of decane confirmed	Cui *et al.* (1996)	[93]
Fundamental studies of molecular systems with spin	Irreversible thermodynamics for molecular fluids with spin	Snider and Lewchuk (1967)	[242]
	Confirmation of nonlinear Born effect via NEMD simulations of liquid chlorine	Edberg *et al.* (1987)	[91]
	NEMD simulations of the vortex viscosity for diatomic fluids	Delhommelle (2002)	[243]
	Tests of extended Navier-Stokes equations	Travis *et al.* (1997), Travis and Evans (1997), Delhommelle and Evans (2002)	[244–246]
Transport in simple molecular fluids	Green-Kubo calculations for shear, bulk, vortex, spin viscosities and thermal conductivity for diatomics	Evans and Streett (1978)	[247]
	NEMD simulation of frequency dependent shear viscosity of methane	Evans (1979)	[248]
	NEMD simulations of oblate ring molecules	Baranyai and Evans (1990)	[60,249]
	Shear and elongational flow for diatomics (liquid chlorine)	Hounkonnou *et al.* (1992)	[250]
	Use of KR boundary conditions for steady-state planar elongational flow of small molecules; comparisons with planar shear	Matin *et al.* (2000), (2001)	[125,251]
Thermostats for molecular systems	Extensive studies of atomic versus molecular thermostats for molecules under shear; proper use of molecular versus atomic SLLOD algorithms elaborated on	Travis *et al.* (1995), (1996)	[95,97,98]
	Further critical examination of use of thermostats for SLLOD applied to molecular fluids	Padilla and Toxvaerd (1996)	[55]
	Configurational thermostats for NEMD molecular systems	Delhommelle and Evans (2001),Chialvo *et al.* (2001), Lue *et al.* (2002), Delhommelle and Evans (2002)	[46,49,77, 78,252]
Thermal and electrical properties	Evans thermal conductivity algorithm extended to flexible molecules	Daivis and Evans (1994)	[253]
	Thermal conductivity for strongly shearing molecular fluid	Daivis and Evans (1995)	[254]
	Temperature dependence of the thermal conductivity of butane	Daivis and Evans (1995)	[255]
	Effects of thermostats on the calculation of the electric conductivity of molten NaCl subjected to strong AC and DC fields	Petravic and Delhommelle (2003), (2004)	[256–258]
	Thermal conductivity of ethanol (use of Ewald summation technique for partial charges)	Petravic (2005)	[259]
	Use of TTCF to compute the electrical conductivity of molten NaCl	Delhommelle *et al.* (2005)	[260]
Simple mixtures	Heat flow and mass diffusion for binary simple liquids	Sarman and Evans (1992)	[261,262]
Liquid crystals	Self-diffusion for rod-like molecules under shear	Sarman *et al.* (1993)	[263]
	Self-diffusion (via colour conductivity algorithm) and heat flow (via Evans algorithm)	Sarman and Evans (1993)	[264]
	Green-Kubo and NEMD algorithms for viscous flow in nematic fluids	Sarman and Evans (1993)	[265]
	Nematic-isotropic interfaces under shear (Lees–Edwards boundary driven algorithm)	Germano and Schmid (2005)	[266]
Ionic and magnetic fluids	Ewald summations for molecular systems under shear	Wheeler *et al.* (1997)	[267]
	NEMD simulations of a simple dipolar fluid under shear	McWhirter and Patey (2002)	[268,269]
	Ferroelectric nematic liquid under shear	McWhirter and Patey (2002)	[270]
	Configurational thermostat for molten salt	Delhommelle and Petravic (2003)	[271]
	Shear viscosity of molten alkalai halides	Galamba *et al.* (2004), (2005)	[272,273]
	Thermal conductivity of molten alkalai halides	Galamba *et al.* (2004)	[274]

Table 2 – *Continued*

General theme	*Details investigated*	*Authors and year*	*References*
	Structure and rheology of ferromagnetic fluids	Ilg *et al.* (2005). See also Ilg *et al.* (2002), Ilg and Kröger (2002)	[275–278]
Alkanes and alcohols	NEMD of linear and branched alkanes	Morriss *et al.* (1991), Daivis *et al.* (1992)	[279,280]
	Rheology of *n*-decane via multiple timestep NEMD algorithm	Cui *et al.* (1996)	[162]
	Rheology of *n*-decane, hexadecane and tetracosane	Cui *et al.* (1996)	[281]
	NEMD as a useful technique to characterize lubricants	Moore *et al.* (1997)	[282]
	NEMD of mixtures of *n*-hexane and *n*-hexadecane	Kioupis and Maginn (1999)	[283]
	NEMD studies of how molecular architecture affects performance of lubricants	Kioupis and Maginn (1999), (2000), Jabbarzadeh *et al.* (2003)	[284–286]
	High pressure NEMD simulations of C_{20}–C_{40} alkanes	McCabe *et al.* (2001)	[287]
	Direct comparison of NEMD simulation with experimental data for shear viscosity of alkanes	Bair *et al.* (2002)	[288]
	Prediction of Newtonian viscosities from high strain rate NEMD simulations for complex fluids	McCabe *et al.* (2002)	[289]
	NEMD simulations of perfluoroalkanes	McCabe *et al.* (2003)	[290]
	EMD and NEMD study of alkanes, alcohols and their mixtures	Zhang and Ely (2004)	[291]
	Study of hydrogen bonding in ethanol under shear	Petravic and Delhommelle (2005)	[292]
Polymer solutions and composites	Explicit solvent NEMD for dilute polymer solutions under shear	Pierleoni and Ryckaert (1995), Aust *et al.* (1999), (2002)	[293–295]
	Concentration dependence of conformational and viscometric of properties polymer solutions via explicit solvent NEMD	Kairn *et al.* (2004)	[296,297]
	NEMD study of polymer/spherical filler systems mimicking polymer nanocomposites	Kairn *et al.* (2005)	[298]
Polymer melts	Melts up to N=100 monomers per chain under steady-state shear, using FENE potential	Kröger *et al.* (1993)	[299]
	Melts under transient elongational flow for N=30 monomers per chain, FENE potential.	Kröger *et al.* (1997)	[300]
	Polyethylene melt under shear—transient rheology, comparisons with Doi–Edwards theory	Moore *et al.* (1999)	[301]
	NEMD simulation of crossover between Rouse and reptation behaviour for FENE chain melt	Kröger and Hess (2000)	[302]
	Supercooled melt under shear	Yamamoto and Onuki (2002)	[303]
	Steady state planar elongation and shear flow studies for up to N=50; FJC chain	Daivis *et al.* (2003)	[85]
	Entanglement studies via Lees–Edwards shearing boundaries for N up to 250; FENE chains	Yamamoto and Onuki (2004)	[304]
	Oscillatory shear studies of unentangled polymer melts	Cifre *et al.* (2004)	[305]
	NEMD of linear polyethylene melt under planar elongation	Baig *et al.* (2006)	[306]
Dendrimers	Structure and rheology of dendrimers under shear, including constant volume and constant pressure simulations; dendrimer melts, blends of dendrimer/polymer melts and dendrimer solutions	Bosko *et al.* (2004), (2005), (2006)	[307–310]
Biomolecular simulation	NEMD simulations of lipid bilayer—computation of bulk modulus	Ayton *et al.* (2002)	[311]
Reviews and books	NEMD applications to non-Newtonian rheology	Cummings and Evans (1992)	[312]
	NEMD of simple and polymeric fluids	Kröger (1998), (2005)	[313,314]
	Overall review of NEMD, including molecular fluids	Sarman *et al.* (1998)	[2]
	Review of models for complex non-equilibrium fluids	Kröger (2004)	[1]

configurational thermostats offers much better prospects for the development of thermostatting techniques that are free of artifacts. Configurational thermostats operate purely on the atomic positions and do not require an estimate of the atomic streaming velocity. The first applications of configurational thermostat to molecular fluids were published by Lue *et al.* [49] and Delhommelle and Evans [77]. The equations of motion for a molecular fluid with a configurational atomic thermostat in the presence of bond constraints are written as

$$\begin{aligned}\dot{\mathbf{r}}_{i\alpha} &= \frac{\mathbf{p}_{i\alpha}}{m_{i\alpha}} + \mathbf{r}_i\cdot\nabla\mathbf{v} + \frac{s}{T}\frac{\partial T_c}{\partial \mathbf{r}_{i\alpha}} + (\mathbf{L}\cdot\boldsymbol{\zeta})_{i\alpha} \\ \dot{\mathbf{p}}_{i\alpha} &= \mathbf{F}_{i\alpha} - \left(\frac{m_{i\alpha}}{m_i}\right)\mathbf{p}_i\cdot\nabla\mathbf{v} \\ \dot{s} &= -Q\frac{(T_c - T)}{T}\end{aligned} \tag{3.115}$$

where $\mathbf{L}$ is obtained from the bond constraint matrix and $\boldsymbol{\zeta}$ is a modified constraint multiplier [49]. The last term in the first equation is added to ensure that bond constraints are not violated by the thermostat force, which is different for each atom in a molecule. For more detail, refer to Delhommelle and Evans, and Lue *et al.* [49,77]. The results obtained with this thermostat generally show that at reduced shear rates above 0.5, the intramolecular properties of the configurational thermostatted system are far less perturbed from their equilibrium values than when a centre of mass kinetic thermostat is used.

4. Homogeneous NEMD: A survey of the literature

Tables 1 and 2 above summarise some of the main contributions to the field of NEMD simulations of homogeneous fluids for both atomic (table 1) and molecular (table 2) fluids. Our summary consists of four columns for each table: a general theme, the detailed investigation of a particular aspect of that theme, the year of publication and authors involved, and the full reference of the relevant work. As the literature on this subject is vast we apologise for inadvertently omitting any significant references. In summarising the field in this way we hope to have produced a useful list of relevant NEMD literature that can be of assistance to other researchers interested in specific publications.

5. Conclusions

We have attempted to not only review the relevant NEMD literature, but also present a useful set of expositions and guidelines to assist readers in the application of NEMD algorithms for homogeneous fluids. It is indeed encouraging that the popularity of NEMD as a useful simulation tool for studying the visco-elastic behaviour of fluids has increased rapidly in recent years. We hope that this trend will continue in the years to come. But we are also aware that there is a degree of doubt in the simulation community, particularly with regard to the application of NEMD techniques to molecular fluids. We hope that this review serves the two purposes of reviewing the relevant literature and assisting readers in formulating the most appropriate equations of motion to help them achieve their objectives in the simulation of homogeneous flows. We look forward eagerly to new developments in the field over the next few years and to an ever-broadening range of applications, in the fields of both materials and biological sciences.

References

[1] M. Kröger. Simple models for complex nonequilibrium fluids. *Phys. Rep.*, **390**, 453 (2004).
[2] S. Sarman, D.J. Evans, P.T. Cummings. Recent developments in non-Newtonian molecular dynamics. *Phys. Rep.*, **305**, 1 (1998).
[3] T.M. Galea, P. Attard. Constraint method for deriving nonequilibrium molecular dynamics equations of motion. *Phys. Rev. E*, **66**, 041207 (2002).
[4] F. Müller-Plathe. Reversing the perturbation in nonequilibrium molecular dynamics: an easy way to calculate the shear viscosity of fluids. *Phys. Rev. E*, **59**, 4894 (1999).
[5] S.R. de Groot, P. Mazur. *Non-Equilibrium Thermodynamics*, Dover, New York, NY (1984).
[6] D.J. Evans, G.P. Morriss. *Statistical Mechanics of Nonequilibrium Liquids*, Academic Press, London (1990).
[7] J.H. Irving, J.G. Kirkwood. The statistical mechanical theory of transport processes. 4. The equations of hydrodynamics. *J. Chem. Phys.*, **18**, 817 (1950).
[8] B.D. Todd, D.J. Evans, P.J. Daivis. Pressure tensor for inhomogeneous fluids. *Phys. Rev. E*, **52**, 1627 (1995).
[9] A.W. Lees, S.F. Edwards. The computer study of transport processes under extreme conditions. *J. Phys. C*, **5**, 1921 (1972).
[10] W.G. Hoover, D.J. Evans, R.B. Hickman, A.J.C. Ladd, W.T. Ashurst, B. Moran. Lennard–Jones triple-point bulk and shear viscosities. Green–Kubo theory, Hamiltonian mechanics, and nonequilibrium molecular dynamics. *Phys. Rev. A*, **22**, 1690 (1980).
[11] D.J. Evans, G.P. Morriss. Non-Newtonian molecular dynamics. *Comput. Phys. Rep.*, **1**, 297 (1984).
[12] D.J. Evans, G.P. Morriss. Nonlinear-response theory for steady planar Couette flow. *Phys. Rev. A*, **30**, 1528 (1984).
[13] A.J.C. Ladd. Equations of motion for non-equilibrium molecular dynamics simulations of viscous flow in molecular fluids. *Mol. Phys.*, **53**, 459 (1984).
[14] P.J. Daivis, B.D. Todd. A simple, direct derivation and proof of the validity of the SLLOD equations of motion for generalized homogeneous flows. *J. Chem. Phys.*, **124**, 194103 (2006).
[15] A.M. Kraynik, D.A. Reinelt. Extensional motions of spatially periodic lattices. *Int. J. Multiphase Flow*, **18**, 1045 (1992).
[16] A. Baranyai, P.T. Cummings. Steady state simulation of planar elongation flow by nonequilibrium molecular dynamics. *J. Chem. Phys.*, **110**, 42 (1999).
[17] B.D. Todd, P.J. Daivis. Nonequilibrium molecular dynamics simulations of planar elongational flow with spatially and temporally periodic boundary conditions. *Phys. Rev. Lett.*, **81**, 1118 (1998).
[18] B.D. Todd, P.J. Daivis. A new algorithm for unrestricted duration molecular dynamics simulations of planar elongational flow. *Comput. Phys. Comm.*, **117**, 191 (1999).
[19] B.D. Todd, P.J. Daivis. The stability of nonequilibrium molecular dynamics simulations of elongational flows. *J. Chem. Phys.*, **112**, 40 (2000).
[20] T. Yamada, K. Kawasaki. Nonlinear effects in shear viscosity of critical mixtures. *Prog. Theor. Phys.*, **38**, 1031 (1967).
[21] T. Yamada, K. Kawasaki. Application of mode-coupling theory to nonlinear stress tensor in fluids. *Prog. Theor. Phys.*, **53**, 111 (1975).
[22] D.J. Evans, G.P. Morriss. Transient-time-correlation functions and the rheology of fluids. *Phys. Rev. A*, **38**, 4142 (1988).

[23] G.P. Morriss, D.J. Evans. Isothermal response theory. *Mol. Phys.*, **54**, 629 (1985).

[24] G.P. Morriss, D.J. Evans. Application of transient correlation-functions to shear-flow far from equilibrium. *Phys. Rev. A*, **35**, 792 (1987).

[25] J. Petravic, D.J. Evans. Nonlinear response for time-dependent external fields. *Phys. Rev. Lett.*, **78**, 1199 (1997).

[26] J. Petravic, D.J. Evans. Nonlinear response for nonautonomous systems. *Phys. Rev. E*, **56**, 1207 (1997).

[27] J. Petravic, D.J. Evans. Nonlinear response theory for time-dependent external fields: shear flow and color conductivity. *Int. J. Thermophys.*, **19**, 1049 (1998).

[28] J. Petravic, D.J. Evans. Time dependent nonlinear response theory. *Trends Stat. Phys.*, **2**, 85 (1998).

[29] B.D. Todd. Application of transient time correlation functions to nonequilibrium molecular dynamics simulations of elongational flow. *Phys. Rev. E*, **56**, 6723 (1997).

[30] B.D. Todd. Nonlinear response theory for time-periodic elongational flows. *Phys. Rev. E*, **58**, 4587 (1998).

[31] C. Baig, B.J. Edwards, D.J. Keffer, H.D. Cochran. A proper approach for nonequilibrium molecular dynamics simulations of planar elongational flow. *J. Chem. Phys.*, **122**, 114103 (2005).

[32] B.J. Edwards, C. Baig, D.J. Keffer. An examination of the validity of nonequilibrium molecular-dynamics simulation algorithms for arbitrary steady-state flows. *J. Chem. Phys.*, **123**, 114106 (2005).

[33] B.J. Edwards, C. Baig, D.J. Keffer. A validation of the p-SLLOD equations of motion for homogeneous steady-state flows. *J. Chem. Phys.*, **124**, 194104 (2006).

[34] B.J. Edwards, M. Dressler. A reversible problem in non-equilibrium thermodynamics: Hamiltonian evolution equations for non-equilibrium molecular dynamics simulations. *J. Non-Newton. Fluid Mech.*, **96**, 163 (2001).

[35] I. Borzsák, P.T. Cummings, D.J. Evans. Shear viscosity of a simple fluid over a wide range of strain rates. *Mol. Phys.*, **100**, 2735 (2002).

[36] R. Bhupathiraju, P.T. Cummings, H.D. Cochran. An efficient parallel algorithm for non-equilibrium molecular dynamics simulations of very large systems in planar Couette flow. *Mol. Phys.*, **88**, 1665 (1996).

[37] D.P. Hansen, D.J. Evans. A parallel algorithm for nonequilibrium molecular dynamics simulation of shear flow on distributed memory machines. *Mol. Simul.*, **13**, 375 (1994).

[38] T.A. Hunt, B.D. Todd. On the Arnold cat map and periodic boundary conditions for planar elongational flow. *Mol. Phys.*, **101**, 3445 (2003).

[39] B.D. Todd. Cats, maps and nanoflows: some recent developments in nonequilibrium nanofluidics. *Mol. Simul.*, **31**, 411 (2005).

[40] F. Frascoli, D.J. Searles, B.D. Todd. Chaotic properties of planar elongational flows and planar shear flows: Lyapunov exponents, conjugate-pairing rule and phase space contraction. *Phys. Rev. E*, **73**, 046206 (2006).

[41] D.J. Evans, W.G. Hoover, B.H. Failor, B. Moran, A.J.C. Ladd. Nonequilibrium molecular dynamics via Gauss's principle of least constraint. *Phys. Rev. A*, **28**, 1016 (1983).

[42] W.G. Hoover. Canonical dynamics: equilibrium phase-space distributions. *Phys. Rev. A*, **31**, 1695 (1985).

[43] S. Nose. A unified formulation of the constant temperature molecular-dynamics methods. *J. Chem. Phys.*, **81**, 511 (1984).

[44] S. Nose. A molecular-dynamics method for simulations in the canonical ensemble. *Mol. Phys.*, **52**, 255 (1984).

[45] B.D. Butler, G. Ayton, O.G. Jepps, D.J. Evans. Configurational temperature: verification of Monte Carlo simulations. *J. Chem. Phys.*, **109**, 6519 (1998).

[46] J. Delhommelle, D.J. Evans. Configurational temperature thermostat for fluids undergoing shear flow: application to liquid chlorine. *Mol. Phys.*, **99**, 1825 (2001).

[47] O.G. Jepps, G. Ayton, D.J. Evans. Microscopic expression for the thermodynamic temperature. *Phys. Rev. E*, **62**, 4757 (2000).

[48] L. Lue, D.J. Evans. Configurational temperature for systems with constraints. *Phys. Rev. E*, **62**, 4764 (2000).

[49] L. Lue, O.G. Jepps, J. Delhommelle, D.J. Evans. Configurational thermostats for molecular systems. *Mol. Phys.*, **100**, 2387 (2002).

[50] H.H. Rugh. Dynamical approach to temperature. *Phys. Rev. Lett.*, **78**, 772 (1997).

[51] D.J. Evans, B.L. Holian. Shear viscosities away from the melting line—a comparison of equilibrium and non-equilibrium molecular-dynamics. *J. Chem. Phys.*, **78**, 5147 (1983).

[52] D.J. Evans, B.L. Holian. The Nose–Hoover thermostat. *J. Chem. Phys.*, **83**, 4069 (1985).

[53] D.J. Evans, S. Sarman. Equivalence of thermostatted nonlinear responses. *Phys. Rev. E*, **48**, 65 (1993).

[54] S.Y. Liem, D. Brown, J.H.R. Clarke. Investigation of the homogeneous-shear nonequilibrium-molecular-dynamics method. *Phys. Rev. A*, **45**, 3706 (1992).

[55] P. Padilla, S. Toxvaerd. Simulating shear flow. *J. Chem. Phys.*, **104**, 5956 (1996).

[56] J. Petravic. Time dependence of phase variables in a steady shear flow algorithm. *Phys. Rev. E*, **71**, 011202 (2005).

[57] J. Petravic, D.J. Evans. Approach to the non-equilibrium time-periodic state in a "steady" shear flow model. *Mol. Phys.*, **95**, 219 (1998).

[58] P.J. Daivis, B.D. Todd. Frequency dependent elongational viscosity by nonequilibrium molecular dynamics. *Int. J. Thermophys.*, **19**, 1063 (1998).

[59] B.D. Todd, P.J. Daivis. Elongational viscosities from nonequilibrium molecular dynamics simulations of oscillatory elongational flow. *J. Chem. Phys.*, **107**, 1617 (1997).

[60] A. Baranyai, D.J. Evans. New algorithm for constrained molecular-dynamics simulation of liquid benzene and naphthalene. *Mol. Phys.*, **70**, 53 (1990).

[61] J.N. Bright, D.J. Evans, D.J. Searles. New observations regarding deterministic, time-reversible thermostats and Gauss's principle of least constraint. *J. Chem. Phys.*, **122**, 194106 (2005).

[62] S. Sarman, D.J. Evans, A. Baranyai. Extremum properties of the Gaussian thermostat. *Physica A*, **208**, 191 (1994).

[63] D.J. Evans, E.G.D. Cohen, G.P. Morriss. Viscosity of a simple fluid from its maximal Lyanpunov exponents. *Phys. Rev. A*, **42**, 5990 (1990).

[64] S. Sarman, D.J. Evans, G.P. Morriss. Conjugate pairing rule and thermal-transport coefficients. *Phys. Rev. A*, **45**, 2233 (1992).

[65] F.D. Ditolla, M. Ronchetti. Applicability of nose isothermal reversible dynamics. *Phys. Rev. E*, **48**, 1726 (1993).

[66] B.L. Holian, A.F. Voter, R. Ravelo. Thermostatted molecular-dynamics—how to avoid the Toda demon hidden in Nose–Hoover dynamics. *Phys. Rev. E*, **52**, 2338 (1995).

[67] S. Toxvaerd, O.H. Olsen. Canonical molecular-dynamics of molecules with internal degrees of freedom. *Ber. Bunsenges. Phys. Chem.*, **93**, 274 (1990).

[68] G.J. Martyna, M.L. Klein, M.E. Tuckerman. Nosé–Hoover chains: the canonical ensemble via continuous dynamics. *J. Chem. Phys.*, **97**, 2635 (1992).

[69] A.C. Branka. Nose–Hoover chain method for nonequilibrium molecular dynamics simulation. *Phys. Rev. E*, **61**, 4769 (2000).

[70] A.C. Branka, M. Kowalik, K.W. Wojciechowski. Generalization of the Nosé–Hoover approach. *J. Chem. Phys.*, **119**, 1929 (2003).

[71] J.J. Erpenbeck. Shear viscosity of the hard-sphere fluid via nonequilibrium molecular-dynamics. *Phys. Rev. Lett.*, **52**, 1333 (1984).

[72] J. Delhommelle, J. Petravic, D.J. Evans. Reexamination of string phase and shear thickening in simple fluids. *Phys. Rev. E*, **68**, 031201 (2003).

[73] D.J. Evans, G.P. Morriss. Shear thickening and turbulence in simple fluids. *Phys. Rev. Lett.*, **56**, 2172 (1986).

[74] D.J. Evans, S.T. Cui, H.J.M. Hanley, G.C. Straty. Conditions for the existence of a reentrant solid-phase in a sheared atomic fluid. *Phys. Rev. A*, **46**, 6731 (1992).

[75] W. Loose, S. Hess. Rheology of dense model fluids via nonequilibrium molecular dynamics—shear thinning and ordering transition. *Rheol. Acta*, **28**, 91 (1989).

[76] J. Delhommelle, J. Petravic, D.J. Evans. On the effects of assuming flow profiles in nonequilibrium simulations. *J. Chem. Phys.*, **119**, 11005 (2003).

[77] J. Delhommelle, D.J. Evans. Comparison of thermostatting mechanisms in NVT and NPT simulations of decane under shear. *J. Chem. Phys.*, **115**, 43 (2001).

[78] J. Delhommelle, D.J. Evans. Correspondence between configurational temperature and molecular kinetic temperature thermostats. *J. Chem. Phys.*, **117**, 6016 (2002).

[79] C. Braga, K.P. Travis. A configurational themperature Nosé–Hoover thermostat. *J. Chem. Phys.*, **123**, 134101 (2005).

[80] D. Kusnezov, A. Bulgac, W. Bauer. Canonical ensembles from chaos. *Ann. Phys.*, **204**, 155 (1990).

[81] C. Braga, K.P. Travis. Configurational constant pressure molecular dynamics. *J. Chem. Phys.*, **124**, 104102 (2006).

[82] D.J. Evans, G.P. Morriss. Isothermal–isobaric molecular dynamics. *Chem. Phys.*, **77**, 63 (1983).

[83] P.J. Daivis, D.J. Evans. Comparison of constant pressure and constant volume nonequilibrium simulations of sheared model decane. *J. Chem. Phys.*, **100**, 541 (1994).

[84] S. Melchionna, G. Ciccotti, B.L. Holian. Hoover NPT dynamics for systems varying in shape and size. *Mol. Phys.*, **78**, 533 (1993).

[85] P.J. Daivis, M.L. Matin, B.D. Todd. Nonlinear shear and elongational rheology of model polymer melts by non-equilibrium molecular dynamics. *J. Non-Newton. Fluid Mech.*, **111**, 1 (2003).

[86] F. Frascoli, B.D. Todd. A nonequilibrium molecular dynamics algorithm for the simulation of planar elongational flow at constant pressure and constant temperature. *J. Chem. Phys.*, **126**, 044506 (2007).

[87] R.D. Olmsted, F.F. Snider. Differences in fluid dynamics associated with an atomic versus a molecular description of the same system. *J. Chem. Phys.*, **65**, 3407 (1976).

[88] H. Yamakawa. *Modern Theory of Polymer Solutions*, Harper and Row, New York, NY (1971).

[89] M.P. Allen. Atomic and molecular representations of molecular hydrodynamic variables. *Mol. Phys.*, **52**, 705 (1984).

[90] G. Ciccotti, J.P. Ryckaert. Molecular dynamics simulation of rigid molecules. *Comput. Phys. Rep.*, **4**, 345 (1986).

[91] R. Edberg, D.J. Evans, G.P. Morriss. On the nonlinear born effect. *Mol. Phys.*, **62**, 1357 (1987).

[92] G. Marechal, J.-P. Ryckaert. Atomic versus molecular description of transport properties in polyatomic fluids: *n*-butane as an illustration. *Chem. Phys. Lett.*, **101**, 548 (1983).

[93] S.T. Cui, P.T. Cummings, H.D. Cochran. The calculation of the viscosity from the autocorrelation function using molecular and atomic stress tensors. *Mol. Phys.*, **88**, 1657 (1996).

[94] D.J. Evans. Non-equilibrium molecular dynamics study of the rheological properties of diatomic liquids. *Mol. Phys.*, **42**, 1355 (1981).

[95] K.P. Travis, P.J. Daivis, D.J. Evans. Computer simulation algorithms for molecules undergoing planar Couette flow: a nonequilibrium molecular dynamics study. *J. Chem. Phys.*, **103**, 1109 (1995).

[96] R. Edberg, G.P. Morriss, D.J. Evans. Rheology of *n*-alkanes by nonequilibrium molecular dynamics. *J. Chem. Phys.*, **86**, 4555 (1987).

[97] K.P. Travis, P.J. Daivis, D.J. Evans. Thermostats for molecular fluids undergoing shear flow: application to liquid chlorine. *J. Chem. Phys.*, **103**, 10638 (1995).

[98] K.P. Travis, P.J. Daivis, D.J. Evans. Erratum: thermostats for molecular fluids undergoing shear flow: application to liquid chlorine. *J. Chem. Phys.*, **105**, 3893 (1996).

[99] A. Baranyai. Temperature of nonequilibrium steady-state systems. *Phys. Rev. E*, **62**, 5989 (2000).

[100] J. Casas-Vázquez, D. Jou. Temperature in non-equilibrium states: a review of open problems and current proposals. *Rep. Prog. Phys.*, **66**, 1937 (2003).

[101] A. Baranyai, D.J. Evans, P.J. Daivis. Isothermal shear-induced heat flow. *Phys. Rev. A*, **46**, 7593 (1992).

[102] W.T. Ashurst, W.G. Hoover. Dense-fluid shear viscosity via nonequilibrium molecular dynamics. *Phys. Rev. A*, **11**, 658 (1975).

[103] D.J. Evans, W.G. Hoover, A.J.C. Ladd. Fluctuation expressions for nonequilibrium distribution functions in adiabatic flows. *Phys. Rev. Lett.*, **45**, 124 (1980).

[104] H.J.M. Hanley, D.J. Evans. Equilibrium and non-equilibrium radial distribution functions in mixtures. *Mol. Phys.*, **39**, 1039 (1980).

[105] D.J. Evans. Rheological properties of simple fluids by computer simulation. *Phys. Rev. A*, **23**, 1988 (1981).

[106] D.J. Evans, H.J.M. Hanley, S. Hess. Non-Newtonian phenomena in simple fluids. *Phys. Today*, **37**, 26 (1984).

[107] J. Delhommelle. Onset of shear-thickening in simple fluids. *Eur. Phys. J. E.*, **15**, 65 (2004).

[108] J.-P. Ryckaert, A. Bellemans, G. Ciccotti, V. Paolini. Shear-rate dependence of the viscosity of simple fluids by nonequilibrium molecular dynamics. *Phys. Rev. Lett.*, **60**, 128 (1988).

[109] D.J. Evans, G.P. Morriss, L.M. Hood. On the number dependence of viscosity in three dimensional fluids. *Mol. Phys.*, **68**, 637 (1989).

[110] D.J. Evans. Enhanced $t^{-3/2}$ long-time tail for the stress stress time correlation-function. *J. Stat. Phys.*, **22**, 81 (1980).

[111] M. Ferrario, G. Ciccotti, B.L. Holian, J.-P. Ryckaert. Shear-rate dependence of the viscosity of the Lennard–Jones liquid at the triple point. *Phys. Rev. A*, **44**, 6936 (1991).

[112] B.D. Todd, D.J. Evans, K.P. Travis, P.J. Daivis. Comment on: molecular simulation and continuum mechanics study of simple fluids in non-isothermal planar Couette flow. *J. Chem. Phys.*, **111**, 10730 (1999).

[113] J. Petravic, D.J. Isbister. Pressure tensor of the hard-disk Lorentz gas. *Phys. Rev. E*, **51**, 4309 (1995).

[114] J. Petravic, D.J. Isbister, G.P. Morriss. Correlation dimension of the sheared hard-disk Lorentz gas. *J. Stat. Phys.*, **76**, 1045 (1994).

[115] J. Petravic, O.G. Jepps. Homogeneous shear flow of a hard-sphere fluid: analytic solutions. *Phys. Rev. E*, **67**, 021105 (2003).

[116] D.J. Evans. Equilibrium fluctuation expressions for wave-vector- and frequency-dependent shear viscosity. *Phys. Rev. A*, **23**, 2622 (1981).

[117] K.P. Travis, D.J. Searles, D.J. Evans. Strain rate dependent properties of a simple fluid. *Mol. Phys.*, **95**, 195 (1998).

[118] K.P. Travis, D.J. Searles, D.J. Evans. On the wavevector dependent shear viscosity of a simple fluid. *Mol. Phys.*, **97**, 415 (1999).

[119] H.H. Gan, B.C. Eu. Theory of the nonequilibrium structure of dense simple fluids—effects of shearing. *Phys. Rev. A*, **45**, 3670 (1992).

[120] H.H. Gan, B.C. Eu. Theory of the nonequilibrium structure of dense simple fluids—effects of shearing. 2. High-shear-rate effects. *Phys. Rev. A*, **46**, 6344 (1992).

[121] Y.V. Kalyuzhnyi, S.T. Cui, P.T. Cummings, H.D. Cochran. Distribution functions of a simple fluid under shear: low shear rates. *Phys. Rev. E*, **60**, 1716 (1999).

[122] J. Ge, G. Marcelli, B.D. Todd, R.J. Sadus. Energy and pressure of fluids under shear at different state points. *Phys. Rev. E*, **64**, 021201 (2001).

[123] J. Ge, G. Marcelli, B.D. Todd, R.J. Sadus. Erratum: energy and pressure of fluids under shear at different state points. *Phys. Rev. E*, **65**, 069901(E) (2002).

[124] G. Marcelli, B.D. Todd, R.J. Sadus. Analytic dependence of the pressure and energy of an atomic fluid under shear. *Phys. Rev. E*, **63**, 021204 (2001).

[125] M.L. Matin, P.J. Daivis, B.D. Todd. Comparison of planar Couette flow and planar elongational flow for systems of small freely jointed chain molecules. *J. Chem. Phys.*, **113**, 9122 (2000).

[126] B.L. Holian. Simulations of vibrational relaxation in dense molecular fluids. II. Generalized treatment of thermal equilibration between a sample and a reservoir. *J. Chem. Phys.*, **117**, 1173 (2002).

[127] B.L. Holian. Evaluating shear viscosity: Power dissipated versus entropy produced. *J. Chem. Phys.*, **117**, 9567 (2002).

[128] J. Ge, B.D. Todd, G. Wu, R.J. Sadus. Scaling behaviour for the pressure and energy of shearing fluids. *Phys. Rev. E*, **67**, 061201 (2003).

[129] B.D. Todd. Power-law exponents for the shear viscosity of non-Newtonian simple fluids. *Phys. Rev. E*, **72**, 041204 (2005).

[130] J. Delhommelle. Should "lane formation" occur systematically in driven liquids and colloids? *Phys. Rev. E*, **71**, 016705 (2005).

[131] J. Delhommelle, J. Petravic. Shear thickening in a model colloidal suspension. *J. Chem. Phys.*, **123**, 074707 (2005).

[132] J. Delhommelle, J. Petravic, D.J. Evans. Non-Newtonian behavior in simple fluids. *J. Chem. Phys.*, **120**, 6117 (2004).

[133] J. Petravic. Shear stress relaxation in liquids. *J. Chem. Phys.*, **120**, 10188 (2004).

[134] J. Petravic. Cooperative effects, transport and entropy in simple liquids. *J. Chem. Phys.*, **121**, 11202 (2004).

[135] M.W. Evans, D.M. Heyes. Combined shear and elongational flow by non-equilibrium molecular dynamics. *Mol. Phys.*, **69**, 2412 (1990).

[136] D.M. Heyes. Molecular dynamics simulations of extensional, sheet and unidirectional flow. *Chem. Phys.*, **98**, 15 (1985).

[137] D.M. Heyes. Tensile viscosities of the Lennard–Jones liquid. *Phys. Lett. A*, **115**, 42 (1986).

[138] C. Pierleoni, J.-P. Ryckaert. Non-Newtonian viscosity of atomic fluids in shear and shear-free flows. *Phys. Rev. A*, **44**, 5314 (1991).

[139] A. Baranyai, P.T. Cummings. Nonequilibrium molecular dynamics study of shear and shear-free flows in simple fluids. *J. Chem. Phys.*, **103**, 10217 (1995).
[140] D.J. Evans, D.J. Searles, W.G. Hoover, C.G. Hoover, B.L. Holian, H.A. Posch, G.P. Morriss. Comment on "Modified nonequilibrium molecular dynamics for fluid flows with energy conservation". *J. Chem. Phys.*, **108**, 4351 (1998).
[141] M.E. Tuckerman, C.J. Mundy, S. Balasubramanian, M.L. Klein. Modified nonequilibrium molecular dynamics for fluid flows with energy conservation. *J. Chem. Phys.*, **106**, 5615 (1997).
[142] M.E. Tuckerman, C.J. Mundy, S. Balasubramanian, M.L. Klein. Response to Comment on "Modified nonequilibrium molecular dynamics for fluid flows with energy conservation" [J. Chem. Phys., **108**, 4351 (1998)]. *J. Chem. Phys.*, **108**, 4353 (1998).
[143] A. Baranyai, P.T. Cummings. Towards the atomistic simulation of phase coexistence in nonequilibrium systems. *J. Chem. Phys.*, **105**, 2378 (1996).
[144] A. Baranyai, P.T. Cummings. Towards a computational chemical potential for nonequilibrium steady-state systems. *Phys. Rev. E*, **60**, 5522 (1999).
[145] B.D. Butler, P. Harrowell. Factors determining crystal-liquid coexistence under shear. *Nature*, **415**, 1008 (2002).
[146] S. Butler, P. Harrowell. Simulation of the coexistence of a shearing liquid and a strained crystal. *J. Chem. Phys.*, **118**, 4115 (2003).
[147] J. Ge, G.-W. Wu, B.D. Todd, R.J. Sadus. Equilibrium and nonequilibrium molecular dynamics methods for detemining solid-liquid phase coexistence at equilibrium. *J. Chem. Phys.*, **119**, 11017 (2003).
[148] J. Petravic. Influence of strain on transport in dense Lennard–Jones systems. *J. Chem. Phys.*, **120**, 7041 (2004).
[149] S.H. Lee, P.T. Cummings. Shear viscosity of model mixtures by nonequilibrium molecular dynamics. I. Argon–krypton mixtures. *J. Chem. Phys.*, **99**, 3919 (1993).
[150] S.H. Lee, P.T. Cummings. Effect of three-body forces on the shear viscosity of liquid argon. *J. Chem. Phys.*, **101**, 6206 (1994).
[151] G. Marcelli, B.D. Todd, R.J. Sadus. The strain rate dependence of shear viscosity, pressure and energy from two-body and three-body interactions. *Fluid Phase Equilib.*, **183**, 371 (2001).
[152] J.-L. Barrat, L. Berthier. Fluctuation–dissipation relation in a sheared fluid. *Phys. Rev. E*, **63**, 012503 (2000).
[153] L. Berthier, J.-L. Barrat. Nonequilibrium dynamics and fluctuation–dissipation relation in a sheared fluid. *J. Chem. Phys.*, **116**, 6228 (2002).
[154] L. Berthier, J.-L. Barrat, J. Kurchan. A two-time-scale, two-temperature scenario for nonlinear rheology. *Phys. Rev. E*, **61**, 5464 (2000).
[155] P.J. Daivis, M.L. Matin. Steady-state thermodynamics of shearing linear viscoelastic fluids. *J. Chem. Phys.*, **118**, 11111 (2003).
[156] T. Taniguchi, G.P. Morriss. Steady shear flow thermodynamics based on a canonical distribution approach. *Phys. Rev. E*, **70**, 056124 (2004).
[157] D.J. Evans, H.J.M. Hanley. A thermodynamics of steady homogeneous shear flow. *Phys. Lett. A*, **80**, 175 (1980).
[158] A. Baranyai. Phase space compression and entropy of nonequilibrium steady states. *J. Chem. Phys.*, **105**, 7723 (1996).
[159] A. Baranyai, D.J. Evans. Calculation of equilibrium entropy differences from non-equilibrium molecular dynamics simulations. *Mol. Phys.*, **72**, 229 (1991).
[160] A. Baranyai, D.J. Evans. Comments on thermodynamic integration methods for the determination of nonequilibrium entropy. *Mol. Phys.*, **74**, 353 (1991).
[161] D.J. Evans. The equivalence of Norton and Thevenin ensembles. *Mol. Phys.*, **80**, 221 (1993).
[162] S.T. Cui, P.T. Cummings, H.D. Cochran. Multiple time step nonequilibrium molecular dynamics simulation of the rheological properties of liquid *n*-decane. *J. Chem. Phys.*, **104**, 255 (1996).
[163] M.L. Matin, P.J. Daivis, B.D. Todd. Cell neighbour list method for planar elongational flow: rheology of a diatomic fluid. *Comput. Phys. Commun.*, **151**, 35 (2003).
[164] G. Pan, J.F. Ely, C. McCabe, D.J. Isbister. Operator splitting algorithm for isokinetic SLLOD molecular dynamics. *J. Chem. Phys.*, **122**, 094114 (2005).
[165] A. Baranyai, P.T. Cummings. Fluctuations close to equilibrium. *Phys. Rev. E*, **52**, 2198 (1995).
[166] A. Baranyai, P.T. Cummings. Directional dependence of the random kinetic energy in planar Couette flow. *Mol. Phys.*, **90**, 35 (1997).
[167] M. Criado-Sancho, D. Jou, J. Casas-Vázquez. Nonequilibrium kinetic temperatures in flowing gases. *Phys. Lett. A*, **350**, 339 (2006).
[168] A. Baranyai. Numerical temperature measurement in far from equilibrium model systems. *Phys. Rev. E*, **61**, R3306 (2000).
[169] J. Casas-Vázquez, D. Jou. Nonequilibrium temperature versus local-equilibrium temperature. *Phys. Rev. E*, **49**, 1040 (1994).
[170] G.P. Morriss, L. Rondoni. Definition of temperature in equilibrium and nonequilibrium systems. *Phys. Rev. E*, **59**, R5 (1999).
[171] D.J. Evans. Homogeneous NEMD algorithm for thermal conductivity—application of non-canonical linear response theory. *Phys. Lett. A*, **91**, 457 (1982).
[172] M.J. Gillan, M. Dixon. The calculation of thermal-conductivities by perturbed molecular-dynamics simulation. *J. Phys. C*, **16**, 869 (1983).
[173] D.J. Evans. Thermal conductivity of the Lennard–Jones fluid. *Phys. Rev. A*, **34**, 1449 (1986).
[174] D. MacGowan, D.J. Evans. A comparison of NEMD algorithms for thermal conductivity. *Phys. Lett. A*, **117**, 414 (1986).
[175] D.J. Evans, G.P. Morriss. The specific heat of non-equilibrium steady states. *Mol. Phys.*, **61**, 1151 (1987).
[176] D.J. Evans. Green–Kubo relations for weak vector processes in strongly shearing fluids. *Phys. Rev. A*, **44**, 3630 (1991).
[177] P.J. Daivis, D.J. Evans. Thermal conductivity of a shearing fluid. *Phys. Rev. E*, **48**, 1058 (1993).
[178] W.T. Ashurst. *Advances in Thermal Conductivity*, University of Missouri-Rolla, Rolla (1974).
[179] A. Baranyai. Heat flow studies for large temperature gradients by molecular dynamics simulation. *Phys. Rev. E*, **54**, 6911 (1996).
[180] A. Tenenbaum, G. Ciccotti, R. Gallico. Stationary non-equilibrium states by molecular-dynamics—Fourier law. *Phys. Rev. A*, **25**, 2778 (1982).
[181] G. Ayton, O.G. Jepps, D.J. Evans. On the validity of Fourier's law in systems with spatially varying strain rates. *Mol. Phys.*, **96**, 915 (1999).
[182] P. Cordero, D. Risso. Nonlinear transport laws for low density fluids. *Physica A*, **257**, 36 (1998).
[183] P.J. Daivis, J.L.K. Coelho. Generalized Fourier law for heat flow in a fluid with a strong, nonuniform strain rate. *Phys. Rev. E*, **61**, 6003 (2000).
[184] D. Risso, P. Cordero. Generalized hydrodynamics for a poiseuille flow: theory and simulations. *Phys. Rev. E*, **58**, 546 (1998).
[185] B.D. Todd, D.J. Evans. Temperature profile for Poiseuille flow. *Phys. Rev. E*, **55**, 2800 (1997).
[186] P.T. Cummings, B.Y. Wang, D.J. Evans, K.J. Fraser. Nonequilibrium molecular dynamics calculation of self-diffusion in a non-Newtonian fluid subject to a Couette strain field. *J. Chem. Phys.*, **94**, 2149 (1991).
[187] S. Sarman, D.J. Evans, P.T. Cummings. Comment on: nonequilibrium molecular dynamics calculation of self-diffusion in a non-Newtonian fluid subject to a Couette strain field. *J. Chem. Phys.*, **95**, 8675 (1991).
[188] S. Sarman, D.J. Evans, A. Baranyai. Mutual and self-diffusion in fluids undergoing strong shear. *Phys. Rev. A*, **46**, 893 (1992).
[189] A. Baranyai, P.T. Cummings. Self-diffusion in strongly driven flows: a non-equilibrium molecular dynamics study. *Mol. Phys.*, **86**, 1307 (1995).
[190] G.P. Morriss. The information dimension of the nonequilibrium distribution function. *Phys. Lett. A*, **122**, 236 (1987).
[191] G.P. Morriss. Lyapunov dimension of two-body planar Couette flow. *Phys. Rev. A*, **37**, 2118 (1988).
[192] B.L. Holian, G. Ciccotti, W.G. Hoover, B. Moran, H.A. Posch. Nonlinear-response theory for time-independent fields: consequences of the fractal nonequilibrium distribution function. *Phys. Rev. A*, **39**, 5414 (1989).
[193] W.G. Hoover, H.A. Posch. Multifractals from stochastic many-body molecular dynamics. *Phys. Lett. A*, **246**, 247 (1998).
[194] G.P. Morriss. Phase-space singularities in planar Couette flow. *Phys. Rev. A*, **39**, 4811 (1989).
[195] G. Ayton, D.J. Evans, D.J. Searles. A local fluctuation theorem. *J. Chem. Phys.*, **115**, 2033 (2001).
[196] D.M. Carberry, J.C. Reid, G.M. Wang, E.M. Sevick, D.J. Searles, D.J. Evans. Fluctuations and Irreversibility: an experimental demonstration of a second-law-like theorem using a colloidal particle held in an optical trap. *Phys. Rev. Lett.*, **92**, 140601 (2004).

[197] D.M. Carberry, S.R. Williams, G.M. Wang, E.M. Sevick, D.J. Evans. The Kawasaki identity and the fluctuation theorem. *J. Chem. Phys.*, **121**, 8179 (2004).

[198] D.J. Evans, E.G.D. Cohen, G.P. Morriss. Probability of 2nd law violations in shearing steady-states. *Phys. Rev. Lett.*, **71**, 2401 (1993).

[199] D.J. Evans, D.J. Searles. Equilibrium microstates which generate second law violating steady states. *Phys. Rev. E*, **50**, 1645 (1994).

[200] D.J. Evans, D.J. Searles. Causality, response theory and the second law of thermodynamics. *Phys. Rev. E*, **56**, 5808 (1996).

[201] D.J. Evans, D.J. Searles. The fluctuation theorem. *Adv. Phys.*, **51**, 1529 (2002).

[202] D.J. Evans, D.J. Searles, L. Rondoni. Application of the Gallavotti–Cohen fluctuation relation to thermostated steady states near equilibrium. *Phys. Rev. E*, **71**, 056120 (2005).

[203] G. Gallavotti, E.G.D. Cohen. Dynamical ensembles in nonequilibrium statistical mechanics. *Phys. Rev. Lett.*, **74**, 2694 (1995).

[204] G. Gallavotti, E.G.D. Cohen. Dynamical ensembles in stationary states. *J. Stat. Phys.*, **80**, 931 (1995).

[205] B.L. Holian, W.G. Hoover, H.A. Posch. Resolution of Loschmidt's paradox: the origin of irreversible behavior in reversible atomistic dynamics. *Phys. Rev. Lett.*, **59**, 10 (1987).

[206] E. Mittag, D.J. Evans. Time-dependent fluctuation theorem. *Phys. Rev. E*, **67**, 026113 (2003).

[207] E. Mittag, D.J. Searles, D.J. Evans. Isobaric–isothermal fluctuation theorem. *J. Chem. Phys.*, **116**, 6875 (2002).

[208] C. Paneni, D.J. Searles, L. Rondoni. Temporal asymmetry of fluctuations in nonequilibrium steady states. *J. Chem. Phys.*, **124**, 114109 (2006).

[209] J.C. Reid, D.M. Carberry, G.M. Wang, E.M. Sevick, D.J. Evans, D.J. Searles. Reversibility in nonequilibrium trajectories of an optically trapped particle. *Phys. Rev. E*, **70**, 016111 (2004).

[210] G.M. Wang, E.M. Sevick, E. Mittag, D.J. Searles, D.J. Evans. Experimental demonstration of violations of the second law of thermodynamics for small systems and short time scales. *Phys. Rev. Lett.*, **89**, 050601 (2002).

[211] S.R. Williams, D.J. Searles, D.J. Evans. Independence of the transient fluctuation theorem to thermostatting details. *Phys. Rev. E*, **70**, 066113 (2004).

[212] S.R. Williams, D.J. Searles, D.J. Evans. Numerical study of the steady state fluctuation relations far from equilibrium. *J. Chem. Phys.*, **124**, 194102 (2006).

[213] D.J. Evans, D.J. Searles. Steady states, invariant measures, and response theory. *Phys. Rev. E*, **52**, 5839 (1995).

[214] G.P. Morriss, D.J. Evans. Yamada-Kawasaki distribution function. *Phys. Rev. A*, **37**, 3605 (1988).

[215] C. Dellago, H.A. Posch, W.G. Hoover. Lyapunov instability in a system of hard disks in equilibrium and nonequilibrium steady states. *Phys. Rev. E*, **53**, 1485 (1996).

[216] G.P. Morriss, C.P. Dettmann, D.J. Isbister. Field dependence of Lyapunov exponents for nonequilibrium systems. *Phys. Rev. E*, **54**, 4748 (1996).

[217] H.A. Posch, C.G. Hoover. Equilibrium and nonequilibrium Lyapunov spectra for dense fluids and solids. *Phys. Rev. E*, **39**, 2175 (1989).

[218] H.A. Posch, W.G. Hoover. Lyapunov instability of dense Lennard–Jones fluids. *Phys. Rev. A*, **38**, 473 (1988).

[219] D.J. Searles, D.J. Evans, D.J. Isbister. The number dependence of the maximum Lyapunov exponent. *Physica. A*, **240**, 96 (1997).

[220] S. Viscardy, P. Gaspard. Viscosity in the escape-rate formalism. *Phys. Rev. E*, **68**, 041205 (2003).

[221] D.J. Evans. On the entropy of nonequilibrium states. *J. Stat. Phys.*, **57**, 745 (1989).

[222] W.G. Hoover. Liouville's theorem, Gibbs' entropy, and multifractal distributions for nonequilibrium steady states. *J. Chem. Phys.*, **109**, 4164 (1998).

[223] C.P. Dettmann, G.P. Morriss. Proof of Lyapunov exponent pairing for systems at constant kinetic energy. *Phys. Rev. E*, **53**, R5545 (1996).

[224] D.J. Evans, A. Baranyai. The Gaussian thermostat, phase space compression and the conjugate pairing rule. *Mol. Phys.*, **77**, 1209 (1992).

[225] G.P. Morriss. Conjugate pairing of Lyapunov exponents for isokinetic shear flow algorithms. *Phys. Rev. E*, **65**, 017201 (2001).

[226] D. Panja, R. van Zon. Pairing of Lyapunov exponents for a hard-sphere gas under shear in the thermodynamic limit. *Phys. Rev. E*, **66**, 021101 (2002).

[227] D.J. Searles, D.J. Evans, D.J. Isbister. The conjugate-pairing rule for non-Hamiltonian systems. *Chaos*, **8**, 337 (1998).

[228] G.P. Morriss. Dimensional contraction in nonequilibrium systems. *Phys. Lett. A*, **134**, 307 (1989).

[229] R. Kubo. Statistical-mechanical theory of irreversible processes .1. General theory and simple applications to magnetic and conduction problems. *J. Phys. Soc. Jpn.*, **12**, 570 (1957).

[230] K. Kawasaki, J.D. Gunton. Theory of nonlinear transport processes: nonlinear shear viscosity and normal stress effects. *Phys. Rev. A*, **8**, 2048 (1973).

[231] D.J. Evans, A. Baranyai, S. Sarman. Response theory of symmetry restricted interactions. *Mol. Phys.*, **76**, 661 (1992).

[232] D.J. Evans. Response theory as a free-energy extremum. *Phys. Rev. A*, **32**, 2923 (1985).

[233] J. Petravic, D.J. Evans. The Kawasaki distribution function for nonautonomous systems. *Phys. Rev. E*, **58**, 2624 (1998).

[234] M.P. Allen, D.J. Tildesley. *Computer Simulation of Liquids*, Clarendon Press, Oxford (1987).

[235] J.P. Hansen, I.R. McDonald. *Theory of Simple Liquids*, Academic Press, New York, NY (1986).

[236] W.G. Hoover. *Computational Statistical Mechanics*, Elsevier, Amsterdam (1991).

[237] W.G. Hoover. *Time Reversibility, Computer Simulation and Chaos*, World Scientific, Singapore (1999).

[238] D. Rapaport. *The Art of Molecular Dynamics Simulation*, Cambridge University Press, Cambridge (1995).

[239] R. Edberg, D.J. Evans, G.P. Morriss. Constrained molecular dynamics: Simulations of liquid alkanes with a new algorithm. *J. Chem. Phys.*, **84**, 6933 (1986).

[240] G.P. Morriss, D.J. Evans. A constraint algorithm for the computer simulation of complex molecular liquids. *Comput. Phys. Commun.*, **62**, 267 (1991).

[241] R.D. Olmsted, R.F. Snider. Symmetry of the pressure tensor in macromolecular fluids. *J. Chem. Phys.*, **65**, 3423 (1976).

[242] R.F. Snider, K.S. Lewchuk. Irreversible thermodynamics of a fluid system with spin. *J. Chem. Phys.*, **46**, 3163 (1967).

[243] J. Delhommelle. Rotational viscosity of uniaxial molecules. *Mol. Phys.*, **100**, 3479 (2002).

[244] J. Delhommelle, D.J. Evans. Poiseuille flow for micropolar fluids. *Mol. Phys.*, **100**, 2857 (2002).

[245] K.P. Travis, D.J. Evans. Molecular spin in a fluid undergoing Poiseuille flow. *Phys. Rev. E*, **55**, 1566 (1997).

[246] K.P. Travis, B.D. Todd, D.J. Evans. Poiseuille flow of molecular fluids. *Physica A*, **240**, 315 (1997).

[247] D.J. Evans, W.B. Streett. Transport properties of homonuclear diatomics II. Dense fluids. *Mol. Phys.*, **36**, 161 (1978).

[248] D.J. Evans. The frequency dependent shear viscosity of methane. *Mol. Phys.*, **37**, 1745 (1979).

[249] A. Baranyai, D.J. Evans. NEMD investigation of the rheology of oblate molecules: shear flow in liquid benzene. *Mol. Phys.*, **71**, 835 (1990).

[250] M.N. Hounkonnou, C. Pierleoni, J.-P. Ryckaert. Liquid chlorine in shear and elongational flows: a nonequilibrium molecular dynamics study. *J. Chem. Phys.*, **97**, 9335 (1992).

[251] M.L. Matin, P.J. Daivis, B.D. Todd. Erratum: "Comparison of planar Couette flow and planar elongational flow for systems of small freely jointed chain molecules". [J. Chem. Phys. 113, 9122 (2000)] *J. Chem. Phys.*, **115**, 5338 (2001).

[252] A.A. Chialvo, J.M. Simonson, P.T. Cummings, P.G. Kusalik. On the determination of orientational configurational temperature from computer simulation. *J. Chem. Phys.*, **114**, 6514 (2001).

[253] P.J. Daivis, D.J. Evans. Non-equilibrium molecular dynamics calculation of thermal conductivity of flexible molecules: butane. *Mol. Phys.*, **81**, 1289 (1994).

[254] P.J. Daivis, D.J. Evans. Thermal conductivity of a shearing molecular fluid. *Int. J. Thermophys.*, **16**, 391 (1995).

[255] P.J. Daivis, D.J. Evans. Temperature dependence of the thermal conductivity for two models of liquid butane. *Chem. Phys.*, **198**, 25 (1995).

[256] J. Petravic, J. Delhommelle. Conductivity of molten sodium chloride in an alternating electric field. *J. Chem. Phys.*, **119**, 8511 (2003).

[257] J. Petravic, J. Delhommelle. Conductivity of molten sodium chloride and its supercritical vapor in strong dc fields. *J. Chem. Phys.*, **118**, 7477 (2003).

[258] J. Petravic, J. Delhommelle. Nonequilibrium molecular dynamics simulations of molten sodium chloride. *Int. J. Thermophys.*, **25**, 1375 (2004).
[259] J. Petravic. Thermal conductivity of ethanol. *J. Chem. Phys.*, **123**, 174503 (2005).
[260] J. Delhommelle, P.T. Cummings, J. Petravic. Conductivity of molten sodium chloride in an arbitrarily weak dc electric field. *J. Chem. Phys.*, **123**, 114505 (2005).
[261] S. Sarman, D.J. Evans. Heat flow and mass diffusion in binary Lennard–Jones mixtures. *Phys. Rev. A*, **45**, 2370 (1992).
[262] S. Sarman, D.J. Evans. Heat flow and mass diffusion in binary Lennard–Jones mixtures. II. *Phys. Rev. A*, **46**, 1960 (1992).
[263] S. Sarman, P.J. Daivis, D.J. Evans. Self-diffusion of rodlike molecules in strong shear fields. *Phys. Rev. E*, **47**, 1784 (1993).
[264] S. Sarman, D.J. Evans. Self-diffusion and heat flow in isotropic and liquid crystal phases of the Gay-Berne fluid. *J. Chem. Phys.*, **99**, 620 (1993).
[265] S. Sarman, D.J. Evans. Statistical mechanics of viscous flow in nematic fluids. *J. Chem. Phys.*, **99**, 9021 (1993).
[266] G. Germano, F. Schmid. Nematic-isotropic interfaces under shear: a molecular-dynamics simulation. *J. Chem. Phys.*, **123**, 214703 (2005).
[267] D.R. Wheeler, N.G. Fuller, R.L. Rowley. Non-equilibrium molecular dynamics simulation of the shear viscosity of liquid methanol: adaption of the Ewald sum to Lees–Edwards boundary conditions. *Mol. Phys.*, **92**, 55 (1997).
[268] J.L. McWhirter, G.N. Patey. Nonequilibrium molecular dynamics simulations of a simple dipolar fluid under shear flow. *J. Chem. Phys.*, **117**, 2747 (2002).
[269] J.L. McWhirter, G.N. Patey. Orientational ordering and disordering of a simple dipolar fluid under shear flow. *J. Chem. Phys.*, **117**, 9016 (2002).
[270] J.L. McWhirter, G.N. Patey. Molecular dynamics simulations of a ferroelectric nematic liquid under shear flow. *J. Chem. Phys.*, **117**, 8551 (2002).
[271] J. Delhommelle, J. Petravic. Shear viscosity of molten sodium chloride. *J. Chem. Phys.*, **118**, 2783 (2003).
[272] N. Galamba, C.A. Nieto de Castro, J.F. Ely. Molecular dynamics simulation of the shear viscosity of molten alkali halides. *J. Phys. Chem. B*, **108**, 3658 (2004).
[273] N. Galamba, C.A. Nieto de Castro, J.F. Ely. Shear viscosity of molten alkali halides from equilibrium and nonequilibrium molecular dynamics simulations. *J. Chem. Phys.*, **122**, 224501 (2005).
[274] N. Galamba, C.A. Nieto de Castro, J.F. Ely. Thermal conductivity of molten alkali halides from equilibrium molecular dynamics simulations. *J. Chem. Phys.*, **120**, 8676 (2004).
[275] P. Ilg, M. Kröger. Magnetization dynamics, rheology, and an effective description of ferromagnetic units in dilute suspension. *Phys. Rev. E*, **66**, 021501 (2002).
[276] P. Ilg, M. Kröger. Erratum: magnetization dynamics, rheology, and an effective description of ferromagnetic units in dilute suspension. [Phys. Rev. E 66, 021501 (2002)] *Phys. Rev. E*, **67**, 049901(E) (2003).
[277] P. Ilg, M. Kröger, S. Hess. Magnetoviscosity and orientational order parameters of dilute ferrofluids. *J. Chem. Phys.*, **116**, 9078 (2002).
[278] P. Ilg, M. Kröger, S. Hess. Structure and rheology of model-ferrofluids under shear flow. *J. Magn. Magn. Mater.*, **289**, 325 (2005).
[279] P.J. Daivis, D.J. Evans, G.P. Morriss. Computer simulation study of the comparative rheology of branched and linear alkanes. *J. Chem. Phys.*, **97**, 616 (1992).
[280] G.P. Morriss, P.J. Daivis, D.J. Evans. The rheology of normal alkanes—decane and eicosane. *J. Chem. Phys.*, **94**, 7420 (1991).
[281] S.T. Cui, S.A. Gupta, P.T. Cummings, H.D. Cochran. Molecular dynamics simulations of the rheology of normal decane, hexadecane, and tetracosane. *J. Chem. Phys.*, **105**, 1214 (1996).
[282] J.D. Moore, S.T. Cui, P.T. Cummings, H.D. Cochran. Lubricant characterization by molecular simulation. *AIChE J.*, **43**, 3260 (1997).
[283] L.I. Kioupis, E.J. Maginn. Rheology, dynamics, and structure of hydrocarbon blends: a molecular dynamics study of *n*-hexane/*n*-hexadecane mixtures. *Chem. Eng. J.*, **74**, 129 (1999).
[284] L.I. Kioupis, E.J. Maginn. Molecular simulation of poly-α-olefin synthetic lubricants: impact of molecular architecture on performance properties. *J. Phys. Chem. B*, **103**, 10781 (1999).
[285] L.I. Kioupis, E.J. Maginn. Impact of molecular architecture on the high-pressure rheology of hydrocarbon fluids. *J. Phys. Chem. B*, **104**, 7774 (2000).
[286] A. Jabbarzadeh, J.D. Atkinson, R.I. Tanner. Effect of molecular shape on rheological properties in molecular dynamics simulation of star, H, comb, and linear polymer melts. *Macromolecules*, **36**, 5020 (2003).
[287] C. McCabe, S.T. Cui, P.T. Cummings, P.A. Gordon, R.B. Saeger. Examining the rheology of the 9-octylheptadecane to giga-pascal pressures. *J. Chem. Phys.*, **114**, 1887 (2001).
[288] S. Bair, C. McCabe, P.T. Cummings. Comparison of nonequilibrium molecular dynamics with experimental measurements in the nonlinear shear-thinning regime. *Phys. Rev. Lett.*, **88**, 058302 (2002).
[289] C. McCabe, C.W. Manke, P.T. Cummings. Predicting the Newtonian viscosity of complex fluids from high strain rate molecular simulations. *J. Chem. Phys.*, **116**, 3339 (2002).
[290] C. McCabe, D. Bedrov, O. Borodin, G.D. Smith, P.T. Cummings. Transport properties of perfluoroalkanes using molecular dynamics simulation: comparison of united- and explicit-atom models. *Ind. Eng. Chem. Res.*, **42**, 6956 (2003).
[291] H. Zhang, J.F. Ely. AUA model NEMD and EMD simulations of the shear viscosity of alkane and alcohol systems. *Fluid Phase Equilibria*, **217**, 111 (2004).
[292] J. Petravic, J. Delhommelle. Hydrogen bonding in ethanol under shear. *J. Chem. Phys.*, **122**, 234509 (2005).
[293] C. Aust, M. Kröger, S. Hess. Structure and dynamics of dilute polymer solutions under shear flow via nonequilibrium molecular dynamics. *Macromolecule*, **32**, 5660 (1999).
[294] C. Aust, M. Kröger, S. Hess. Rotation and deformation of a finitely extendable flexible polymer molecule in a steady shear flow. *Macromolecule*, **35**, 8621 (2002).
[295] C. Pierleoni, J.-P. Ryckaert. Deformation and orientation of flexible polymers in solution under shear flow: a new picture for intermediate reduced shear rates. *Macromolecule*, **28**, 5097 (1995).
[296] T. Kairn, P.J. Daivis, M.L. Matin, I.K. Snook. Concentration dependence of viscometric properties of model short chain polymer solutions. *Polymer*, **45**, 2453 (2004).
[297] T. Kairn, P.J. Daivis, M.L. Matin, I.K. Snook. Effects of concentration on steady-state viscometric properties of short chain polymer solutions over the entire concentration range. *Int. J. Thermophys.*, **25**, 1075 (2004).
[298] T. Kairn, P.J. Daivis, I. Ivanov, S.N. Bhattacharya. Molecular-dynamics simulation of model polymer nanocomposite rheology and comparison with experiment. *J. Chem. Phys.*, **123**, 194905 (2005).
[299] M. Kröger, W. Loose, S. Hess. Rheology and structural changes of polymer melts via nonequilibrium molecular dynamics. *J. Rheol.*, **37**, 1057 (1993).
[300] M. Kröger, C. Luap, R. Muller. Polymer melts under uniaxial elongational flow: stress-optical behavior from experiments and nonequilibrium molecular dynamics computer simulations. *Macromolecule*, **30**, 526 (1997).
[301] J.D. Moore, S.T. Cui, H.D. Cochran, P.T. Cummings. Transient rheology of a polyethylene melt under shear. *Phys. Rev. E*, **60**, 6956 (1999).
[302] M. Kröger, S. Hess. Rheological evidence for a dynamical crossover in polymer melts via nonequilibrium molecular dynamics. *Phys. Rev. Lett.*, **85**, 1128 (2000).
[303] R. Yamamoto, A. Onuki. Dynamics and rheology of a supercooled polymer melt in shear flow. *J. Chem. Phys.*, **117**, 2359 (2002).
[304] R. Yamamoto, A. Onuki. Entanglements in quiescent and sheared polymer melts. *Phys. Rev. E*, **70**, 041801 (2004).
[305] J.G.H. Cifre, S. Hess, M. Kröger. Lienar viscoelastic behavior of unentangled polymer melts via non-equilibrium molecular dynamics. *Macromol. Theory Simul.*, **13**, 748 (2004).
[306] C. Baig, B.J. Edwards, D.J. Keffer, H.D. Cochran, V.A. Harmandaris. Rheological and structural studies of linear polyethylene melts under planar elongational flow using non-equilibrium molecular dynamics simulations. *J. Chem. Phys.*, **124**, 084902 (2006).
[307] J.T. Bosko, B.D. Todd, R.J. Sadus. Internal structure of dendrimers in the melt under shear: a molecular dynamics study. *J. Chem. Phys.*, **121**, 1091 (2004).

[308] J.T. Bosko, B.D. Todd, R.J. Sadus. Viscoelastic properties of dendrimers in the melt by nonequilibrium molecular dynamics. *J. Chem. Phys.*, **121**, 12050 (2004).

[309] J.T. Bosko, B.D. Todd, R.J. Sadus. Molecular simulation of dendrimers and their mixtures under shear: comparison of isothermal-isobaric (NpT) and isothermal-isochoric (NVT) ensemble systems. *J. Chem. Phys.*, **123**, 034905 (2005).

[310] J.T. Bosko, B.D. Todd, R.J. Sadus. Analysis of the shape of dendrimers under shear. *J. Chem. Phys.*, **124**, 044910 (2006).

[311] G. Ayton, A.M. Smondyrev, S.G. Bardenhagen, P. McMurtry, G.A. Voth. Calculating the bulk modulus for a lipid bilayer with nonequilibrium molecular dynamics simulation. *Biophys. J.*, **82**, 1226 (2002).

[312] P.T. Cummings, D.J. Evans. Nonequilibrium molecular dynamics approaches to transport properties and non-Newtonian fluid rheology. *Ind. Eng. Chem. Res.*, **31**, 1237 (1992).

[313] M. Kröger. Nonequilibrium dynamics simulations of simple and polymeric fluids. *Curr. Opin. Colloid Interface Sci.*, **3**, 614 (1998).

[314] M. Kröger. *Models for Polymeric and Anisotropic Liquids*, Springer, New York, NY (2005).